REPEATABLE MANUFACTURE OF WINGS FOR FLAPPING WING MICRO AIR VEHICLES USING MICROELECTROMECHANICAL SYSTEM (MEMS) FABRICATION TECHNIQUES

THESIS

David "Bob" Dawson, Captain, USAF

AFIT/GAE/ENY/11-M06

DEPARTMENT OF THE AIR FORCE
AIR UNIVERSITY

AIR FORCE INSTITUTE OF TECHNOLOGY

Wright-Patterson Air Force Base, Ohio

AFIT/GAE/ ENY/11-M06

REPEATABLE MANUFACTURE OF WINGS FOR FLAPPING WING MICRO AIR VEHICLES USING MICROELECTROMECHANICAL SYSTEM (MEMS) FABRICATION TECHNIQUES

THESIS

Presented to the Faculty

Department of Aeronautics and Astronautics

Graduate School of Engineering and Management

Air Force Institute of Technology

Air University

Air Education and Training Command

In Partial Fulfillment of the Requirements for the

Degree of Master of Science in Aeronautical Engineering

David "Bob" Dawson, BS

Captain, USAF

March 2011

REPEATABLE MANUFACTURE OF WINGS FOR FLAPPING WING MICRO AIR VEHICLES USING MICROELECTROMECHANICAL SYSTEM (MEMS) FABRICATION TECHNIQUES

David "Bob" Dawson, BS

Captain, USAF

Approved:

_____   _____
Dr. Richard Cobb, USAF (Chairman)   Date

_____   _____
Dr. Ronald Coutu, USAF (Member)   Date

_____   _____
Dr. Mark Reeder, USAF (Member)   Date

AFIT/GAE/ENY/11-M06

Abstract

While there have been great advances in the area of Flapping Wing Micro Air Vehicles (FWMAV), prototype parts have been constructed with the objective of scientific discovery and basic research. There has been little effort to make parts that could be consistently and repeatedly manufactured. Until recently, there has been little, if any, focus on methods that could be used and verified by subsequent researchers. It is herein proposed that Microelectromechanical System fabrication methods will provide a fast, cheap, and highly repeatable manufacturing method for the FWMAV wings. The wings manufactured to demonstrate this process, bio-inspired by the *Manduca Sexta*, were patterned and manufactured from titanium. The process took a relatively short amount of time: three and a half hours from start to finish. Multiple wings were fabricated as a batch during this time. A repeatable method for producing camber in the wing and mounting a membrane on the titanium structure is also presented. These processes will allow parametric testing of FWMAV wings. These wings will be exactly the same, except for specific changes made by the designer, so wing iterations can be compared and studied precisely. The best possible FWMAV wing can be discovered and exactly recreated in this manner. This process may also be easily adapted to mass manufacture of FWMAV wings in industry.

Acknowledgments

I would like to express my appreciation to my faculty advisor, Dr. Richard Cobb, for his guidance, support, and trust throughout the course of this thesis effort. His insightful questions have been invaluable. I would also like to thank: Dr. Ron Coutu, for his support and expertise on all aspects of MEMS fabrication; Michael Anderson, for his support and clarity of vision; and Ryan O'Hara, for wing design and material property analysis, as well as for his guidance and prodding. Thanks to Travis Tubbs for his work with hawkmoths, and for providing the wings that made wing camber measurements and wing design possible. And, of course, thanks to my wife, Olga, and our children, for all the support they have given.

Bob Dawson

Table of Contents

List of Figures

List of Tables

List of Acronyms

c_l Coefficient of Lift

c   chord length

D   Drag

L   Lift

L'   Lift per unit span of an airfoil

FWMAV   Flying Wing Micro-air Vehicles

h   saggita, or segment height of a circle, representing camber

HF   Hydrofluoric Acid

MEMS   Microelectromechanical Systems

μm micron, or micro meter; 1/1,000,000 of a meter

q_∞ freestream dynamic pressure, –

ρ_∞ freestream density of air

r   radius of a circle

S   Generalized symbol for length scale

V_∞ freestream air velocity

REPEATABLE MANUFACTURE OF WINGS FOR FLAPPING WING MICRO AIR VEHICLES USING MICROELECTROMECHANICAL SYSTEM (MEMS) FABRICATION TECHNIQUES

I. Introduction

1.1 Miniaturizing Air Vehicles

The term Micro Air Vehicle (MAV) generally refers to an air vehicle the size of a bird. Micro-MAV has been used to describe a MAV in the small bird to large insect range, and will be used throughout this thesis. Research and development of Micro-MAVs is a growing area across the country because of potential applications in intelligence gathering, search and rescue and exploration. Micro-MAVs cannot be fabricated however, by simply miniaturizing a conventional airplane. There are two main difficulties preventing miniaturization: aerodynamics and scaling.

Aerodynamically, as the chord of an airfoil shrinks, flight velocity needs to be increase in order to maintain lift. Equation 1 shows the relationship between the chord and the freestream velocity of the aircraft:

$$ \overline{\qquad} \qquad\qquad - \qquad\qquad\qquad\qquad\qquad [1] $$

where L' is the lift per unit span, c_l is the dimensionless coefficient of lift, q_∞ is the dynamic pressure (∞ denotes freestream value), V_∞ is the freestream velocity of the air, ρ_∞ is the density of air, and c is the chord length (1). So as the chord gets smaller, the lift per unit span shrinks for any given velocity, lift coefficient (determined by geometry and angle of attack), and atmospheric conditions. As an air vehicle gets smaller, it becomes impossible to maintain enough lift to keep the vehicle in the air at desirable speeds.

Miniaturized conventional structures do not scale well for several reasons. First and foremost among these reasons is the scaling of forces. As the length dimension decreases, the corresponding force scales according to the power of the length dimension. For example, surface tension (or friction) scales as follows:

$$[2]$$

where S is a generalized length scale, γ is the surface tension (or friction) coefficient, and constants are scaled as S^0. Gravity, however, has a much smaller effect on an object as it scales down:

$$\rule{2cm}{0.4pt} \quad \rule{2cm}{0.4pt} \qquad [3]$$

where M_1 and M_2 are masses, G is the gravitational coefficient, and r is the distance between M_1 and M_2. As the length is scaled down, gravitational effect is diminished to the fourth power, giving it a proportionally smaller effect than surface tension or friction.

The effects of these and other common forces are summarized in Table 1, which shows that surface tension scales proportionately to length. Surface tension, then, makes a much more significant fraction of the force that needs to be overcome for small joints, surfaces, or mechanisms that rely on or are effected by friction, than for larger ones. Large-scale fabrication relies on surface forces being relatively small, but small flying vehicle joints, flaps, and other mechanisms tend to "bind up" mechanically under similar conditions. As a result, small control surfaces are difficult to reliably manufacture, and both structures and control systems must be devised to overcome such limitations. Mechanisms must be simple to use and to maintain. Many solutions to these problems have been devised (2), and the manufacture of small structures and control surfaces is currently an area of intense research.

2

Table 1: Scaling factors of common forces (F) with relation to their length dimension (S), as well as their scaled relationship to acceleration (a) and time (t)

$$F = \begin{bmatrix} S^1 \\ S^2 \\ S^3 \\ S^4 \end{bmatrix} = \begin{bmatrix} \text{Surface Tension} \\ \text{Electrostatic} \\ \text{Electromagnetic} \\ \text{Gravitational} \end{bmatrix}, a = \begin{bmatrix} S^{-2} \\ S^{-1} \\ S^0 \\ S^1 \end{bmatrix}, t = \begin{bmatrix} S^{1.5} \\ S^1 \\ S^{0.5} \\ S^0 \end{bmatrix}$$

The relative sizes of commonly known objects are shown in Figure 1, with common air vehicles at or above the top of the scale, and Micro-MAVs between the second and third categories from the top of the figure. The relative scales of these objects, and how they scale as dimensions are reduced, can be seen in Figure 2 using the length scales across the top of the figure.

As length is scaled down and forces such as friction begin to dominate fabrication considerations, new fabrication methods must be explored. For example, it is difficult to cast or mold a very small part because the surface tension of the mold. This is not a considerable factor for large molds, but can make it very difficult to inject material into a small mold, and to remove the material once molded. 2-D manufacture, when feasible, is simplest. Likewise, when friction dominates movement considerations, ball joints and other sliding mechanisms are no longer feasible, and a new means of movement must be devised. Flexures, piezoelectrics, and thermal expansion may take their place. The smaller the manufactured item, the more important these forces become, and the more vital it is to find solutions. Micro-MAVs are on a scale small enough that these considerations are too important to overlook.
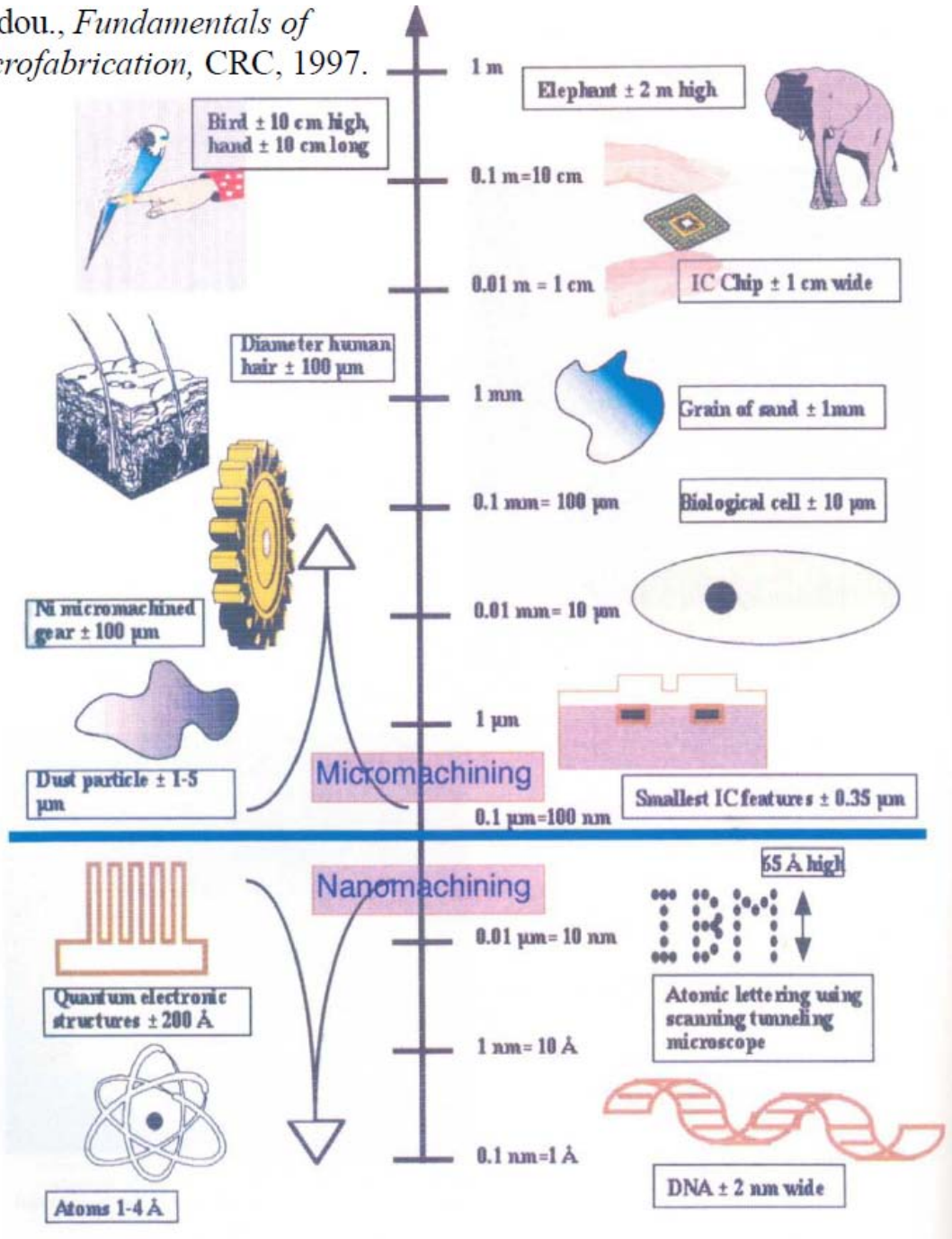
Figure 1: Representative scale of commonly known objects from macro down to nano dimensions (3)
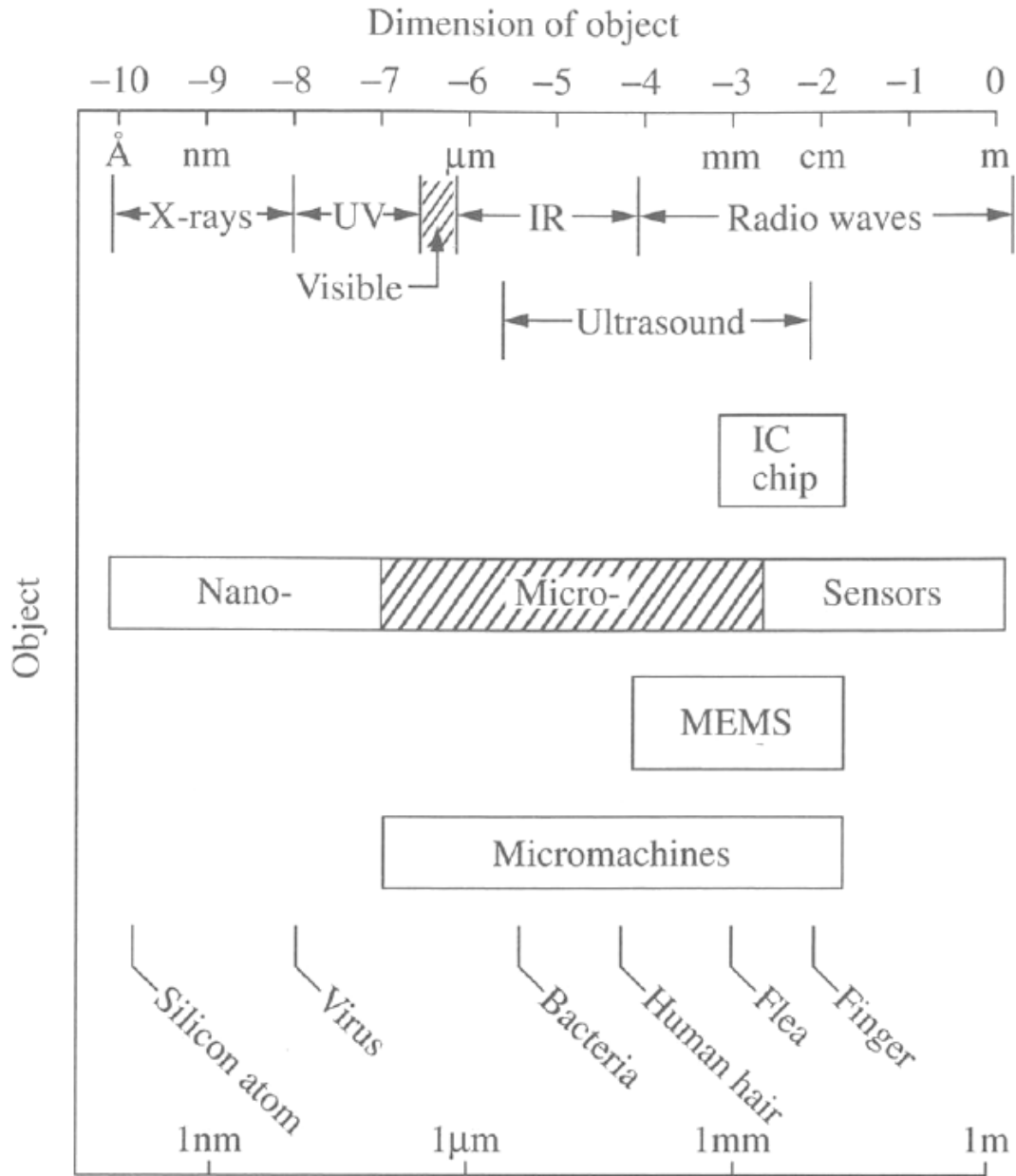
Figure 2: Logarithmic scale of common nano, micro, and macro objects show the vast difference in their relative length scale (4)

The scale of Micro-MAVs will require a different approach to fabrication, locomotion, and power storage. New mechanisms must be developed to overcome the effects of scaling in each of these areas. The focus of this thesis will be on wing fabrication, with the other areas being addressed briefly in the following paragraphs.

Power storage has the same scaling problem mentioned above. While the surface area of a battery is reduced by the square of the length scale, the volume available to store the reactive chemicals that supply power is reduced by the cube of the length scale. There is currently no chemical reaction that technology has been able to harness that will provide more than a few minutes of power at the light weight required by a Micro-MAV. Either a new and more dense source of power must be invented, or a new method to store and deliver power to the Micro-MAV must be pioneered.

Locomotion for Micro-MAVs has been studied more in depth than the power storage problem. The flapping wing ornithopter is currently thought to be the most promising solution to the locomotion problem. It has been postulated that flapping wing ornithopters have several advantages over traditional flying mechanisms by virtue of mimicking nature's flyers. Thus they should not only be able to overcome problems of scale, but may mimic the natural flyers' agility, which exceeds anything man has been able to make at any size (5). As the principles behind the natural flyer's flight is better understood, the ability to create similar flyers, for a myriad of uses, may be realizable (6). Such uses include surveillance/reconnaissance, search and rescue, hazardous environment exploration, and even future planetary exploration.

Due to their size, Micro-MAVs will require a unique blend of fabrication techniques for the various parts of a MAV. A Micro-MAV body has been successfully

manufactured at Harvard and UC Berkeley using a laser-cut 2-D carbon fiber pattern that

can be folded into a 3-D structure (6) (7). Wing actuators have been cut, at a suitably

light and small size, using power-dense piezoelectric material (8). MEMS fabrication

techniques have been shown to be useful in manufacturing wings. The wing structures,

as well as wing membranes, that have been manufactured through these techniques to

great success will be outlined below (9) (10). As research is refined and repeatability is

emphasized, the advantages outlined in this thesis may make MEMS techniques the

prevalent wing fabrication method.

1.2 Principles of Micro-MAV Flight

A number of universities that have interest in the micro-robotics area have done

outstanding preliminary work in the study of Micro-MAV flight principles. UC Berkely

has a strong Biomimetics programs, and has innovated micro-sized robotics in many

areas (11) (12). Their research in the area of MAVs, biomimetics (i.e. ornithopters) and

flapping-wing Micro Air Vehicles (FWMAVs) has revealed many principles important to

Micro-MAV design. From a Caltech/UCLA study of flyers in the size category of small

bird to large insect, the researchers found that an ornithopter would have to have a

wingspan less than 15 cm and weigh less than 10 g (13). The ornithopter would have to

fly in the unsteady state aerodynamic regime, meaning the airflow over the wings is not

constant in time, and cannot be modeled using steady-state aerodynamics. These

constraints on the flight of the ornithopter outline several considerations in manufacturing

its wings.

Such a wing must be light, but also be able to withstand the strong forces used to generate lift and thrust during unsteady-state flight. It must withstand strong inertial forces. The initial MEMS fabrication process pioneered by Caltech and UCLA yielded wings with a structural depth of 350 µm, made from silicon wafers. Unfortunately, the wings were found to be too brittle. They broke easily under the stresses of ornithopter-style wing flapping. Caltech/UCLA then developed a new process using titanium-alloy metal for their wing frames (9).

Results of a joint venture between Harvard and UC Berkeley demonstrate that all apparatus available for larger scale mechanical systems become more challenging to sythesize as size decreases, since surface effects begin to dominate over Newtonian forces (7). Motors, joints, bearings, and structural members are all affected. Macroscale manufacturing techniques are morphologically limited, and joints that assume surface effects to be small are ineffectual. For body and joints, MEMS techniques have limited application. Their solution was to use reinforced composites for body structures and parylene for compliant joints, eliminating surface effects.

These composite structures were fabricated together using laminate technology for strength. For body structures, this allowed true 3-D results, and could be done much more flexibly than MEMS fabrication techniques. The researchers concluded that it was also faster. However, for the wing system, largely a 2-D structure that needs to be reliably repeated, the MEMS fabrication techniques will work well. The process could also be much less expensive than other techniques, such as laser machining. The greatest strength of MEMS fabrication techniques may lie, however, in the ability to be easily scaled into mass production.

8

1.3 Problem Statement: Why Make Repeatable Wings?

Typical of original research, the initial wings for MAV testing were made "on the fly," with convenient material found in the lab, or with "ideal materials," with little forethought to mass production, availability, or affordability. The frames were made by hand out of what materials the researchers could find, normally carbon fiber spars with a polymer membrane. Testing, while well-planned, was improvised based on the wing that was made (14). For instance, the wings made by Micro-MAV pioneer R. J. Wood for his first insect scale MAV were made from a correctly oriented carbon fiber/epoxy composite, with a 1.5 micron-thick polyester membrane. As initial concepts were refined and enlarged upon by other researchers, more consistent results became desirable. Yet, an experiment is of little worth if it cannot be duplicated. The advantage of MEMS manufacturing is that researchers can develop a mask[*] that will yield the same results every time, with little variation between products. There is less opportunity for human error. MEMS production also offers advantages of a quicker turnaround time and wing size control. Also with MEMS, there is no need to use glue to fabricate the wing structure, so MEMS techniques also afford weight minimization. When a wing is found to work, it can be reliably manufactured, again and again. Even a complex wing can be easily mass produced. Mass production will factor significantly in the future of MAVs.

---

[*] A mask provides an exact means of masking photoresist polymers from a controlled UV light exposure, in order to control which portions of the substrate remain masked from a given etchant after the photoresist is developed. More details in manufacture process can be found in Section 2.4

1.4 Research Hypothesis

The main hypothesis of this thesis is that MEMS fabrication techniques can batch produce wings in a methodical, repeatable manner that can be tested and compared to similar wings. Due to the small size of MAV wings, normal manufacturing techniques will have difficulty reliably producing such a small wing. Additionally, these techniques will facilitate parametric testing, to explore which wing spars are important to structure, flight, and wing dynamics, and to assess which can be eliminated in order to save weight.

1.5 Research Focus

Wings have been made with materials available in labs where MAVs have been invented and tested. These wings worked, but could not have been mass produced, or even reproduced exactly for testing purposes. MEMS fabrication techniques provide a reliable manufacturing method to mass produce wings that can be tested and used to gather reproducible data.

1.6 Investigative Questions

Can MEMS fabrication techniques, which are optimized for micron-scale devices, be used to repeatedly manufacture reliable MAV wings on the centimeter scale, with features on the order of millimeters?

Can this method be used to control changes to wings so that these changes can be tested against a control to yield quantifiable, comparable results?

Are there any additional manufacturing methods needed to complete the wing, such as processes for placing the membrane or for imparting wing camber?

Can these MEMS fabrication, camber, and membrane application techniques be used in MAV mass production?

1.7 Methodology

Flapping wing MAV wings will be reproduced by making a MEMS mask of chrome on soda lime, coating a substrate with a photoresist, exposing it through the mask, and developing the photoresist. The substrate can then be etched in a suitable material etchant (usually an acid). Once the wing has been etched, the photoresist can be stripped, leaving only the wing. The wing will then be tested against wings manufactured using different methods (such as laser machining) and materials (such as carbon fiber).

The repeatability of the wing will be determined in two ways. First, pictures of various wing structures will be taken through a microscope and compared. Second, weight and structural integrity will be compared between wings made as a batch.

Repeatability and scalability to mass production are the goals, and will define the success of this thesis. Repeatability is defined above. Scalability to mass production is defined as the ability to use the fabrication methods outlined in this thesis to produce multiple wings repeatably and as a batch.

1.8 Implications

The Air Force Research Laboratory (AFRL) has a goal of making insect-size MAVs by 2030. The testing done on the wings will help to achieve that goal, and the manufacturing methods will be a viable path for AFRL MAVs. The MAVs made by AFRL for the U.S. Air Force will be invaluable tools for Surveillance and Reconnaissance, as well as for Search and Rescue in areas where normal-sized vehicles

or humans may not be able to gain access. In effect, they will be used to save the most valuable resource the Air Force has: human lives.

1.9 Preview

Chapters II and III provide background and experimental setup information for the manufacturing methods described. Chapter IV analyzes the resulting manufactured wings and compares them to the methodology criteria above. Chapter V discusses conclusions and possible future areas of study.

II. Literature Review

2.1 Chapter Overview

The purpose of this chapter is to further investigate the reason for using flapping wings in MAVs, and to explore the optimum wing shape for a flapping wing MAV in the size range of small bird to large insect. Also discussed are the efforts made by pioneers in the MAV field, the results of their testing, and how said results can be used to further the wing manufacturing techniques described in the introduction.

2.2 FWMAV Aerodynamics

Flapping-wing aerodynamics is a difficult subject, and has not been as completely explored as fixed-wing aerodynamics. Unfortunately, it is not likely that fixed wings would work for the MAV size range. This hypothesis is not only based on the proposed difficulty of providing a power source capable of powering a fixed-wing MAV, but is also largely based on observations of nature. Natural flyers have evolved unique systems of flight, but there are visible trends that depend upon the size of the flyer. Large-bird flight can be approximated by fixed-wing models. They soar and glide in a manner that is similar to fixed-wing aircraft manufactured by humans, and their flight can be modeled using quasi-steady-state assumptions. However, once the size of the bird scales down to the tens of grams, the style of flight changes. Small bird and large insect flight is always in the unsteady regime, meaning that wingtip speed exceeds flight speed, as shown in Figure 3 (9). This plot of wingtip speed and flight speed vs. mass of insects and birds was obtained by combining the upper and lower wingtip speed equations, derived from statistical data, as represented in equation [4]:

$-$
[4]

where U is the flight speed, and $U_{vert,x}$ are the upper and lower wingtip speeds. From this

figure, the quasi-steady and unsteady regimes are clearly divided.
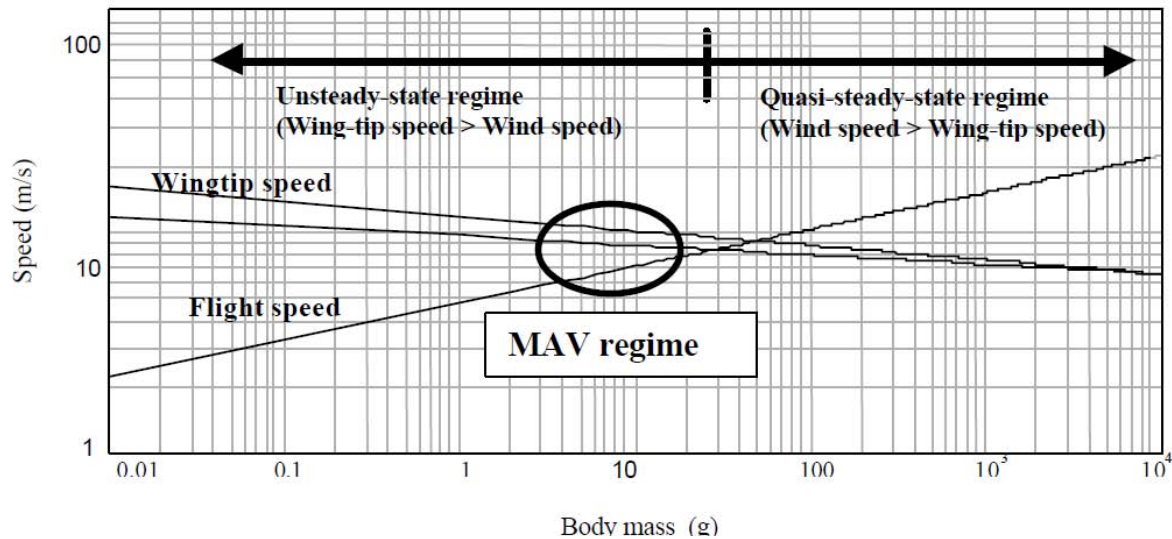
Figure 3: Flight Speed and Wingtip speed differ for steady and unsteady state

regime flyers (9)

For the unsteady regime, lift cannot be predicted and measured in the same

manner as in the quasi-steady regime. If one were to use steady-state assumptions, one

would predict that the unsteady-state flyer cannot produce enough lift to fly at all.

However, progress has been made in understanding the aerodynamics of this regime of

flight, discussed in section 2.3.1 below, which has been of great use those who seek the

ability to control the flight of MAVs.

Furthermore, the MAVs of the large insect range and small hummingbirds have

similar flight mechanisms, which will be discussed below. It indeed seems that there is a

14

naturally optimized manner of flight for the size of MAV to be constructed through this and similar research, so an optimal wing for that MAV may be found. Considerations on this wing structure will include manufacturability and ability to control flight through wing characteristics, as well as strength and structure of the final wing. The following investigation is of accomplished flyers from the small bird to large insect range, as shown in Figure 4.
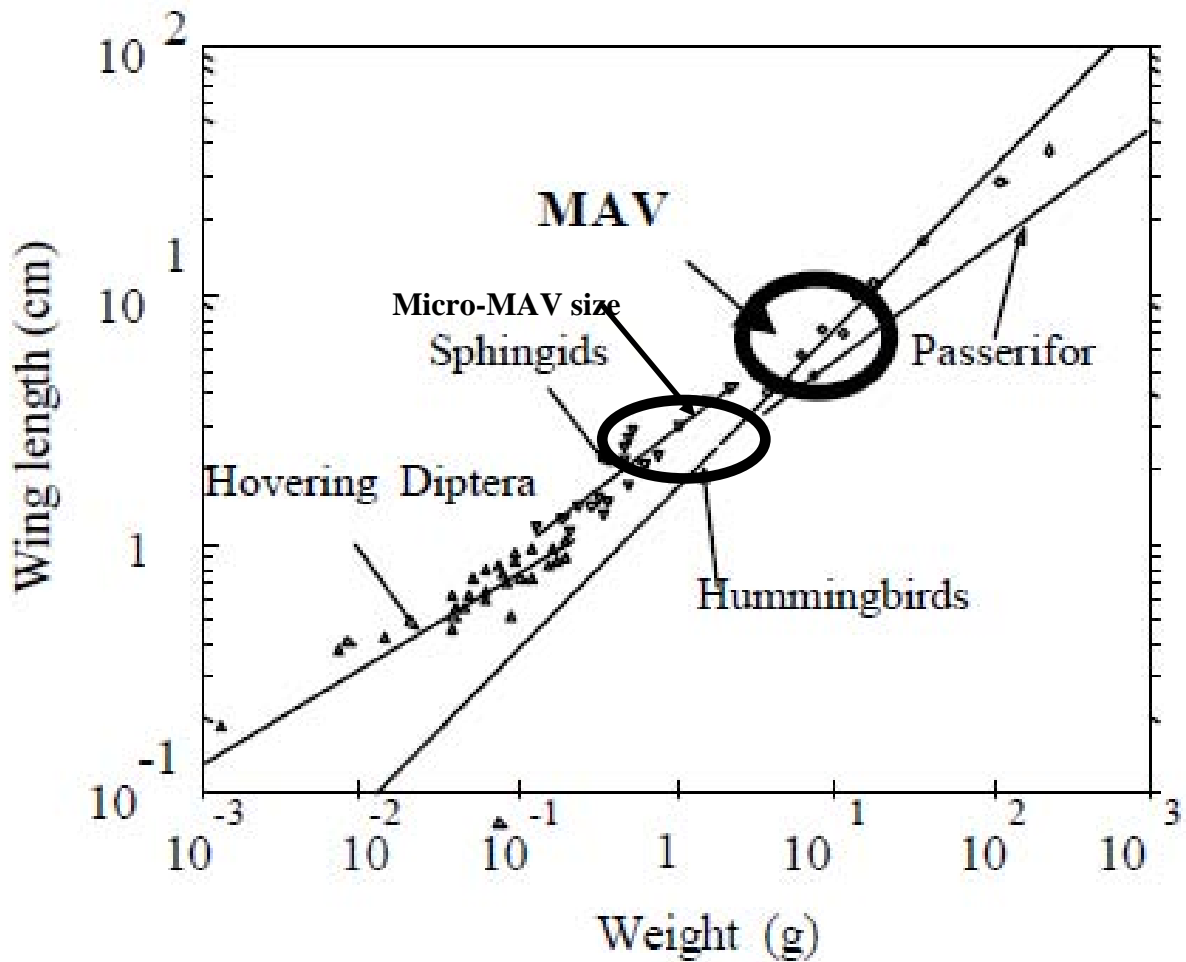
Figure 4: MAV and the smaller Micro-MAV sizes compared to a range of natural flyer sizes (9)

15

2.3 Relevant Research

2.3.1 Lift

Steady-state aerodynamic theory cannot account for the lift generated by unsteady-state flyers. When insect wings are tested in a wind tunnel at velocities encountered during natural flight, the measured forces are substantially smaller than those generated by the insect (15). The complex flapping motion generates more lift than can be predicted by steady-state aerodynamic theory (16) (17).   Research has shed some light on these phenomena, and Micro-MAV wing design will need to include the unsteady-state principles found through that research if flight is to be achieved.

Lift is generated in a similar manner by bats, hummingbirds, and hawkmoths. The lift generated by these flyers is very different from the lift modeled for quasi-steady-state flappers and fixed-wing aircraft. It has been posited that the wing-tip vortex of the flyer's downstroke is among the most important aspects of lift generated by unsteady-state flyers. Time-resolved vortex wake structures of the bat, hummingbird, and hawkmoth can be seen below in Figures 5, 6 and 7.
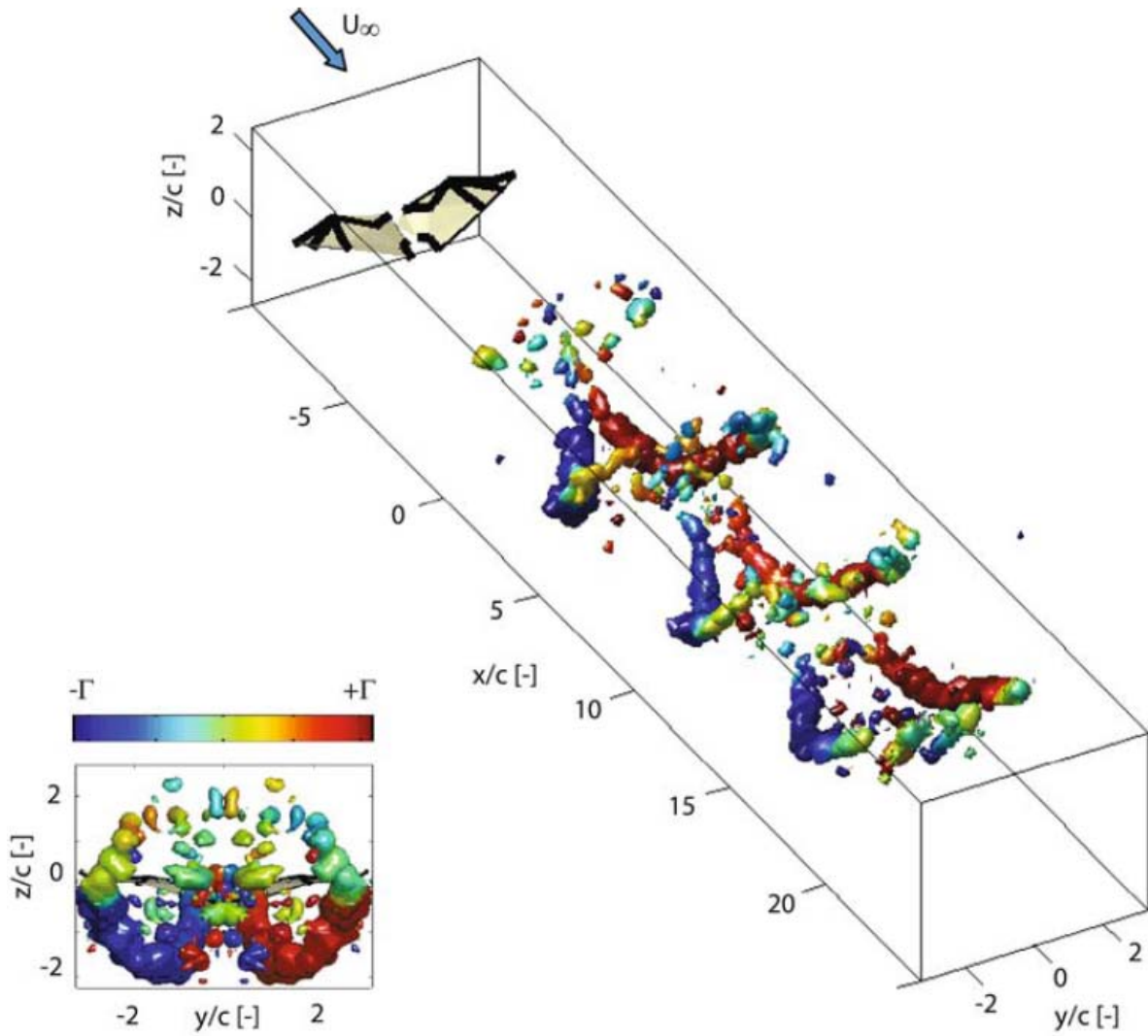
Figure 5: Bat wake at Re=16,700 and k=0.38; isosurfaces from right wing tip vortex (mirrored to left side for ease of viewing), showing changes in circulation(From (18), used with permission from the author)
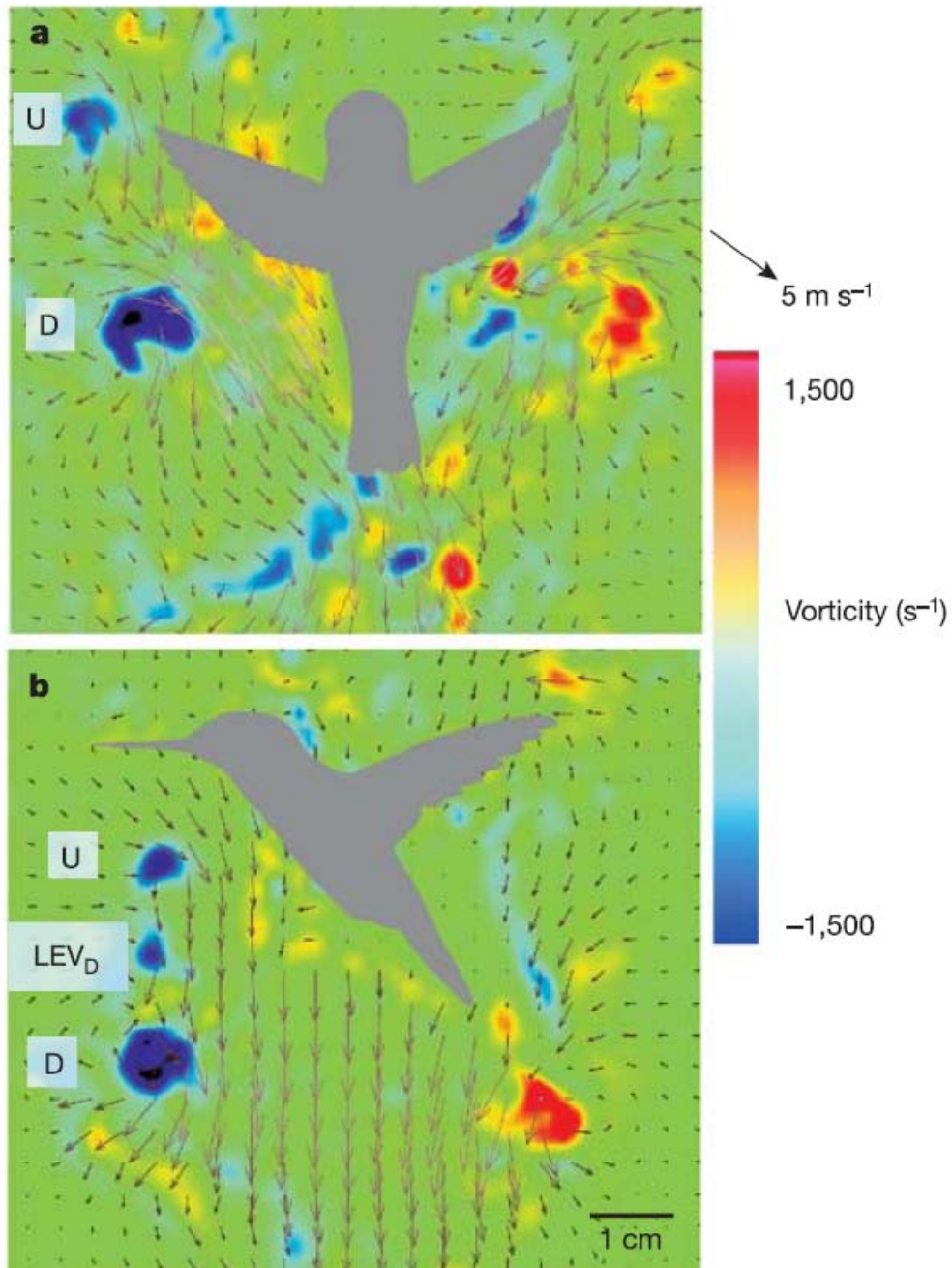
Figure 6: Wake vortex shedding in hummingbird hovering flight; A) wake at end of upstroke, showing tip vortices of downstroke (D) and upstroke (U); B) wake at end of upstroke, showing vorticity pocket LEV$_D$ created by rapid pronation at leading edge of wing, carried through downstroke, and shed during upstroke supination (From (19), used with permission from the author)

The position of vorticity in the wake of the flapper

(a) Complete downstroke (b) $t \leq 0.5s$ (c) $0.5s < t \leq 1.0s$ (d) $1.0s < t \leq 1.6s$ (e) Wake model

16° (SD 15°) 51° (SD 11°) 16° (SD 14°) 8° (SD 17°) 20 cm
25 cm s⁻¹ (SD 2.5) 25 cm s⁻¹ (SD 3.7) 28 cm s⁻¹ (SD 4.2) 24 cm s⁻¹ (SD 5.1)
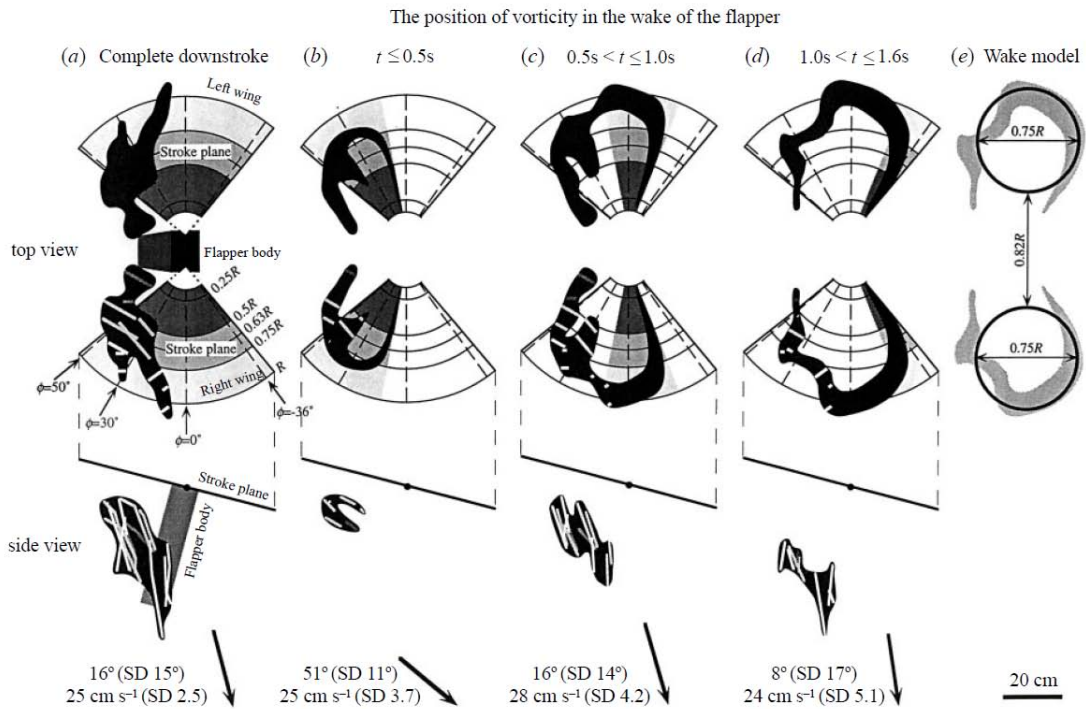
Figure 7: Approximate shape and movement of vortex wake, tracking center of downstroke vortex, in orientation of hovering moth; shed vorticity during complete downstroke shown in (a); (b)-(d) show both shed and leading-edge voriticity during shorter timespans (From (20), used with permission from the author)

The similarities in these figures show that the lift is generated in a similar manner for all three unsteady-state flyers. A wing tip vortex is generated during the downstroke and shed at the end of the downstroke (by rapid supination for the hummingbird and hawkmoth, and by bringing the wing into the body for the bat). A separate wing tip vortex is generated during the upstroke, and is again shed at the end (by rapid pronation for the hummingbird and hawkmoth, and by wing extension for the bat). This leading

19

edge vortex is stabilized by the presence of axial flow, augmenting lift throughout the downstroke. This combination of translational and rotational effects is hypothesized to be among the greatest lift generators for unsteady-state flyers (15). If it can be controlled in a similar manner, a wing that is fabricated to create lift in the same manner as a natural wing should be able to mimic, or at least approximate, these lift characteristics. The natural way to accomplish this feat is to mimic the wing itself, and approximate its 3-D motion, as proposed and described by Anderson (21). An investigation into which wing would be most easily fabricated so as to take advantage of what has been learned of unsteady-state flight characteristics follows.

2.3.2 Natural Wings

Small flyers in the size range being investigated include bats, swallows, hummingbirds, butterflies, beetles, dragonflies, and moths. A short synopsis of the strengths and weaknesses of each flyer, from a MAV perspective, follows. Examples of pictures of each of these flyers, with close-ups of their wings for structural comparison, are included in Appendix 1. Also included are notes from lectures and extended research into the wings and rationalization for the the final choice made for wing design. Following is a brief summary of strengths and weaknesses of each type of wing.

Butterflies and beetles are not "good" flyers for purposes of MAV design. MAVs could not be controlled using principles of flight based upon their flight mechanisms. While their wing structures are somewhat similar to those of the better, or more precise, flyers, they fly in an erratic fashion. It would neither be feasible nor desirable to control

a MAV in that manner, so butterfly and beetle wing structures were not used to provide guidance in designing a MAV wing.

Dragonflies are precise and controlled flyers, with the ability to hover and accelerate quickly, both from a dead stop as well as from a hovering attitude. These are characteristics favorable to a controllable MAV. Dragonfly wing structure is simple, and while it is corrugated, it has little camber or features to complicate manufacturing. However, the delicate wings have numerous structural cells that would make the wing relatively heavy for MAV flight, if replicated entirely, as seen in the silicon wing fabricated by Caltech and UCLA in Figure 8. Also, a study of dragonfly flight shows that the interaction of their double wing structure and the dual control of the wings for take-off and hovering appears to be a more difficult mechanism to mimic mechanically than the flight mechanisms of other natural flyers (22). For these reasons, the dragonfly wing was not used as a prototype for wing design, either.

The only bird with the controlled flight that would be amenable to MAV control is the hummingbird. Other non-steady-state regime flyers, such as swallows and bats, are very nimble and able flyers, but do not fly with the precision desired in a MAV. Their flying mechanism would be very difficult to mimic mechanically because their wings have extra degrees of freedom (23) (24) (25). The hummingbird has been thoroughly studied in areas of flight mechanism, kinematics, musculature, bone structure, and aerodynamics (26) (27). The flight mechanism is one that, while difficult to mimic, is not as complex as that of the dragonfly, and may be possible to control in a MAV. The hummingbird wing structure would be difficult to replicate, however. The bone structure takes up only about one fifth of the wing, and the rest is feather. The bone structure is

21

actively controlled, but the feathers, which perform much of the vortex generation and vortex shedding that aid in flight, passively respond and bend excessively (~35%). These characteristics would be difficult to mimic mechanically, so if a wing could be found that is less difficult to mimic mechanically, this would be preferable.

Bats are precise flyers with the characteristics needed in flying a MAV. They are able to turn and weave in the air in pursuit of equally nimble insects. The bone structure of their wings extends along the entire length of the wing membrane, and is simple. A bat wing could be simply manufactured, and a silicon bat wing was fabricated by Caltech and UCLA by a technique similar to that proposed in this thesis (9), shown in Figure 8. However, the motion of the bat wing in flight includes control through four degrees of freedom that would be difficult to mimic mechanically (24), including an upstroke that is retracted close to the body in order for the downstroke to generate more aerodynamic force (28) (29). Also, the wing membrane is highly elastic and highly anisotropic in a manner that has proven to be very difficult to engineer. The bat has hair sensors covering the entire wing that provide constant feedback, allowing it to adjust in flight. These factors would make bat flight extremely difficult to replicate mechanically.
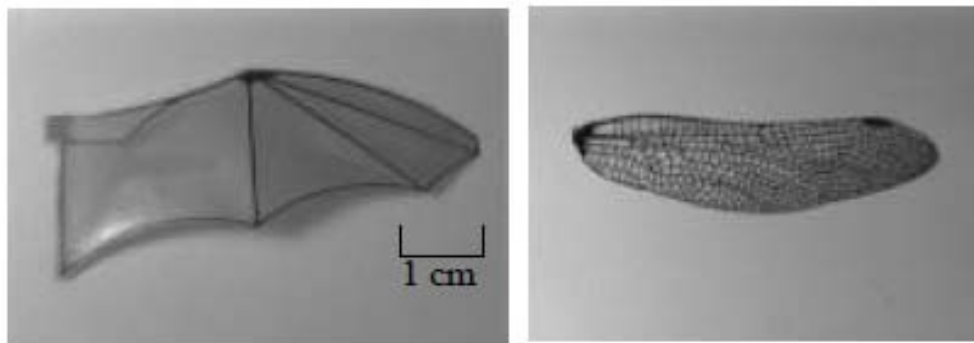
Figure 8: Caltech/UCLA MEMS fabricated silicon wings (13)

The hawkmoth wing has many of the strengths of the wings described above, and is often considered the best choice for wing design. The flight mechanism is very similar to that of the hummingbird, and it is a very precise flyer. Based on research performed by AFRL, Michael Anderson has proposed that complex, 6 degree-of-freedom MAV motion can be performed by controlling only one or two degrees of freedom in the wing. This capability would reduce the complexity and increase reliability of the mechanically-designed flight mechanisms (21). The hawkmoth, specifically the *Manduca Sexta*, has been studied extensively, providing a strong base of knowledge from which to work (20) (30) (31) (32) (33). The hawkmoth wing has structural membranes from shoulder to tip, and could be designed with relative ease when compared to other wings and wing properties. For these reasons, the hawkmoth wing is the best choice of biological design from which to mimic a mechanical wing.

2.3.3 Mimicking Wing Properties

While the structure of the hawkmoth wing is obviously important to its function, there are other properties, that must be copied if the manufactured wing is to flap like the natural hawkmoth wing. The camber of the wing will be important to the passive properties of wing flapping. Likewise, the wing membrane must be similar to the natural wing to provide lift and minimize drag.

2.3.3.1 Camber

There was little information in literature about the actual camber of a hawkmoth wing. The majority of wings used to gather experimental data were given nondescript structures that only approximate wings (34) (35) (36) (8). While many wings have been created based on the *Manduca Sexta*, for both experimental as well as applicational studies, most have simply used the wing outline (20) (31). Others have simply used the *Manduca Sexta* wing (37). Two experiments used camber as a variable, though the basis for their respective choices for camber, is not given (33) (38). Both used between 5-10% camber. While much valuable data has come from these experiments, the role of camber in hawkmoth flight has not been explored. The *Manduca Sexta*, however, is cambered, so the wings used in this thesis will be cambered to more closely mimic their properties.

According to Usherwood, in a study that used propeller models to investigate forces acting on model hawkmoth wings in propeller-like rotation (revolution), the model wings used produced high vertical and horizontal (L & D) force coefficients because of a leading-edge vortex, but L & D were remarkably unaffected by considerable variation in leading-edge detail, twist, and camber (30). While camber may not affect lift and drag to a great degree, an un-cambered wing flaps very differently from a cambered wing. Experiments by Deleon suggest that the structure of the wing contributes enormously to its movement in the air, its stiffness, and its strength (39). A natural hawkmoth wing, with its camber intact, flaps very differently from a flat replica made from carbon fiber. The natural wing is much more resistant to breakage. These properties reflect more than the simple strength of the material out of which the actual hawkmoth wing is made. The structure, including the camber, adds to the strength and performance of the wing.

The answer to another question may also shed light on the role of camber in the wing: is wing loading dominated by fluid dynamic pressure forces, or inertial-elastic forces that bend a wing even in the absence of air? Or do they have equal effect? Experimental data by Daniel et al. suggests that the inertial-elastic bending moments are far greater, and therefore far more influential on wing flapping, than the fluid dynamic moments (37). This could help to explain the difference in performance between extant hawkmoth wing prototypes and the *Manduca Sexta* wing. In order to mimic the natural movement of the flapping hawkmoth wing, and especially the pronation and suponation that have been shown to have such great effect on flight, camber would need to be introduced into wings manufactured by this process.

The actual camber of a hawkmoth wing would be extremely difficult, if not impossible, to manufacture into a titanium wing using the process outlined in this thesis. The hawkmoth wing has camber in two different directions. However, the spring back of titanium, coupled with the amount of camber in a hawkmoth wing, make this sort of camber difficult to manufacture, as will be demonstrated in the following paragraphs. For this reason, it has been determined that only one chord-wise direction of the hawkmoth wing will be imparted camber for the wings manufactured for this thesis.

2.3.3.2 Membrane Strength

The membrane had to match the titanium structure in its ability to resist tearing or breaking under adverse conditions. While one of the great advantage of flapping wings is the maneuverability they enable, that maneuverability means putting stress on the wing during quick maneuvers such as take-off, or sudden changes in direction of flight.

25

Many engineered materials fit this criteria, so a secondary concern with membrane strength was to balance it with affordability and availability. Parylene, for instance, was used by Caltech to deposit a very thin but strong membrane on their manufactured wings. But without manufacturing facilities or materials available at AFIT, the material is too expensive to contract out (priced at over $1000 per batch). Kapton, on the other hand, is used for other Micro-MAV manufacturing processes, such as joints, and fits the strength criteria.

2.3.3.3 Membrane Weight

The *Manduca Sexta* wing weighs 50-60 mg and is very strong. About 8-12 mg of that weight are scales, which cannot be produced in a laboratory with the current technology level available for purposes of this thesis (40). While scale function is not well-understood, they could help to keep flow attached to the wing, act as sensors, act as solar collectors, and serve to protect the moth, from both predators and water (41) (42). When scales are removed, the weight of a *Manduca Sexta* wing is 40-50 mg. Titanium, while light and strong, is comparitavely heavy when manufactured using a stiffness comparable to the *Manduca Sexta* wing. The membrane must not add too much to the weight of the manufactured wing.

Kapton is available at 12.5 μm and 7.5 μm thicknesses, but was not necessarily needed in those thicknesses. Experimentation demonstrated that RIE plasma etching could reliably reduce the thickness of the membrane. More details on the process and other applications of this plasma etching of Kapton are discussed in section 4.2.6.3, but more experimentation is still needed to analyze the extent to which the membrane

26

material may be thinned before it is no longer strong enough to meet the strength criteria. The answers to these questions will determine the lightest membrane that still meets the strength criterion for the Micro-MAV to be able to fly.

2.3.4 Other Fabricated Wings

Early MAV wings were made entirely by hand. Dr. Robert Wood's robotic insect wing, for instance, was composed of 30 μm thick ultrahigh modulus carbon fiber "veins," with a 1.5 μm thick polyester "membrane" that can be seen in Figure 9. While ingenious in design, it cannot be exactly replicated because no template was used in design or production.
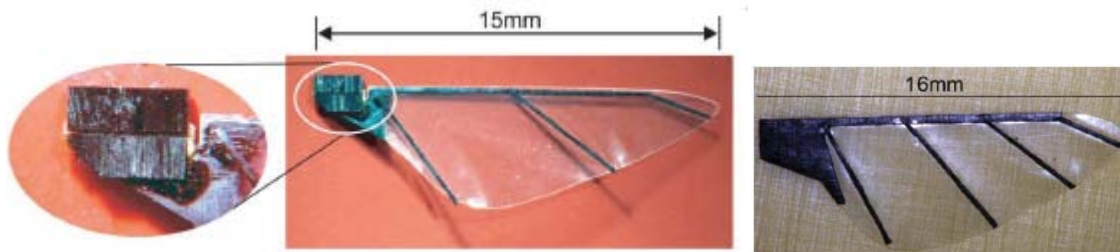
Figure 9: Wing composed of 30 μm ultra high modulus carbon fiber and 1.5 μm polyester membrane (5), and 70 μm ultra high modulus carbon fiber wing and 1.5 μm polyester membrane (14)

Similar efforts have been made in both the construction of models meant only to measure aerodynamic forces as well as in models meant to fly. Many of these efforts,

covering a time period from 2001 to 2010, are shown in Figure 10. While these specialty

wings were effective and yielded results that have furthered our understanding of

unsteady state aerodynamics, many of these wings would be difficult to reproduce

exactly in order to duplicate results, and they would cost much time and effort in the

process. The larger experimental wings may be simpler and thus more reproducible, but

would not be effective for Micro-MAV flight.
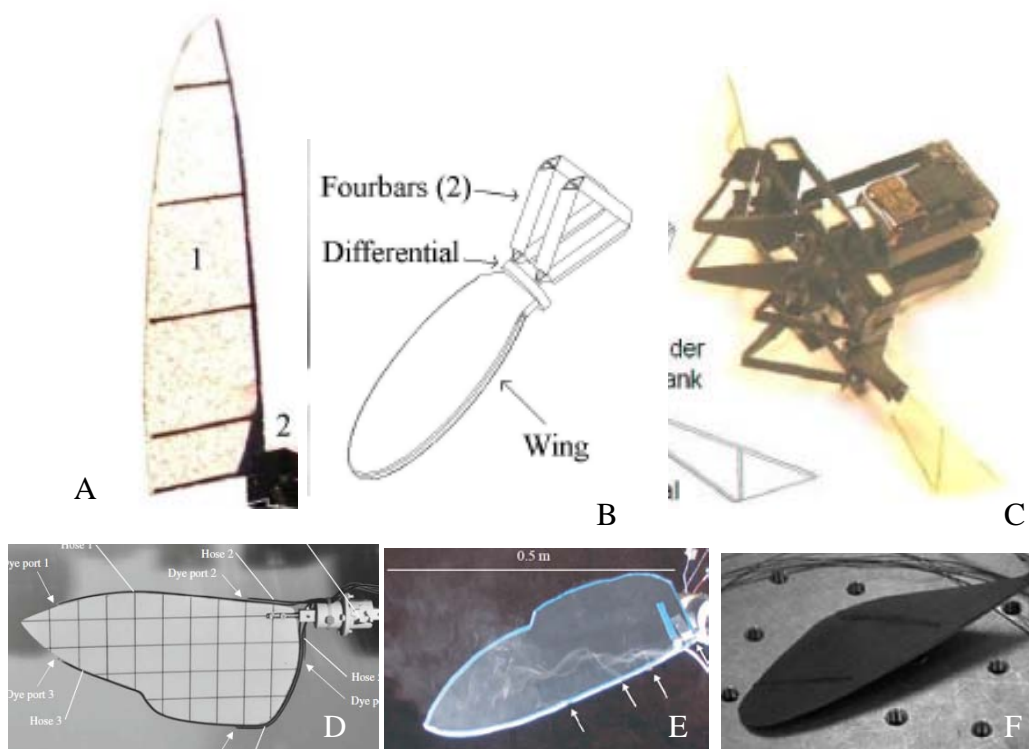
Figure 10: Experimental wings used for data collection, but not made to be exactly

reproducible; A) wing built by Wu and Ifju out of unidirectional carbon fiber (0.8

mm width) and Capran membrane, used for flapping wing structure optimization

((34), 2010); B) spars and wing built by Wood and Fearing for flight force

measurements ((35), 2001); C) carbon fiber body and wings made by Avadhanula,

Wood, et. al. to test lift force improvements for the Micromechanical Flying Insect

(MFI) ((8), 2003); D) Wings cut from template of aluminum, Perspex, and rapid

prototyping photopolymer, built by Lua et. al. for testing aerodynamic

characteristics of hovering hawkmoth-like wings ((31), 2010); E) Revolving

hawkmoth wing built by Usherwood and Ellington out of black plastic "Fly-weight"

envelope stiffener for aerodynamics study ((30), 2002); F) elastodynamic wing built

by Cox, et.al. ((43), 2002)

Caltech and UCLA worked together to pioneer a very effective reproducible wing based on MEMS fabrication technology (9) (13). The fabrication techniques in this thesis were inspired by their pioneering effort. The purpose of their fabrication was to produce a wing that could be tested parametrically and studied in a wind tunnel. A bird-sized MAV was then constructed and shortly flown based on their findings. While they constructed some beautiful and complex wings using this method, they found that they performed poorly when compared to the corresponding natural wings, which were lighter and more rigid. The manufactured wings that were studied and used for the Caltech/UCLA MAV were much larger than the target for this thesis, and were fabricated simply for generating thrust. The size of their MAV wings was much larger than those being fabricated and tested for Micro-MAVs.

It has not been until recently that any serious effort to fabricate reproducible Micro-MAV sized wings has been made. Figure 11 shows a recent 2010 effort to make reproducible carbon fiber wings using an aluminum mold. The wings are very simple,

specifically built for reproducible results in aerodynamic tests and experiments. These

wing molds would be more difficult to use for more complex wings.
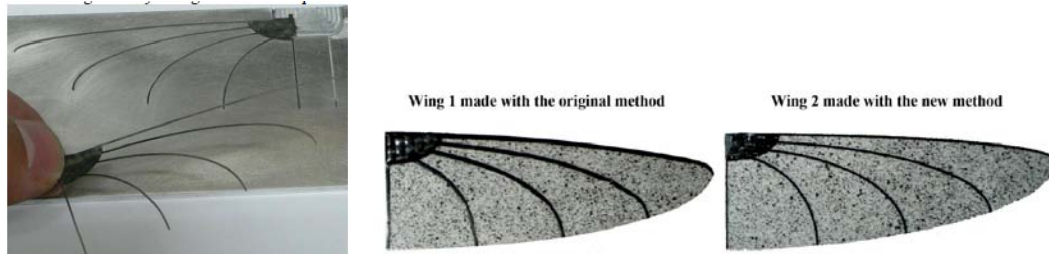
Figure 11: Carbon fiber and Capran wings made using aluminum mold by Xie, Wu,

and Ifju ((36), 2010)

2.4 MEMS Technique

MEMS fabrication technology was originated to reliably fabricate microscopic

mechanisms on 2-D surfaces en masse. It has been adapted for macroscopic

manufacturing, as noted above, by Caltech and UCLA. MEMS manufacturing has two

advantages over laser cutting. First, the wings can be made in batches. Once mask has

been made, each piece of titanium can be coated in photoresist, baked, exposed, and

etched in about a half hour. There is no limit to the number of wings that can be made in

a batch. The second advantage is that there is no heat hardening or deformity as there can

be in laser cutting, though pulsed lasers largely avoid this problem. Additionally, the

materials involved can be very cheap. At AFIT a cleanroom is already set up, but a laser

will have to be purchased in order to laser cut wings. In this case, MEMS fabrication is

significantly less expensive.

MEMS fabrication is the process of selectively etching material, and is specialized for semi-conducting compounds such as silicon or Gallium Arsenide. By growing epitaxial layers and alternating with silicon oxide, or other layers that have greater solubility in a given etchant than the base layer, mechanisms can be built up to complex levels and actuated to produce complex machines and structures. In general, the process involves 7 steps (these steps assume a positive photoresist).

1. Device design is performed with specialized software that takes into account the several layers of silicon that can be used. In Figure 12, each different color shown represents either a different layer, or a series of stacked layers. The devices range from 50 μm to 400 μm in length and 3 μm to 40 μm in width.

2. Create masks. Each layer will need a separate mask. A mask is made from a clear material, such as fused silica or soda lime, with a reflective layer on it, such as chrome. The reflective layer blocks out all light and electromagnetic radiation from exposing photoresist. The mask usually contacts the photoresist-covered substrate directly so that only the desired portions are exposed. The mask looks like the layer it will be protecting, i.e. the "polysilicon 1" mask for the design in Figure 12 will include only the pink and red areas in chrome, and the rest of the mask will be transparent.

3. Spin photoresist onto a silicon wafer. Bake off solvent to harden the photoresist and prepare it for contact with the mask, then expose wafer through the mask.
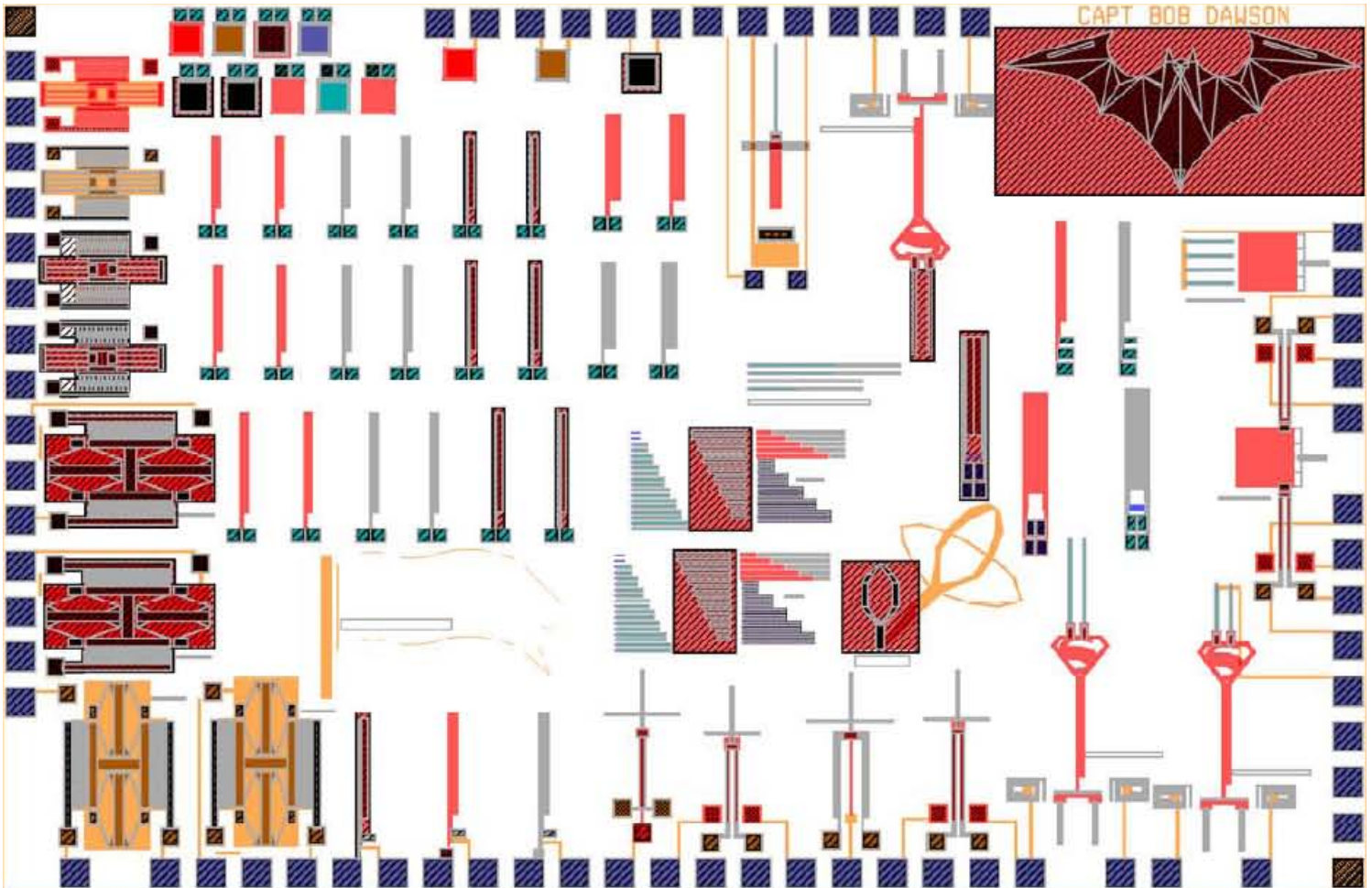
Figure 12: MEMS wafer design covering an area of 0.33 cm x 0.5 cm, entailing 180 separate devices and four functionless patterns

4. Use a developer to remove exposed photoresist. For the "polysilicon 1" layer of the design in Figure 12, all areas that are not pink would be exposed to UV radiation, and would be dissolved in the developer. Only the pink and red areas would be covered in photoresist.

5. Etch the exposed substrate with an etchant specific to the need. The etchant may be a wet chemical such as HF, a plasma, or a directed energy beam such as

an electron beam. All areas of substrate not covered by photoresist will be
etched away.

6. Layers can be evaporated, grown, vapor deposited, or oxidized. A structural
layer will usually be alternated with a sacrificial layer with different solubility
from the structural layer. Each successive layer will be masked with photoresist
and exposed through a separate chrome mask, then etched as above.

7. The final device will be released by immersing it in an etchant specific to the
sacrificial layer.

2.5 Summary

Flapping wing MAVs are being designed because research has strongly suggested that
flight of natural flyers of a similar size and weight to the proposed MAVs must take place
in the unsteady state regime, where wing tip speed exceeds horizontal flight speed.
Much care was taken in choosing a design for the Micro-MAV wing, and it was decided
that the hawkmoth, *Manduca Sexta*, would be the most ideal basis for design. The
motion of the hawkmoth wing as it flies, coupled with its relatively simple structure,
make it easier to mimic than other natural flyers in the unsteady-state regime. The wing
design will then be fabricated based on simple MEMS fabrication principles, using
Caltech's method as a rough guide for etching. While many wings have been fabricated,
including hawkmoth wings, the size, detail, and repeatability of the wings proposed
herein make them unique.

III. Design and Fabrication Methodology

3.1 Chapter Overview

The purpose of this chapter is to lay out steps to repeatably fabricate a Micro-MAV wing. These steps will be easy to follow in order to consistently replicate wings for parametric testing, mass production, or any other purpos that requires exact duplication of a wing.

3.2 Test Subjects

3.2.1 Wing Structure

The process for making the wing structure is as follows:

1. Liberate *Manduca Sexta* wing

2. Scan wing and capture major wing structure in a wing design

3. Write wing design to mask

4. Transfer wing design to titanium

5. Etch titanium

Specifics of each of these step will be addressed in order in the following sections.

3.2.1.1 Use *Manduca Sexta* Wing for Wing Design

The wing design was carried out as a team effort between biologist Travis Tubbs and design engineer Ryan O'Hara. The *Manduca Sexta* have a short life span, and must be cared for and used expeditiously. Once a hawkmoth hatches from its cocoon, its wing is liberated, taking care to cut the entire shoulder out while leaving structures that are

important to flight. The wing in Figure 21, for instance, was based on a wing that was cut off at the point where the wing meets the body. The wing design in Figure 20 includes the structure of the shoulder joint inside the body, making it stonger and more structurally sound in flight than the previous wing, which was shown in Figure 21. The detailed steps of this process are as follows:

1. Travis Tubbs raised the *Manduca Sexta* from worms, through pupa and emergence into full-grown hawkmoths. He took measurements on their musculature and physiology, then carefully liberated the wings for further study and experimentation by other members of the team.

2. Ryan O'Hara scanned the wings using a Computerized Tomography (CT) scanner, which sends several X-ray beams simultaneously from different angles to measure the relative density of tissues being examined. Major structures can be easily discerned, as well as the wing membrane, as seen in Figure 13.
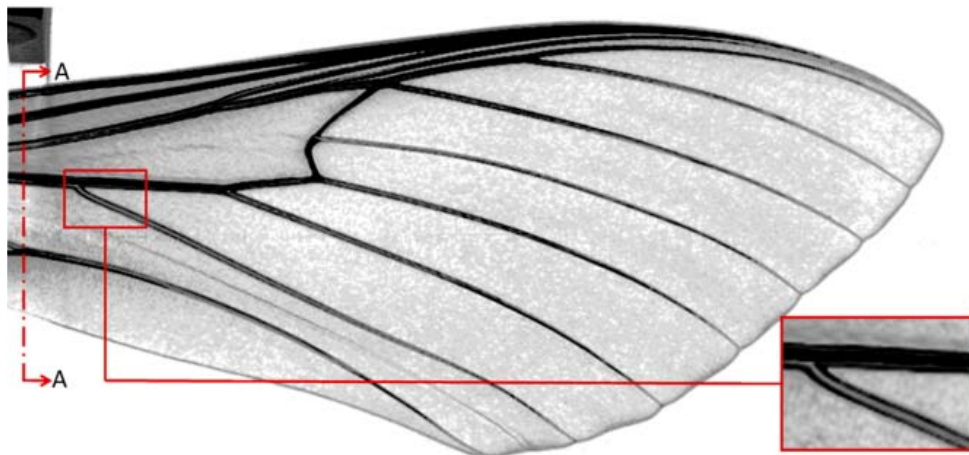
Figure 13: CT scan of hawkmoth wing yields a detailed scan of the relative density of each feature of the wing

3. MATLAB was then used to generate a point cloud of about 1.2 million points from data taken from the CT scan. The point cloud contains the CT scan information about both the structure and the membrane of the wing, but they cannot easily be discerned visually, as can be seen in Figure 14.
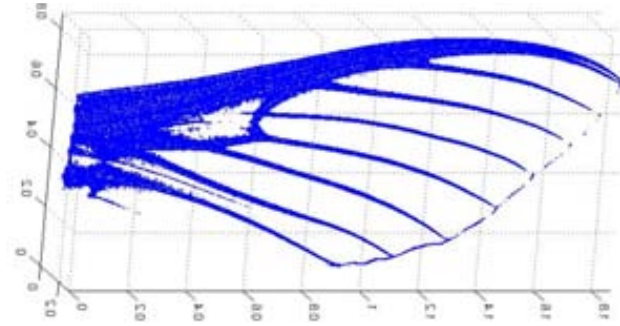
Figure 14: MATLAB generated figure of a point cloud taken from CT scan data

4. The data cloud was then reduced to about 200,000 points in order to reveal much more information about the veination and structure of the wing. Figure 15 shows that the dense structural members remain. The information in these points includes their spatial location relative to each other.
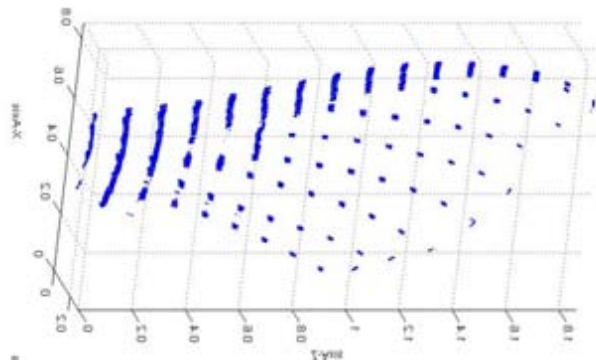
Figure 15: MATLAB figure of reduced point cloud shows wing structure of most

dense features

36

5. These points were then used to generate a surface fit to find the shape of the wing in MATLAB. The MATLAB surface shown in Figure 16 represents the wing data visually, including the camber and wing structures.
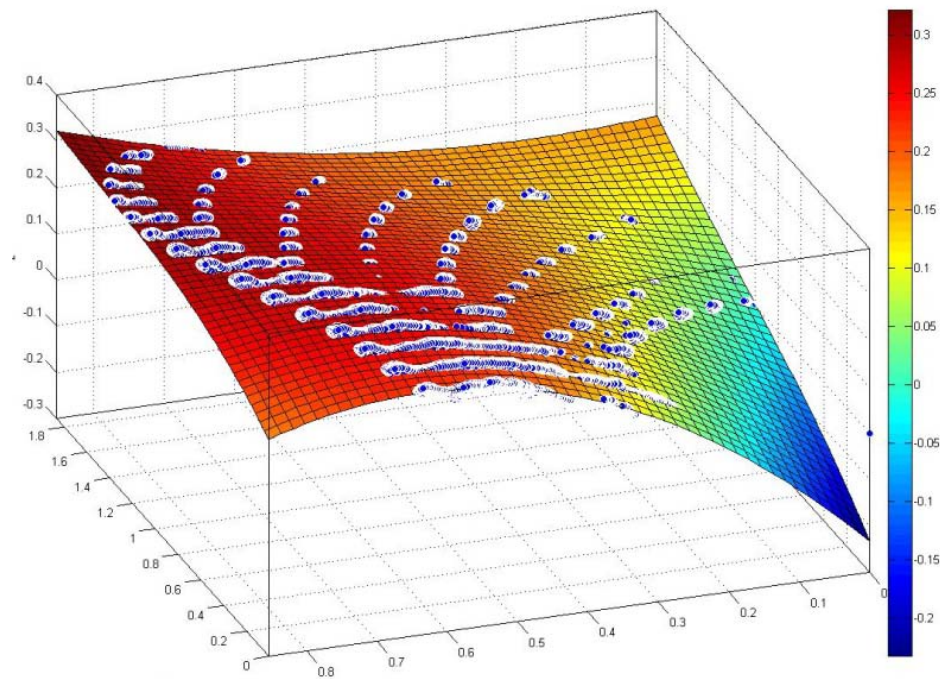
Figure 16: 3-D MATLAB figure of surface curvature of wing can be used to measure wing camber

6. Next, a two-dimensional image of the wing was loaded into a drawing program. This 2-D image was used to take points along major structures of the wing by hand. These points were taken at close enough intervals that they could be easily used to draw the curvature of each structueal member by using a CAD program.

The points in Figure 17 clearly shows the curvature of each major structure of the hawkmoth wing.
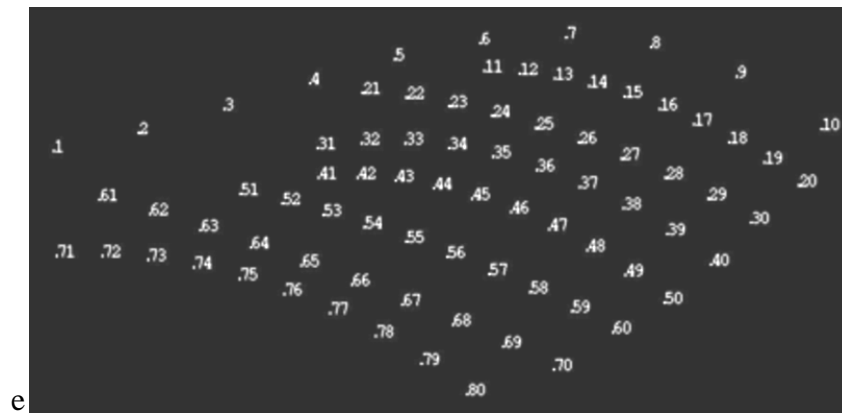
Figure 17: 2-D image of points taken manually along major structures of the wing will be comined with MATLAB figure

7. These points were applied to the MATLAB figure of the surface fit of the wing to yield a three dimensional surface for the wing. Figure 18 connects the points taken in the 2-D picture over the 3-D MATLAB surface to yield an accurate representation of the hawkmoth wing.
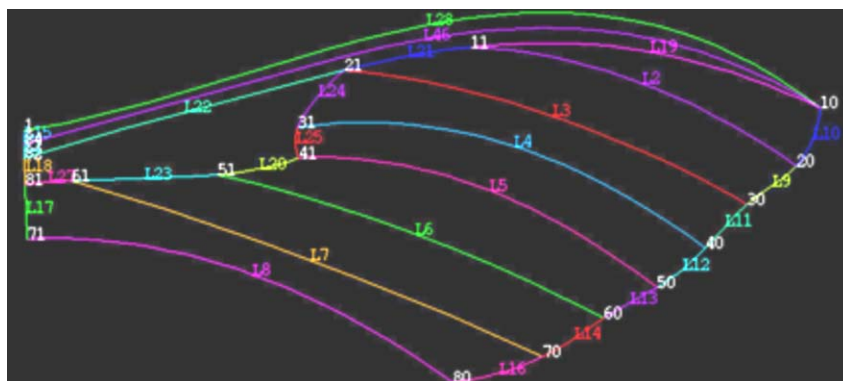
Figure 18: 2-D structural outline and 3-D MATLAB figure are combined to create an accurate representation of the hawkmoth wing

8. SolidWorks, CorelDraw, or other CAD or drawing programs could then be used to create a faithful representation of the wing. Each line from the accurate representation of the wing could be manipulated to create a structural member with the properties needed for the material that will be used to fabricate the hawkmoth wing. Figure 19 shows the initial structure used to fabricate titanium wings, with spars calculated to match the stiffness of the hawkmoth wing structures to the stiffness of titanium.

Figure 19: CAD program is used to make a representation of the wing that can be used to make the fabrication mask

The final wing designed through this process is shown in Figure 20. This design is superior to that shown in the process steps above in that the entire shoulder of the hawkmoth is included, while the wing design above was cut off. This should give the wing properties closer to that of the natural hawkmoth wing.
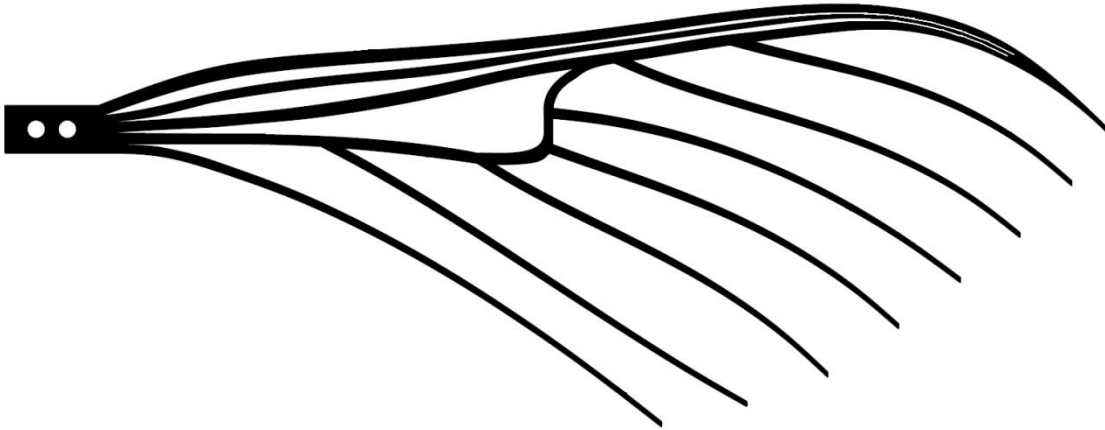
Figure 20: Hawkmoth wing design based on scan of the entire hawkmoth wing, including the shoulder

3.2.1.2 Wing Material and Manufacture Process

Once a wing has been selected, the manufacturing process for a Micro-MAV wing will be similar to that outlined by Pornsin-Srirak, et. al. (9), but improved to accommodate materials available as well as better manufacturing processes. Wing design was carried out by another AFIT student, Maj. Ryan O'Hara, based on the scans of biological hawkmoth wings perfomed by himself and AFIT student Capt. Travis Tubbs. The design takes into account the flexibility of the titanium vs. the stiffness of the moth wing, and the spar members are tapered to mimic the hawkmoth wing properties. The resulting wing, of which an early example is show in Figure 21, can then be used to design the mask upon which the fabrication process will be based.

The material to be used as the wing structural material, titanium, was chosen for several reasons. It is common and its properties are well known. Titanium is light, but

strong and flexible. It can be purchased as titanium foil in thicknesses and quantities

suitable for wing design, and the design can then be tailored to its stiffness properties. It

is not difficult to etch titanium, and it can be seen more clearly in its clear HF etchant

than stainless steel can be seen in its dark brown $FeCl_3$ etchant. Titanium is harder than

aluminum and will not break as easily. Carbon fiber has excellent properties, but would

be very difficult to adapt to a MEMS fabrication process. Nitinol was also considered as

a structural material for its excellent qualities, but was not as readily available, and was

more expensive than titanium. However, some of these materials may be considered in

further research.
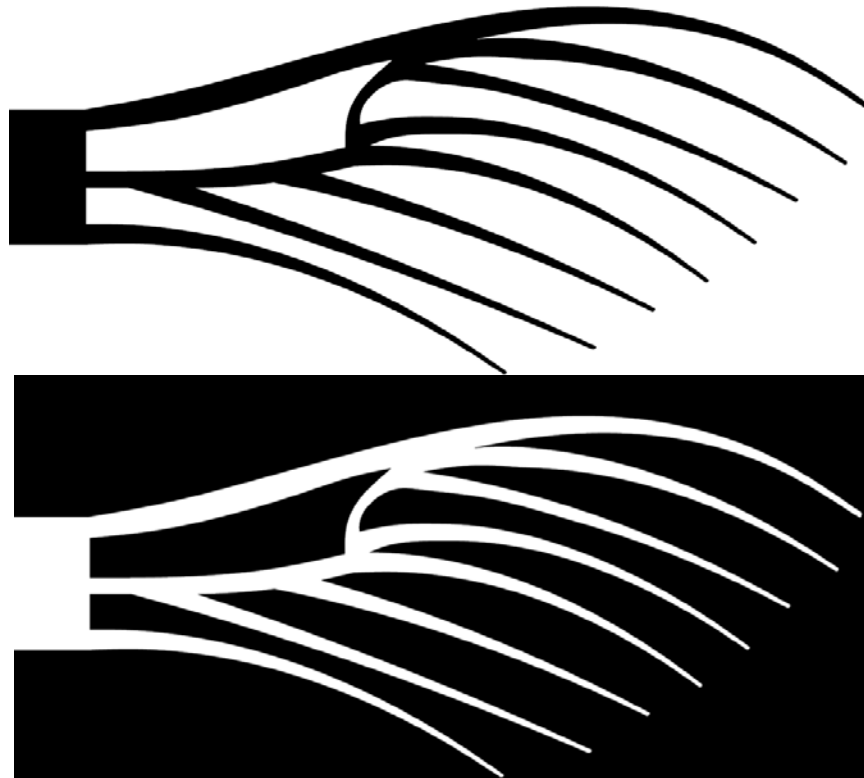
Figure 21: Positive and negative stylized wing designs based on material properties analogous to hawkmoth wing structure (design courtesy of Ryan O'Hara)

The Micro-MAV wing fabrication process is outlined as follows, and is synopsized in Figure 22:

1) Make mask

2) Deposit photoresist

3) Expose photoresist through mask

4) Develop photoresist

5) Etch away unwanted material

6) Strip photoresist

This process is discussed in detail in the the fabrication process section of the Methodology section.
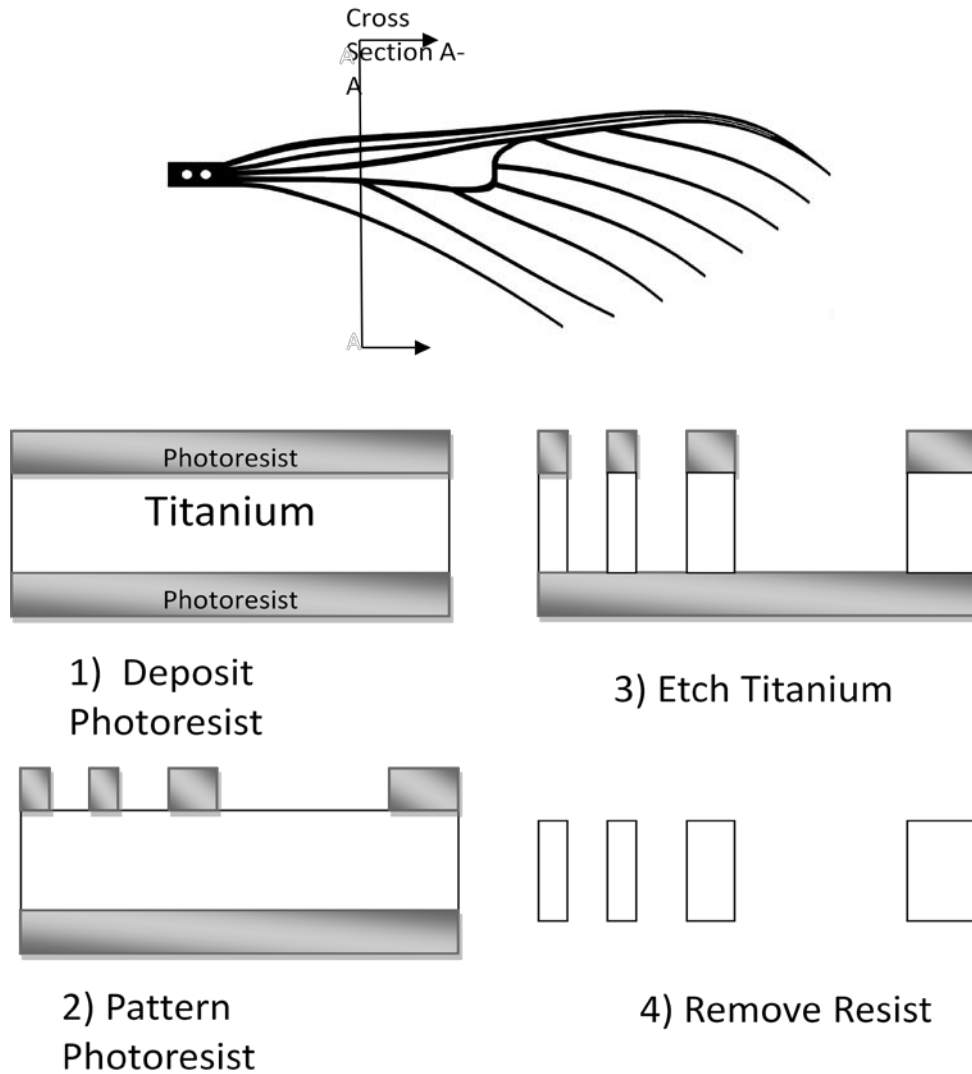
Figure 22: MEMS Wing fabrication process

3.2.1.3 Write Wing Design to a Mask

In order for the wing design to be produced on a mask, it must be in a format that could be read by the laser mask writer. The mask writer used was a Heidelberg μpg101, which uses .cif, .dxf, and .bmp files. Each file type must follow rules that will allow it to remain readable to the Heidelberg software. The general design rules are as follows:

1. Keep in mind that defined areas will be exposed.

2. Do not use special characters (spaces, punctuation marks, umlauts ..) in the design name.

3. The design coordinate origin must be the center of the design.

4. If possible, create the whole design in only one layer. If several layers are used, they will be merged using an OR function.

5. All polylines must be closed. Keep in mind that interiors of polyline structures will be filled out completely, covering any structures within.

6. Do not cross polylines, or create doubled vertices (vertices with no distance between them). This will create data errors.

7. Do not use single lines without width.

8. Limits:

   a. maximum design size: 100mm x 100mm

   b. 1,000,000 vertices/polygon

   c. maximum definition or reference depth: 16

   d. maximum number of definitions or references: 100,000

There are also specific rules that must be followed for each file type. The first, .cif, is a file format used by L-Edit, a common MEMS design tool. The rules for a .cif file are:

1. Use only one layer. If several layers exist in a design file, only the layer with the most references will be written.

2. Maximum definition or reference depth is 50.

3. The subroutine with the highest number definition will be taken as main routine.

The second type of file, .dxf, can be written by most common CAD packages, including SolidWorks, AutoCad, as well as other drawing packages such as CorelDraw. The .dxf spedific design rules are:

1. Use a 100% AutoCAD compatible editor.

2. The design has to be created in metric units.

3. As far as possible, only use the structure types "polyline", "circle", and "text".

4. Only one text font is provided. This will replace any other font used in the design creation. The only supported text attributes are "rotated", "mirrored", and "scaled".

5. Try to use as few layers as possible. All layers will be merged via an OR operation.

6. Do not use special characters in the layer names.

7. Polylines with width must not change their width (tapered lines).

8. When inserting blocks, the same scaling has to be used for x and y.

9. External blocks are not supported.

The .bmp files are common and easy to generate, but can be more pixelated than the other files. The .bmp specific design rules are:

1. Maximum image file size is 4 GB.

2. For grayscale exposures, use 8-bit format (the 256 gray values will be interpolated down to 100 gray values.)

3. Create the design in a 90° counter-clockwise rotated version, as the design will be rotated 90° clockwise during data processing.

Once the file is in a format that could be read by the mask writer, the process is simple:

1. Copy file to Heidelberg μpg101 controlling computer hard drive

2. Turn on nitrogen to mask writer

3. Initiate µpg writer software and follow on-screen directions to find the file that was copied to the hard drive

4. Ensure settings are correct: standard settings of 90% power at 8 mW are sufficient for an average mask

5. Write mask

6. Immerse mask in positive photoresist developer to remove areas that were exposed by laser; rinse with distilled water and dry with nitrogen

7. Immerse mask in chrome developer to remove all chrome unprotected by photoresist; rinse with distilled water and dry with nitrogen

Figure 23: Finished mask of final wing design, chrome on soda lime, taken in cleanroom (hence the yellow light) to avoid dust contamination

3.2.1.4 Transfer wing design to titanium

Cut a titanium foil rectangle 2.5 cm x 1 cm. In the cleanroom, apply photoresist. There are two kinds of photoresist, positive photoresist and negative photoresist. Both require different methods of application.

3.2.1.4.1 Positive Photoresist

Positive photoresist is sensitive to UV radiation, and breaks down when exposed to UV light. The purpose of a mask for the positive photoresist is to protect the features that will be kept during the etch step, allowing light to expose the photoresist in the areas that are to be etched away, as shown in Figure 24. Photoresist developer then dissolves the exposed photoresist, leaving a pattern that looks exactly like the mask. The reason it is called positive photoresist because the "picture" left after exposure is positive. When etched, the resulting features will look like the mask.
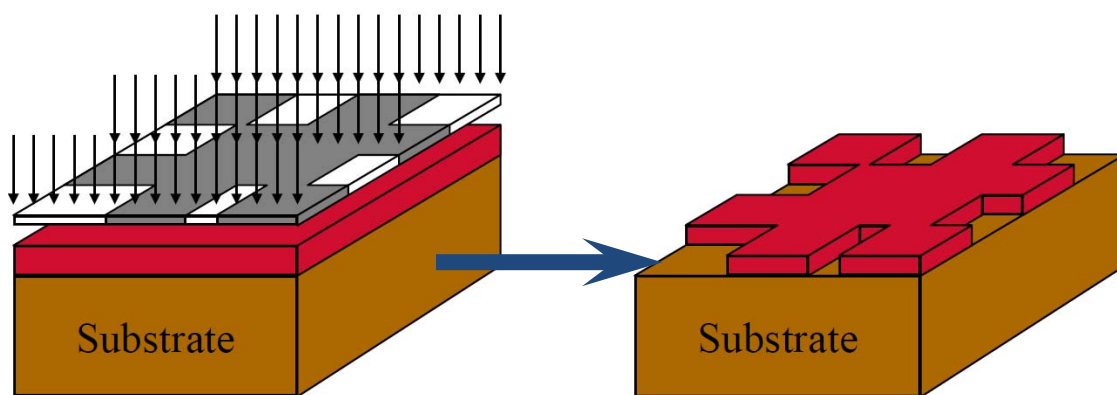
Figure 24: Photolithography mask and results after exposure for a positive photoresist; photoresist protected from UV light remains after developing process

The mask for positive photoresist will block the light for the wing spar structure, allowing the area between structures to be exposed to UV radiation, as show in Figure 25. Several considerations need to be taken into account for this design.
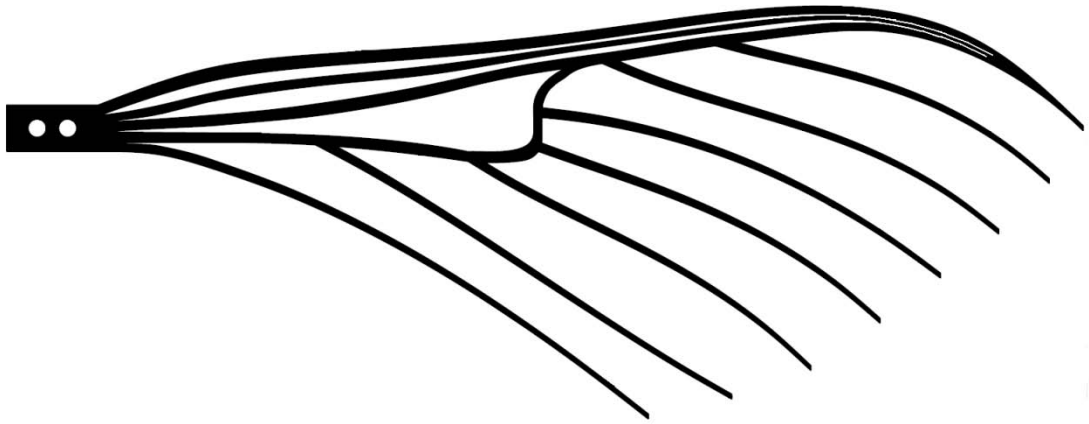
Figure 25: Positive mask for Micro-MAV wing

3.2.1.4.2 Positive Photoresist Process

1. Clean titanium:

    a. Fix titanium rectangle to spinner head

    b. Clean with a steady stream of acetone, followed by methanol; follow with distilled water, and finish with nitrogen to dry

    c. Repeat for other side

    d. Dry on hot plate at 110ºF for 30 s.

2. Spin on Shipley 1818 positive photoresist

3. Bake on hot plate at 110ºF for 75 s.

4. Apply photoresist to opposite side of titanium with a foam or cotton swab, and bake on hot plate at 110ºF for 75 s.

5. Expose to UV light through mask using Suss MJB3 mask aligner. Both CI1 (365 nm) or CI2 (405 nm) settings could be used for positive photoresist(44):

   a. Time of exposure = exposure energy required for photoresist/lamp intensity; S1818 needs 150 mJ/cm^2

   b. For setting 1, $\frac{\overline{\quad}}{\overline{\quad}}$

   c. For setting 2, $\frac{\overline{\quad}}{\overline{\quad}}$

6. Develop titanium rectangle in S1818 developer for 30 s.
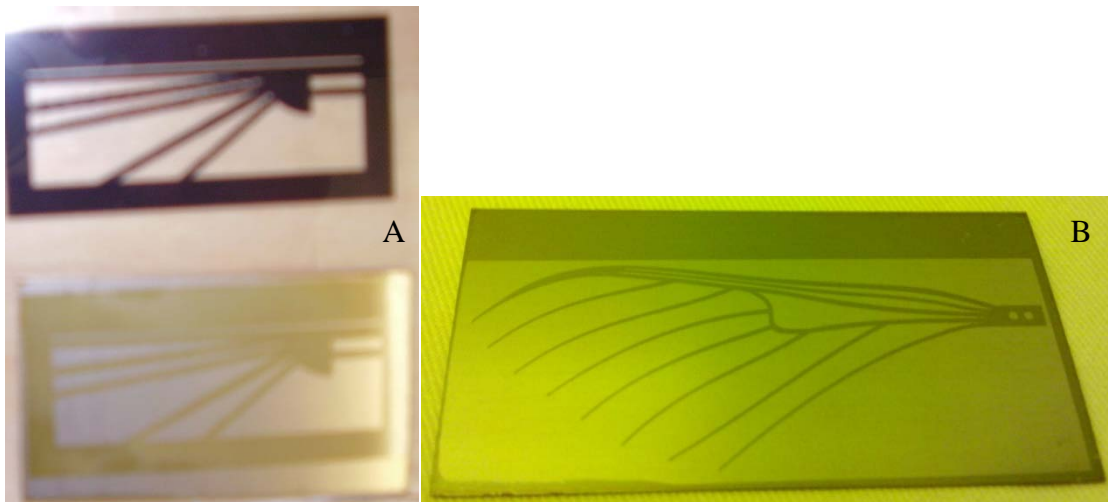
Figure 26: Positive photoresist on titanium; A) initial crude wing design and its ink-on-transparency mask; B) final wing design (taken in yellow light of cleanroom to avoid exposure and weakening of photoresist)

3.2.1.4.3 Negative photoresist

Negative photoresist does not break down when exposed to UV radiation. UV light causes the polymer chains to break and cross link. When the exposed negative photoresist is baked, this cross-linking becomes permanent, so that the developing process will dissolve the un-exposed areas of photoresist. It is called negative resist because the "negative of the picture" on the mask remains after the substrate is etched, as shown in **Figure 27**.
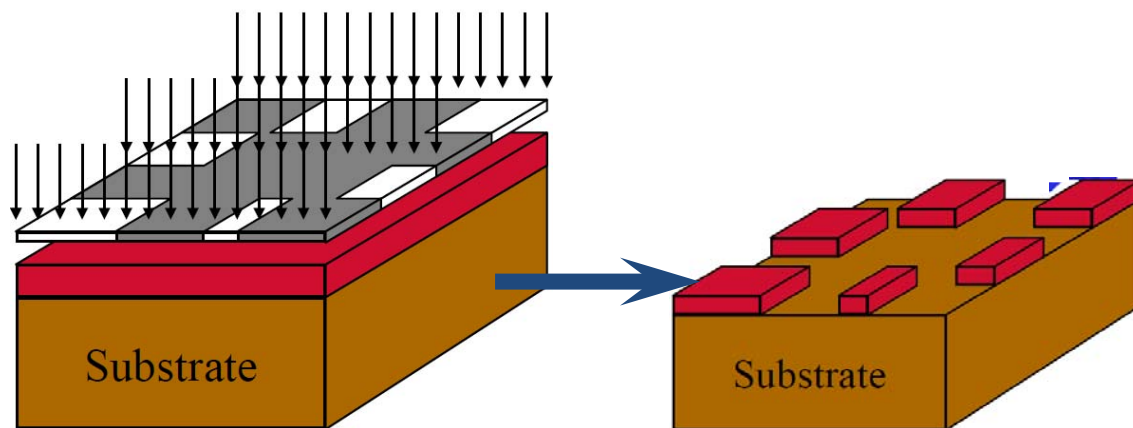
Figure 27: Photolithography mask and results after exposure for a negative photoresist; photoresist exposed to UV light remains after developing process

The mask for negative photoresist will block the light for all non-wing parts of the mask, allowing the wing spar structures to be exposed to UV radiation, as shown in Figure 28. Like the positive resist, several considerations must be taken into account for this design. The considerations are similar, so only the differences between the two processes will be explained. The similarities between the processes will only be pointed out briefly.
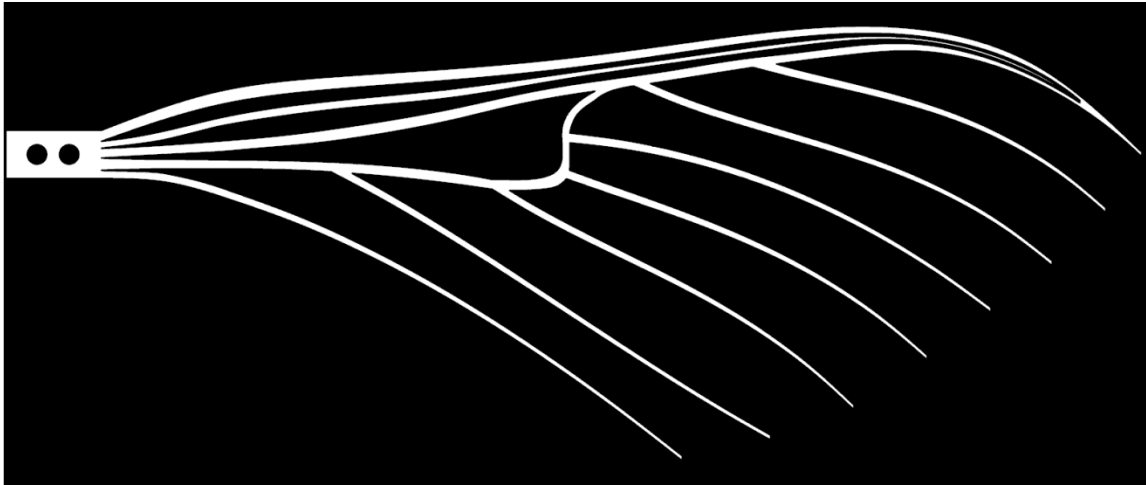
Figure 28: Negative mask for Micro-MAV wing

3.2.1.4.4 Negative Photoresist Process

1. Clean titanium:

    a. Fix titanium rectangle to spinner head

    b. Clean with steady a stream of acetone, followed by methanol; follow with distilled water, and finish with nitrogen to dry

    c. Repeat for other side

    d. Dry on hot plate at 110ºF for 30 s.

2. Spin on SU8 negative photoresist

3. Soft bake on hot plate at 65ºC for 2 minutes, followed by 95ºC for 5 min.

4. Once one side is soft baked, the second side may be spun on (it need not be applied by cotton swab due to the robustness of SU8) and soft baked

5. Expose to UV light through mask using Suss MJB3 mask aligner; only CI1 (365 nm) could be used for negative photoresist (SU-8 is optimized for near UV (350-

400 nm), and is virtually transparent, and therefore insensitive, to wavelengths above 400 nm(45)):

    a. Time of exposure = exposure energy required for photoresist/lamp intensity; SU8 needs ~125 mJ/cm^2

    b. Using setting CI1, ═══

6. Expose opposite side to UV light for 11 s without mask

7. Cross link exposed SU8 by baking on hot plate at 65ºC for 1 minute, followed by 95ºC for 1 min.

8. Immerse in SU8 developer for 1 min., agitating gently
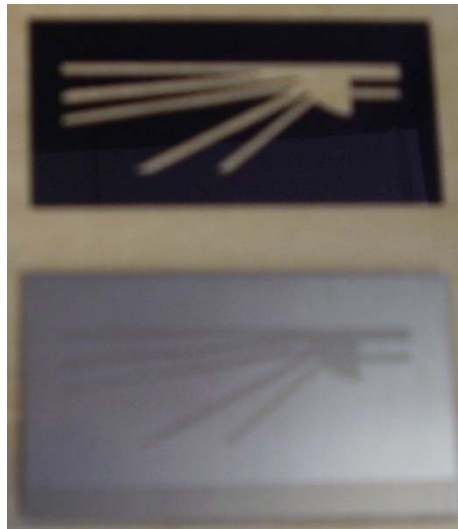
Figure 29: Original SU8-on-titanium crude test moth wing and its ink-on-transparency mask

3.2.1.5 Etch Titanium

Titanium may be easily etched with Hydrofluoric (HF) acid using the following steps (please note that great care must be used in handling HF, and proper protective gear must be worn to protect from injury or death):

1. Prepare dilute mixture of HF:DI water in proportion of 1:10

2. Immerse titanium rectangle in HF mixture for approximately 26-31 minutes, until exposed titanium has been dissolved completely

3. Remove from HF mixture when exposed titanium has been removed, and immerse in DI water for 30 seconds; agitate gently

4. Strip baked on positive resist with acetone (unfortunately, baked-on SU8 is extremely robust and must be removed mechanically, if at all)
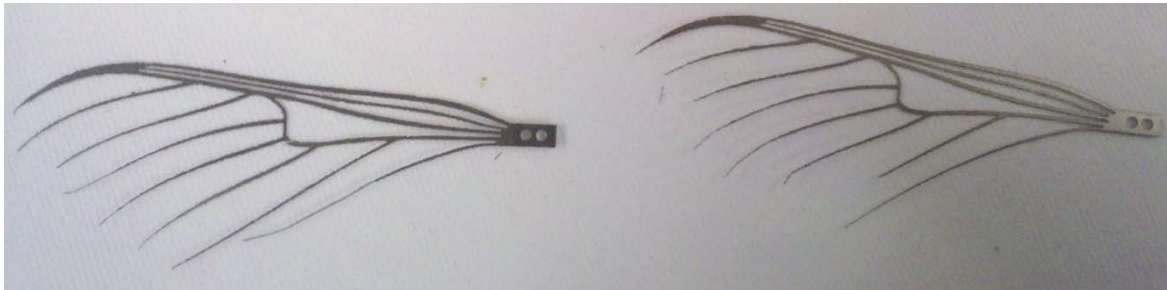
Figure 30: Two final-design wings from a batch

3.2.2 Camber

Once the titanium structure has been fabricated, the natural camber of the hawkmoth wing must be imparted so that it will act similarly when flapped. While it has been speculated that wing camber has very little effect on the lift produced by the

wing(30), it affects the stiffness and modulus of the wing in motion, and therefore may be a large factor in controlling the complex motion of the natural wing. Wing camber for a natural hawkmoth wing is complex, including bi-directional camber. While such camber would be nearly impossible to impart to a titanium wing, the major camber of the wing may be fairly simply imparted once the camber of the natural wing is measured. The modulus of elasticity and the spring-back of the titanium must be taken into account during this process, and a suitable model must be rigged to consistently impart the same camber to a wing.

There are few structural members in this (crosswise) direction. Titanium has a great deal of springback, and great care was taken to estimate the right amount of camber in a pressed mold to produce the final camber as seen in a hawkmoth wing (see section 4.2.5).

A wing pressed in a mold with a 0.625" diameter will spring back sufficiently to yield ~5% camber. A mold made using a rapid prototyper was used repeatedly to impart camber to wings.

3.2.3 Kapton Membrane

A Kapton film should then be adhered to the structure so that it can be tested. The thickness of the Kapton and the amount of glue used to adhere to the metal could have a great effect on the overall weight of the wing. Also, the method of adhering the film to the structure must not change the camber of the wing, nor allow the membrane to wrinkle.

If a membrane were applied before the wing were given camber, the membrane could resist the camber. However, the Kapton membrane would be more difficult to apply once camber has been imparted. Membranes cannot provide compressive resistance, and will wrinkle if not applied correctly. In order to avoid wrinkling and to ensure a properly applied Kapton membrane, tensile stress may be applied to the Kapton while draped over a cylinder with 5% camber (~4" outer diameter) by hanging weights from the film. Adhesive may then be applied to the inside camber of the wing, which may then be gently pressed onto the membrane (a fine spray on adhesive was found to work well). The residual Kapton around the wing perimeter may then be removed with a razor, or other cutting implement.

Once applied, the membrane was weighed on an OHAUS Voyager Pro scale, and compared with the etched titanium wing only. From these measurements, the 12.5 μm membrane weighed 15.6 mg, the 7.5 μm membrane weighed 8.8 mg, and the 2.5 μm membrane weighed 4.0 mg. The strength of the membrane was not tested, but etching the membrane clearly has a significant weight saving.
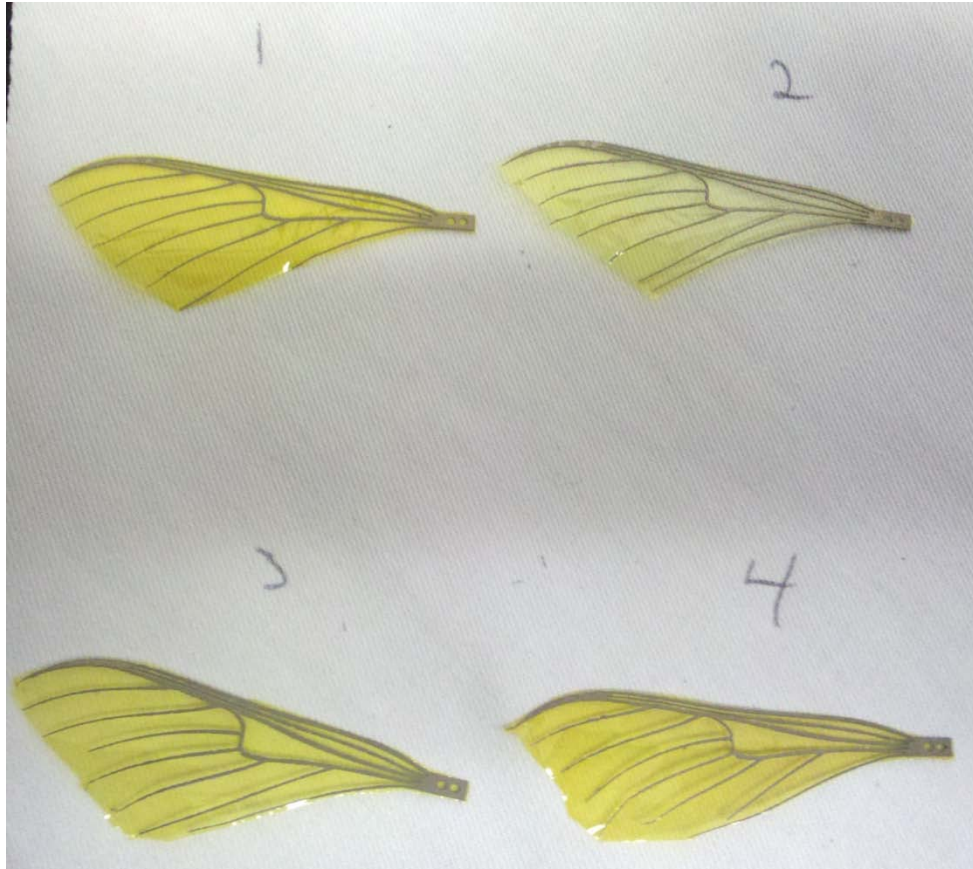
Figure 31: Final wing design, made as a batch of four wings, with Kapton membranes 1) 12.5 μm Kapton membrane on wing weighs 65.5 mg; 2) 12.5 μm Kapton etched to 2.5 μm weighs 60.0 mg (56.0mg for Ti only); 3) 7.5 μm Kapton membrane on wing weighs 64.7 mg (55.9 mg for Ti only); 4) A second 12.5 μm membrane on wing weighs 64.3 mg (48.7mg for Ti only)

3.3 Summary

In order to most correctly mimic the motion and properties of the hawkmoth wing, a fresh hawkmoth wing was scanned, and points taken from that scan were used to

draw a wing in a CAD program. That drawing was transferred to a photoresist mask. The mask was used to transfer the wing pattern to a piece of titanium, with photoresist covering the portions of the wing structure that were needed for wing fabrication. The wing was etched in a 10:1 distilled water:HF solution for a half hour.

This process yielded a wing structure very similar to the hawkmoth wing. This structure could be given properties closer to that of the actual hawkmoth by imparting camber and applying a membrane. The camber was imparted by pressing the wing in a cylinder, and a Kapton membrane was glued to the titanium structure.

IV. Analysis and Results

4.1 Chapter Overview

Int this chapter, the results based on the method in Chapter III are now compared to expectations and qualified and quantified as appropriate. Actual rate of HF etch was gained through experimentation, as was actual springback of titanium. Experiments on Kapton thinning and application to manufacturing are discussed. Other manufacturing possibilities and alternatives are taken into account.

4.2 Results of Experimentation and Fabrication

4.2.2 Write Wing Design to Mask

The mask writer needs very specific .dxf drawings, and the .dxf files written by SolidWorks could not be read by it. They had to be changed. There are two methods that could be used to make the file into a format that could be read by the mask writer. First, L-Edit could be used to import the .dxf file and make it into a .cif file. Second, it could be made into a .bmp file. Both of these file types could be read by the mask writer software. Both methods are laid out below.

In order for L-Edit to write a .dxf file as a .cif file, the file cannot have splines, so the following steps must be taken:

1. AutoCad or a similar CAD package (DraftSight was used for this thesis) must
   be used to write polylines over the splines

2. Delete the splines and save as a .dxf file (most programs will not do this

automatically, but they do offer this option during the save process)

3. Use L-Edit to import the .dxf file; this may be done in some versions using the

file menu, or in other versions using the SoftMEMS toolbar:

a. Change scale from microns (default) to centimeters

b. Import .dxf file

c. Move the origin of the file to the wing base

A .dxf file cannot be directly read by Microsoft paint, or other image files, but

can be read by Adobe Acrobat:

1. Use Adobe Acrobat to open the .dxf file; version 9.4 was used for this process;

Use PDF/E-1 PDF standard, and no security; all boxes should be checked, and

layout options set to "all layers"

2. Minimize all borders and maximize the drawing on the screen, until it touches

screen borders, but does not exceed it; take a screenshot (alt+print screen)

3. Open a graphics program, such as Microsoft paint, and paste the screenshot into

the program

4. The wing is imported as a wire outline; fill in the lines

5. Save as 24 bit .bmp, or 256 color .bmp (monochrome .bmp will be very jagged,

and will not make a good mask)

CAD programs can also export the image as .bm files. For this report DraftSight was

used, and an export was performed simply by using the export function in the file menu

of the toolbar.

The mask writing process is basic. The mask blank is made of fused silica or

soda lime, covered with chrome to block the light. The chrome is covered with positive

photoresist, which could be exposed very exactly via laser. The laser exposes the pattern

that was loaded into the computer, using a horizontally striated pattern. The resolution of

the Heidelberg μPG 101 used for the wings analyzed herein was 3 μm.

The exposed photoresist was dissolved using S1818 photoresist developer. The

mask blank was then submerged in a chrome developer, which removes all exposed

chrome from the mask blank, leaving only the image of the mask file that was loaded into

the computer. This mask will allow light to pass through and expose the photoresist that

is not blocked by chrome.

4.2.3 Transfer wing design to titanium

The mask was used to transfer the wing design onto the titanium rectangle via the

process outlined in 3.2.1.4.2 Positive Photoresist Process, or 3.2.1.4.4 Negative

Photoresist Process. This was a simple MEMS fabrication process that represented a

number of modifications that needed to be solved in order to modify the process to meet

the specifications for making wings. These modifications are outlined in the following

subsections.

4.2.3.1 Photoresist Thickness

Photoresist thickness depends on the viscosity of the photoresist and the speed (in

rpm's) at which it was spun onto the substrate. Photoresist is named according to the

average thickness of photoresist when spun on at 4000 rpm. For instance, Microposit's

Shipley 1813, or S1813 photoresist, will average 1.3 µm thick when spun on at 4000 rpm. The photoresist used in these experiments, S1818, is more viscous, and averages 1.8 µm thick when spun on at 4000 rpm.

Photoresist is not highly susceptible to etching by HF. It will etch at a much slower rate than the titanium. However, to ensure protection during etching, S1818 was chosen over other photoresists, and was spun on at 3000 rpm, giving an average thickness of about 2.2 µm. This proved to be adequate in all etches.

4.2.3.2 Adhesion

The first consideration for choosing a photoresist was adhesion. In trial runs with stainless steel, positive photoresist did not adhere to the steel, possibly due to fine tooling marks, which appeared as scratches on the face of the material. As the etch progressed, the HF began to lift off of the photoresist, etching the material that was meant to be protected by the photoresist. Figure 32 shows the rough surface of the portion that was supposed to be covered by photoresist. The resulting etch was not recognizable, and the etch was stopped prematurely, before all photoresist could be lifted from the stainless steel surface by the HF.

It was hypothesized that two factors must be fulfilled to prevent repetition of this adhesion problem. First, the surface of the material needed to be smooth. Second, the photoresist needed to adhere well. During initial runs with titanium, adhesion did not seem to be an issue, though fine tooling marks were present. If it turned out that smoothness were not as big an issue for titanium as for the stainless steel, it could be further postulated that this was due to the differences between the interaction between

61

titanium and HF, and those between stainless steel and HF. Grain boundaries and other stainless steel material inconsistencies could haved played a part in these interactions. If the same process were to be used for stainless steel, these interactions would need to be explored in greater detail. Since titanium is so reactive with HF, positive photoresist makes an ideal mask. For the same reason, great care must be taken in applying the photoresist, because any scratch in the photoresist will cut straight through the titanium during the etch. This could cut off structural members and weaken the wing.
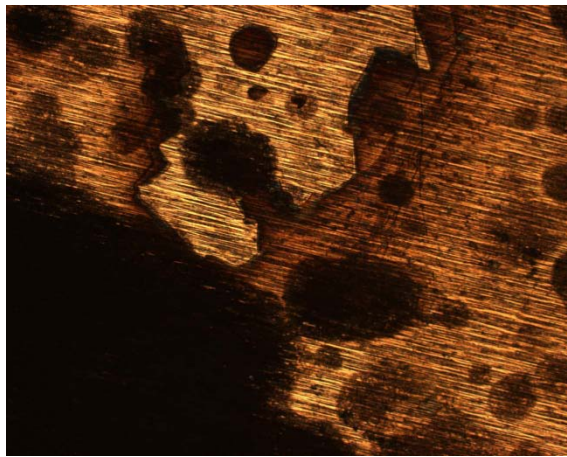
Figure 32: 5x magnification of edge of stainless steel etch

4.2.3.3 Feature Resolution

The second consideration in choosing photoresist was feature resolution. The fine features at the end of each of the spars, and the point at which the top three spars join structurally, need to be taken into account in mask design. HF is anisotropic, so it will etch under the mask as far as it etches down into the material. Since the titanium foil is 0.005" thick, the mask needs to be 0.01" thicker than the fine features in the final wing. Any feature smaller than 0.01" would be obliterated by the etching process. However, it was expected that the large scale of the wing, as opposed to the micro scale normally

used in the MEMS etching process, will mean that even the fine wing features are large enough that this would not greatly affect mask design.

In order to test the hypothesis, two tests were devised. First, a fine-featured mask was made, shown in Figure 33. The mask was drawn, using Microsoft Paint, exactly from the veination of the CT scan of the hawkmoth wing, without taking material stiffness into account. Its purpose is solely to test fine etch capability. Note the rough edges of the etched wing. The edges were pixelated according to the lines drawn in Microsoft Paint. The resulting wing shows very little visible difference between the mask and the wing. A quick measurement with a caliper showed that the mask features were slightly larger than the wing features, as would be expected in an anisotropic etch. However, the etch was very exact, which was very encouraging indeed.
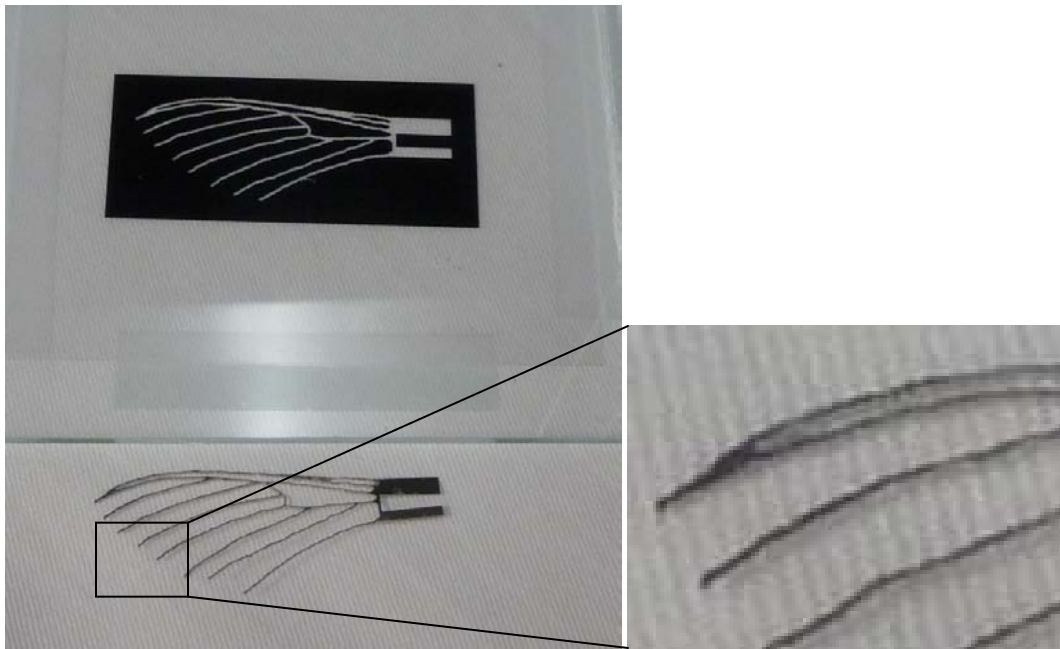
Figure 33: Fine featured wing, testing feature resolution; the enlarged portion shows the pixilation caused by drawing the wing in Microsoft Paint reflected in the etch

To further test the resolution capability of the etch, a series of fingers was devised, and a true chrome-on-soda lime mask was made. The mask consisted of two halves of the comb, with five different fingers repeated five times on each side. On one side, the fingers were 100μm, 200μm, 300 μm, 400 μm, and 500 μm. The other side of the comb increased each of those measurements by twice the thickness of the titanium foil, to account for anisotropic etching: 350 μm, 450 μm, 550 μm, 650 μm, and 750 μm. The finger mask, and the resulting etch, are shown in Figure 34.
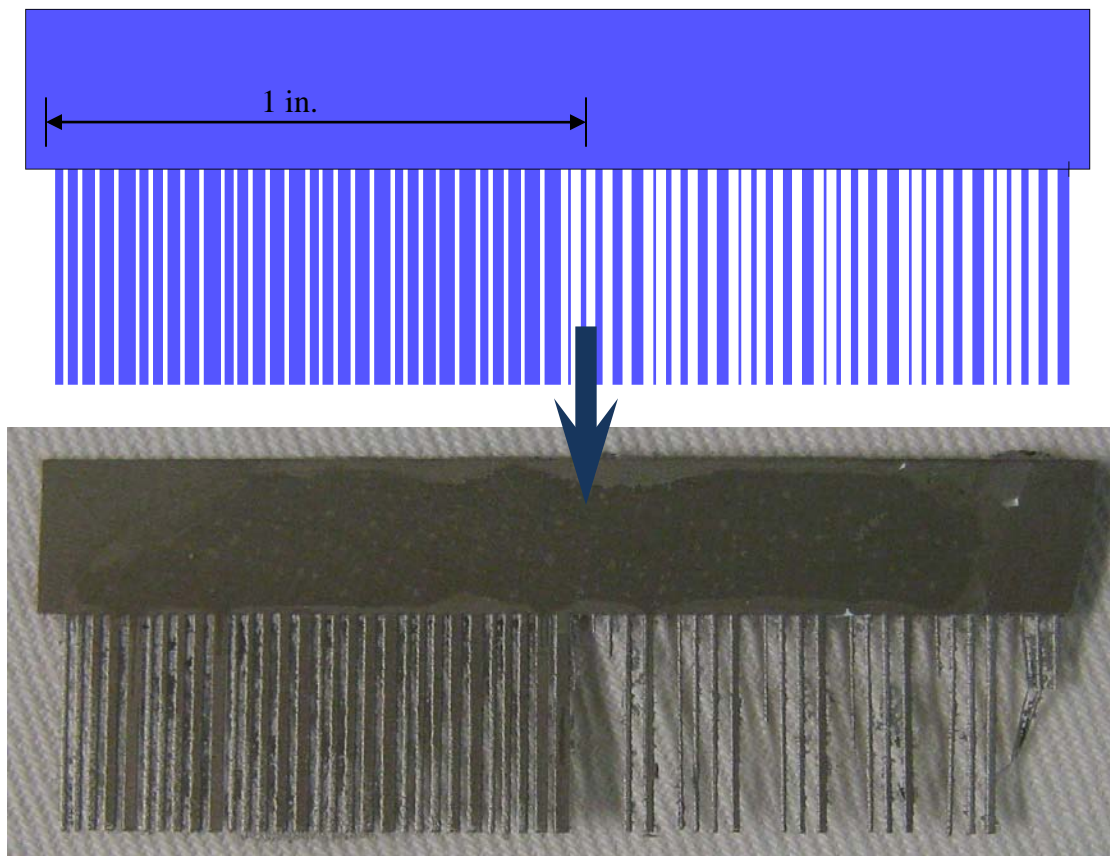
Figure 34: Mask CAD drawing and resulting etch of fingers used to measure the resolution capability of the proposed etching process

The results of the process verified that the resolution of the etching process was twice the thickness of the titanium foil, because the anisotropic etch worked on both sides of each feature. 0.005"=~125μm, so both the 100 μm and the 200 μm fingers were entirely dissolved. On the side that was made to take the anisotropic etch into account, the 350 μm finger was etched to just more than 100 μm, seen in Figure 35. The picture on the left was taken of the 100 μm photoresist finger at a magnification of 20x before the etch was performed. The picture on the right was of the 350 μm finger after the etch was performed, also at 20x. The base of the finger is wider than the face due to the anisotropic nature of the etchant. Since the back of the titanium foil rectangle was protected, the base was exposed to the etchant for less time than the face. The change in cross section may add to the properties of the wing, but that hypothesis will not be tested in this thesis.
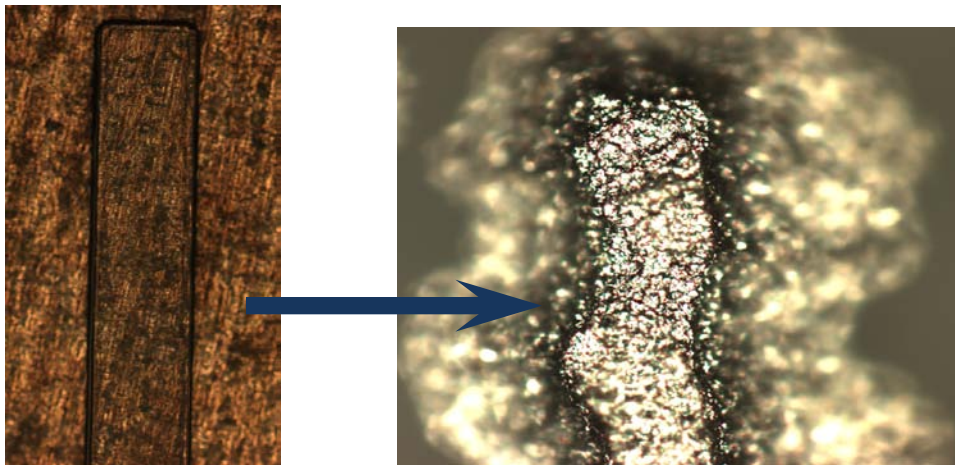
Figure 35: Comparison of 100 μm finger before HF etch and 350 μm finger after HF etch shows they are nearly the same width, as predicted; A) 100 μm finger,

photoresist on titanium, before etching and B) 350 μm finger after etch; both

pictures were taken at 20x magnification; note that the titanium finger is nearly the

same thickness as the thinner finger, because of the anisotropic nature of the HF

etch from both sides of the masked area.

4.2.3.4 Mask Material

One last consideration in choosing a photoresist was mask material. Initial test masks were made using a printer and transparencies. Ink does not block out light as chrome does, and the photoresist was partially exposed. Positive photoresist consists of a photosensitive compound, a base resin, and an organic solvent, so it has limited solubility in the developer even before exposure to energy. As energy exposure is increased, positive photoresist becomes more soluble until the threshold is reached, at which point it becomes completely soluble(46). Enough energy was able to get through the ink of the crude mask to partially expose the photoresist. The face of the resulting wing, as seen in Figure 36, was partially etched. Though the photoresist could be seen on the entire surface of the masked titanium, the HF was able to etch through the photoresist that remained after development, and it pock marked the wing.

Figure 36: Surface of initial stylized wing was rough due to partially exposed positive photoresist

Subsequent testing with a chrome mask showed that ink was indeed the culprit for this rough surface. Chrome blocked the light entirely, protecting the photoresist from exposure. Using this process, the wings that were made had a smooth surface.

4.2.3.5 Photoresist Thickness

Since negative photoresist is a polymer combined with a photosensitive compound, it is viscous by nature. Negative photoresist yields a thicker shield layer than positive photoresist, and is more adhesive. The SU8 photoresists are named according to the thickness of the photoresist when spun on at 3000 rpm. For instance, the least viscous of the SU-8 series, SU8-2, averages 2 μm thickness when spun on at 3000 rpm. Both SU8-2 and SU8-5 were used during these experiments.

SU8 is very robust, and resistant to HF etching. SU8-2 was expected to be sufficient to protect the substrate in all cases, and this assumption turned out to be

correct. There is a small amount of swelling of the photoresist during the development step, which is exacerbated in thicker coatings. This swelling was not deemed to be sufficient to effect the shape of the wing members for a macro scale etch of the process used for these experiments.

4.2.3.6 Adhesion

Negative photoresist adheres differently than positive photoresist because of the nature of polymers used. It adheres more strongly and is very difficult to remove. When the positive photoresist was unable to adhere to the stainless steel, the first solution was to make a negative mask and try a negative photoresist. The mask remained without a problem throughout all of the processing and the etching.

4.2.3.7 Resolution and Mask Material

Due to the problem with the ink and the transparency mask material, all of the early protoypes were made with negative photoresist, including the fingers in Figure 34 that were made to test etch resolution. Negative photoresists consist of polymers combined with a photosensitive compound that initiates a polymer cross-linking reaction once enough energy is absorbed. A negative photoresist will not cross-link appreciably until a given threshold energy is reached, so the energy absorbed through the crude ink and transparency mask is not enough to change the solubility of the photoresist in the developer. There is no partial exposure, resolving the positive photoresist problem.

4.2.4 Etch titanium

While it is known that HF is one of the better titanium etchants, very little could

be found in extant literature about the etch rates(47)(48). The etch rate sheet in the

cleanroom claims that concentrated HF (49%) was "not tested, but known to be fast, i.e.

>10,000 Angstroms/minute (1 µm/minute)." True indeed.

Initial immersion of a 1cm x 1 cm x 125 µm titanium foil sample resulted in

complete dissolution before an initial ten minute check could be completed. A second

sample that was checked after only two minutes was also found completely dissolved,

with very small pieces still producing H_2 bubbles. Table 2 shows experimental results for

titanium samples in different solutions of HF and distilled water. The 3:1 dilution was

initially used for a titanium sample. Then, another two parts of water were added and

another titanium sample was dissolved. Lastly, another three parts of water were added

and another titanium sample was dissolved.

Table 2 : 1 cm x 1 cm x 125 µm Ti samples immersed in various solutions of distilled

water and HF (one sample tested in each dilution), and etch rate (one side etch only)

DI:HF	Holes form (min.)	Breaks apart (min.)	Completely dissolve (min.)	Max/Min Etch Rate (µm/min.)
1:1	Not measured	Not observed	2:00	Not measured/31.25
3:1	5:15	Not observed	6:15	11.9/10
5:1	9:00	9:45	10:00	6.94/6.25
8:1	12:55	13:30	13:45	4.84/4.55

A dilution of between 5:1 and 10:1 was deemed to be a sufficiently slow etch rate

to avoid mistakes in etching. The question of surface quality still remained however, so a

separate experiment was carried out with separate samples in dilutions of 5:1 and 10:1; surface finish was then compared. Dilutions were prepared using a pre-marked beaker, which was marked using water measured from a graduated cylinder. After the given time of immersion, the samples were removed and immersed in a container of distilled water.

Table 3: Samples etched at 5:1 and 10:1 distilled water : HF solutions to test surface finish of etch

Sample	Dimensions Before (mm)	Dimensions After (mm)	Photoresist	Dilution	Time (min)
1	32.2 x 6.2 x 0.12	32.1 x 7.0 x 0.11	SU8	10:1	8:30
2	32.2 x 6.1 x 0.12	32.2 x 6.1 x 0.12	SU8	5:1	4:30
3	20.8 x 9.3 x 0.12	20.7 x 9.2 x 0.12	S1818	5:1	4:30
4	17.6 x 10.4 x 0.12	17.4 x 10.35 x 0.10	S1818	10:1	8:30
5	11.3 x 10.1 x 0.12	11.25 x 10.0 x 0.12	None	5:1	4:30

The results clearly showed that the 5:1 dilution yielded a deeply pitted surface finish, while the 10:1 dilution yielded a much smoother finish, seen in Figure 37. Aggressive etches often pit surfaces in this manner for a number of reasons. First, an uneven chemical makeup on the material surface can quickly allow one area to be etched more deeply than another. The titanium being used for these etches is pure, however, and this should not be a significant factor. Second, an area that is temporarily stagnant due to insufficient etchant agitation will quickly fall behind the fast etch of surrounding areas. Frequent agitation of the HF solution should mitigate this effect. However, the biggest factor causing pitting in the titanium surface will be the hydrogen bubbles that form on

the surface of the titanium during the chemical reaction between HF and titanium. These

bubbles slow the etch rate in the area they cover until they are large enough to float to the

surface of the HF solution. This process can be mitigated by agitating the solution, but

hydrogen bubbles form so quickly that the etched surface will never be as smooth as the

machine tooled surfaces. The slower etch, however, has more time to make up

differences in material transfer, and yields a smoother surface than the quicker etch. A

higher dilution would likely yield an slightly smoother etch, but the etch rate would be

slower. Balancing these two considerations concluded that a 10:1 dilution would yield an

acceptable surface finish at an acceptable etch time. The hydrogen bubbles would not

likely allow a significantly smoother etch, even in a dilute acid solution that takes a much

longer time to etch.
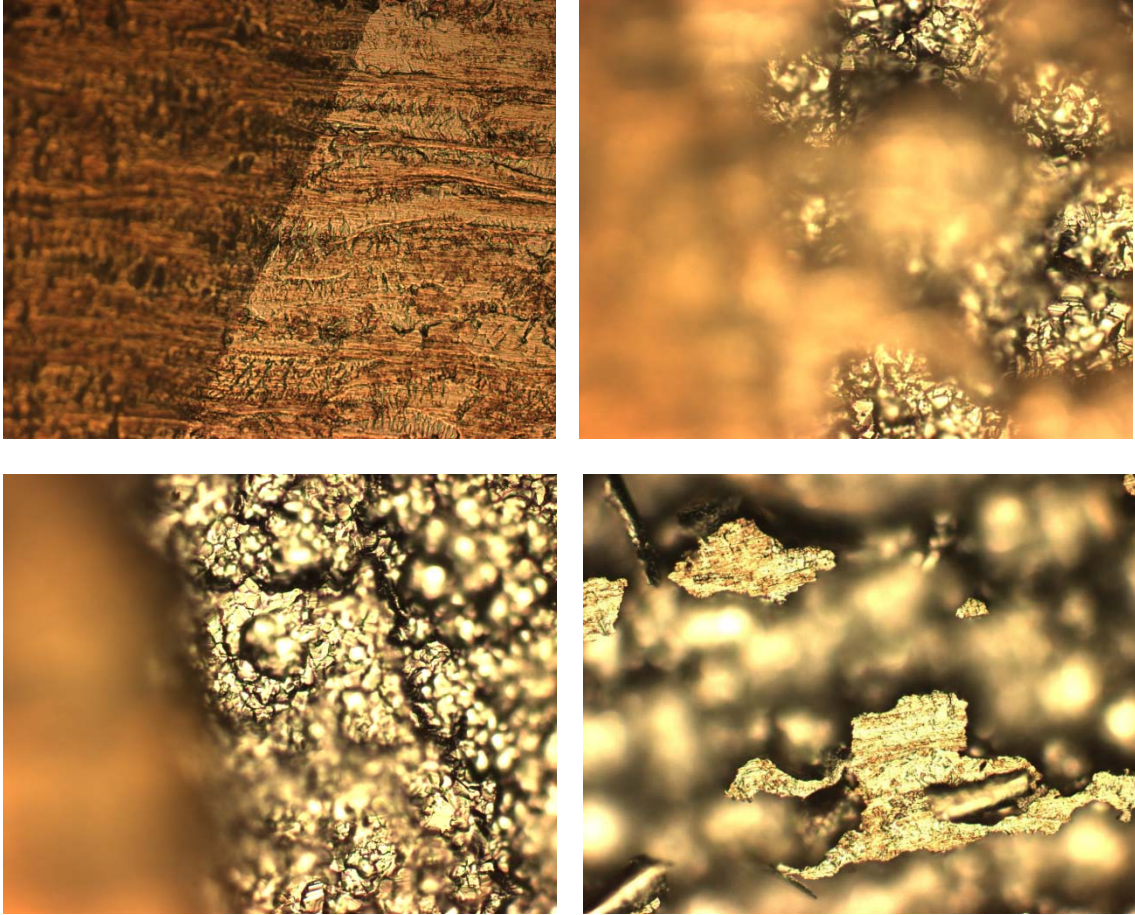
Figure 37: Etch rate effect on surface finish; A) sample 3 before etching (baseline surface); B) sample 3 after etching shows high peaks and valleys on a highly pitted surface C); sample 4 after etching, with a much less pitted, more even surface D); sample 5 after etch had a highly pitted surface

The experiment also showed that both the SU8 negtive photoresist and the S1818 positive photoresist worked well as masks. Neither peeled up, as was seen with the stainless steel etch. Both were "painted" on with a foam swab, and then baked at 110ºC for 75 seconds. This gave another indication that the pitting of the first positive

photoresist covered wing was due to the partial exposure, and the subsequent partial developing, of the photoresist.

It should be noted that some of the dimensions of the samples noted in Table 3 seem to have etched at an inconsistent rate when compared both before and after the etch. The samples were cut unevenly, and the length and width dimensions were taken with a caliper at the spot judged to be the middle of the sample. For a skew rectangle, a small variation in the point at which the measurement was taken could yield a different result, and that is most likely the reason for the inconsistent dimensions. The difference of measured thickness in sample four was also anomalistic, but cannot be explained in the same manner. It was more likely due to a poorly taken measurement, coupled with an insufficently sensitive measurement tool.

The chemical etch rate for sputtered titanium, found in an experimental paper called *Etch Rates for Micromachining Processing* (48), is experimentally given as 1100 angstroms/minute, or 1.1 microns/minute, for 10:1 a dilution of distilled water : HF. While that is more exact than other sources, and somewhat closer to the etch rate of titanium foil discovered in these experiments, it was still roughly a quarter of the actual rate of 4030-4810 angstroms/minute. This could have been due in part to density uniformity, and other differences between sputtered titanium and rolled titanium foil. It could also reflect a difference in chemical age, dilution, or measurement. It can be noted from the data, however, that the etch rate steadies as dilution increases. Figure 38 shows that the rapidly diminishing etch rate, as more water dilutes the HF, approximates a logarithmic decrease. If this trend continues, the etch rate may be assumed to remain between 3 and 4 μm/min. for increasing dilutions.
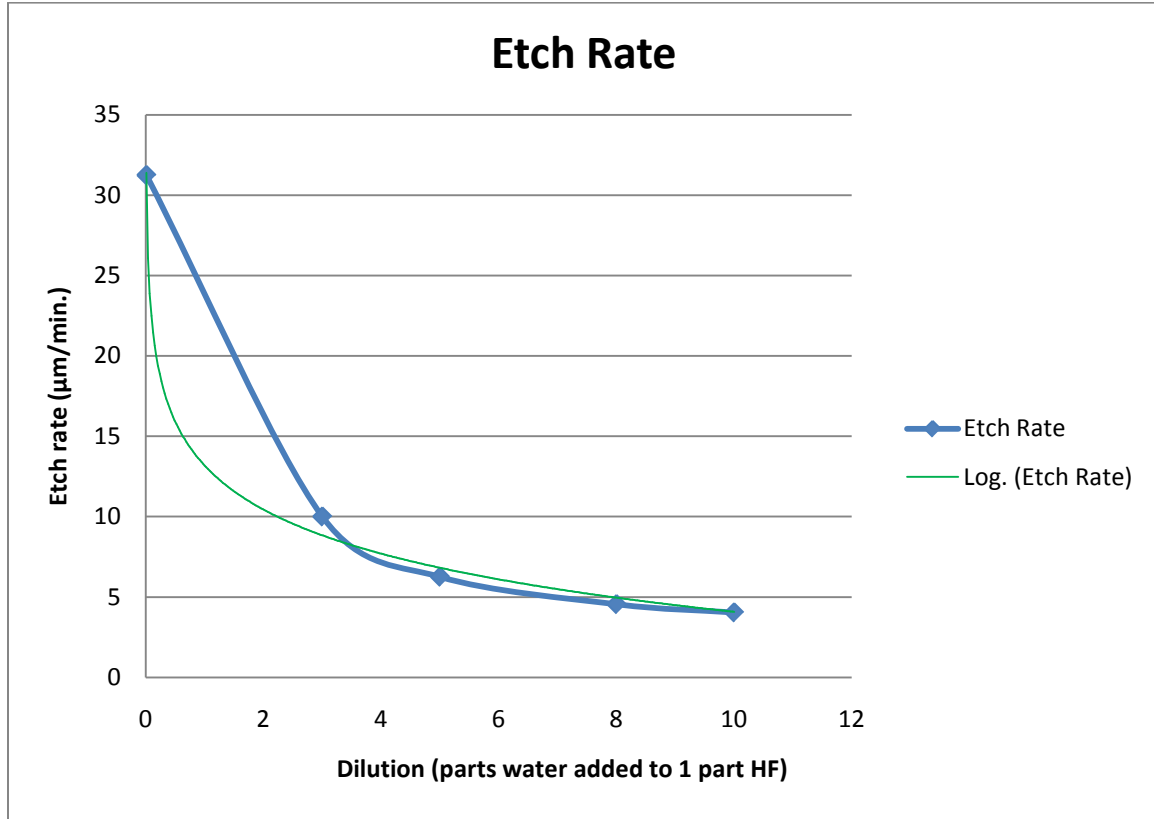
Figure 38: Etch rate vs. HF dilution shows that the change in etch rate vs. dilution becomes significantly less as dilution is increased

4.2.5 Impart Camber

Unfortunately, little information was found in a literature search to quantify the spring-back of titanium after it has been bent. While the modulus of elasticity and other properties have been well documented and characterized, a spring-back constant was not part of these data. It was decided, then, that experimental determination would be sufficient for the purposes of the wing manufactured for this thesis. A series of strips of titanium foil of differing widths were cut to approximately 1 cm and 2 cm pieces. They

were pressed into cylindrical molds of differing radii. The full data from these experiments can be found in the appendix. It was discovered that in order to impart 5% camber to a thin foil member 1 cm long, a cylinder of 0.625" diameter yields the best results, as seen in Figure 39.
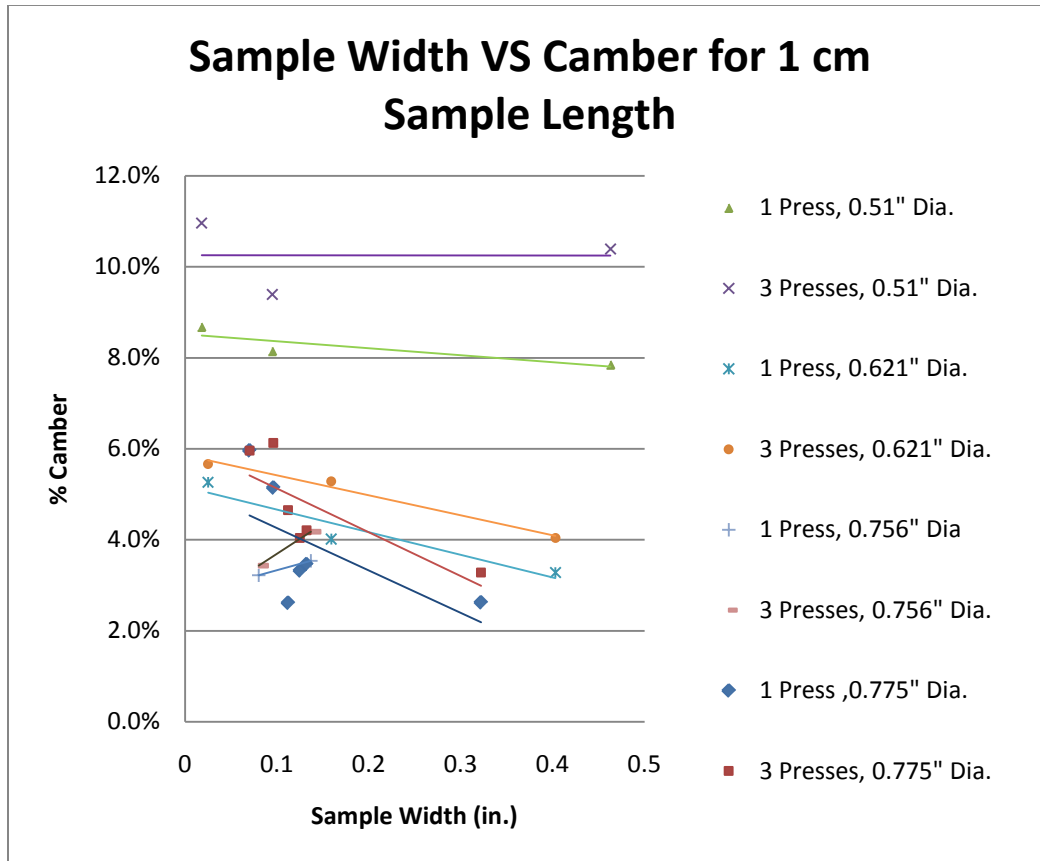
Figure 39: Camber imparted to 0.005" thick titanium foil strips when various diameter cylinders were used to press them into tight-fitting cylindrical molds

A cylinder and cylindrical mold of this diameter were modeled using Solidworks and printed with a rapid prototyper. This mold, shown in Figure 40 was used to impart camber to the wings manufactured for this thesis. The cubic structures at the mouth of

the camber mold were set to fix the wing into place, using the wing's shoulder plate, so that the camber in the same parts of the wing structure could be set exactly the same for wing manufactured. The hollow core of the camber cylinder has no structural or camber significance, but was simply a precaution to save rapid prototyping material, since the middle was not needed for camber and was thick enough to remain structurally sound.
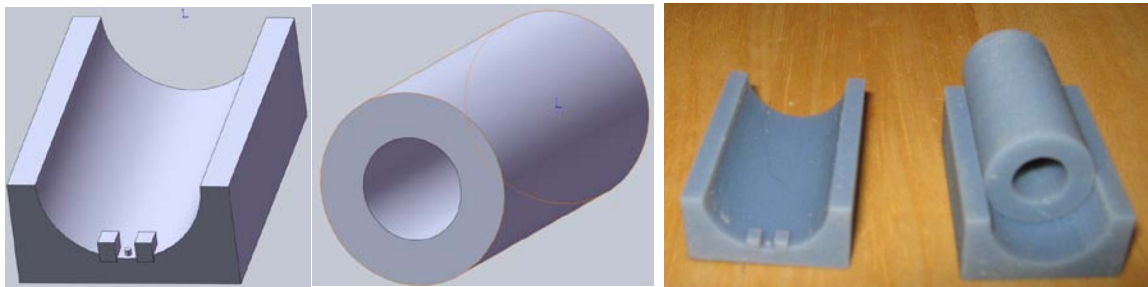
Figure 40: Design and rapid prototyped cylinder and mold calculated to produce 5% camber in the manufactured titanium hawkmoth wing

4.2.6 Apply Membrane

The membrane is the most important lift producing component of the wing, so care was taken in planning and assembling this member. The main considerations to take into account were weight and strength. It needed to be strong enough to resist ripping or tearing under stressful conditions, yet remain light enough to avoid producing too much drag on the Micro-MAV. Additionally, it needed to be easily attached to the wing structure, or it would not be a feasibly repeatable membrane. The attachment process could not affect other wing properties, such as camber.

4.2.6.1 Matching Camber

The membrane must be attached in such a way as to enhance wing properties, rather than detract from them. If it were to be attached before camber was imparted to the wing, for instance, it would provide additional resistance and springback during the process of pressing it into the mold, and could counteract the camber. Also, since titanium must be bent far beyond the degree to which it will spring back, Kapton could break, wrinkle, or deform in the process. For these reasons, a method was devised for attaching the membrane to the wing in instances where camber has already been applied.

This process provided its own set of problems. It was difficult to smoothly apply a membrane to a curved surface in which there was little surface area for it to be pressed or flattened against. Plus, the membrane must be in tension or it would wrinkle and cause additional drag during the flying process. In order to overcome these problems, a method was devised to apply the wing to the membrane while the membrane was in tension, using a cylinder with 5% camber, as shown in Figure 41. A fine spray adhesive was applied to the wing structure, which was then pressed against the membrane on the camber cylinder. Note that the cylinder, like the camber pressing cylinder, is hollow in the middle, for purposes of saving rapid prototyping material rather than for structural reasons.
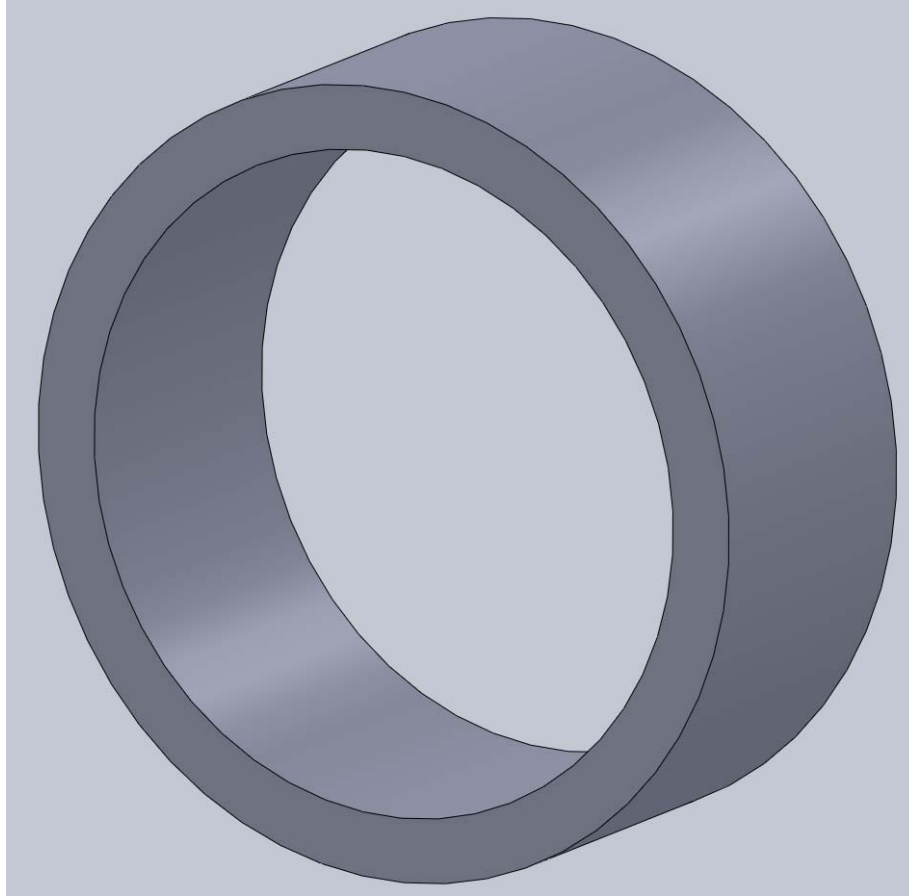
Figure 41: Cylinder with 5% camber for a wing that is 2 cm wide

Since camber is defined as:

$$\text{—} \qquad\qquad\qquad [5]$$

Where h = maximum deflection of the airfoil above the chord, as measured perpendicular to the chord, and a = arc length(1). The camber of any cylinder, then, will be:

$$\text{—} \quad \text{–} \qquad\qquad\qquad [6]$$

To accommodate a wing with 5% camber, the cylinder would have to be significantly larger than the wing; the camber of the 2 cm chord was 5%, though the camber of the cylinder was 31.8%

In order to find the dimensions of a cylinder that fit this criteria, the chord was found by iterating on the radius of the cylinder (r) and the height of the arc (h) using the following equations, based on the diagram in Figure 42:

$$\overline{}$$

$$\overline{} \tag{7}$$

The image contains a diagram of a circle with points C (top), A (bottom left), B (bottom right), O (center), D (bottom), and E, with a red triangle and green segment. Accompanying text:

Lines AO, OD and OB are called radii.
Lines AC, BC and AB are called chords.
The angle ACB is an inscribed angle.
The angle AOB is a central angle.
The curved line AB is called an arc.
Line OE is the apothem and is the height of triangle AOB.
Line ED is the segment height or the sagitta - a rarely used term.
The length of an arc equals (Central Angle / 180°) · π · r
The green area is called a segment.
The red triangle plus the green segment is called a sector.
Sector Area = (Angle AOB/360°) · π · r²
Segment Area = Sector Area Minus Triangle AOB Area.

Figure 42: Parts of a circle used to define formulae for finding the radius of the circle, given the arc and height above the chord(49)

Iterating to find the radius yielded r = 4.985 cm, or a cylinder with a diameter of 3.94 in.

Once this cylinder was manufactured, the Kapton could then be stretched over it with a given tension by fixing weights to each side. An adhesive was applied to the concave camber of the wing, and the wing is pressed down against the Kapton membrane. The excess membrane could then be trimmed away. The resulting membrane was smooth, without interfering with the camber already bestowed on the titanium wing structure, as seen in Figure 43.
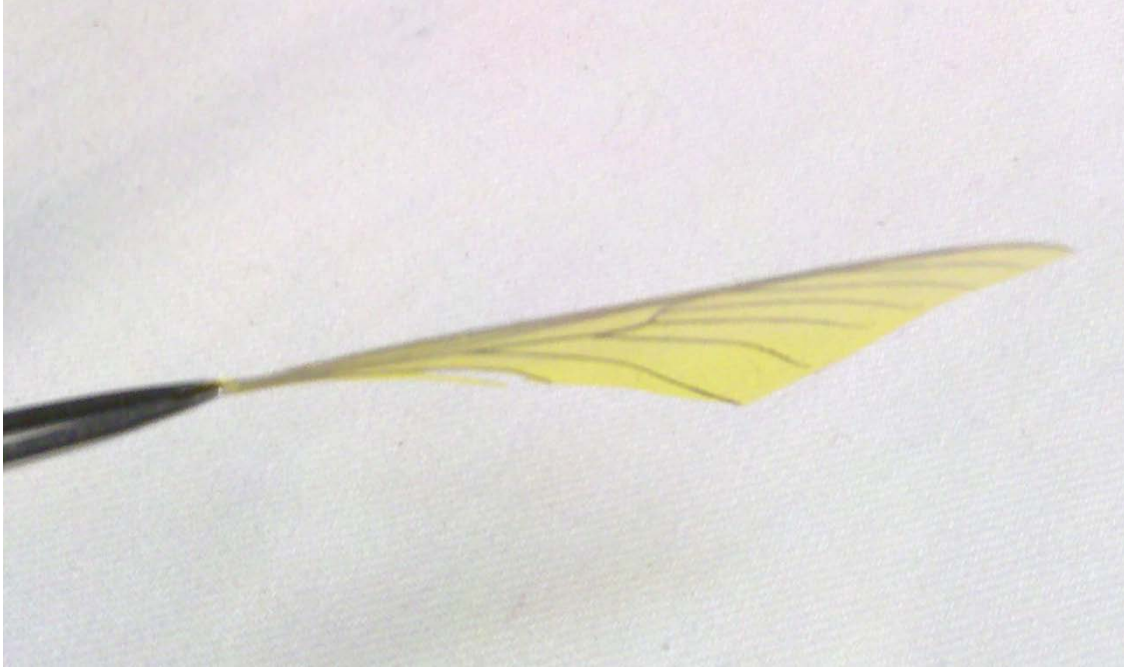
Figure 43: Camber of finished wing is small, but visible

4.2.6.2 Kapton Etching

Kapton etching was used for two main purposes. Thinning the membrane, mentioned above, was ideal for weight reduction. When making wings out of other materials, such as carbon fiber, it could also serve to clean and roughen up the surface so as to adhere to the structural surface. For both purposes, a series of experiments were performed to quantify the rate of etch on the Kapton substrate using O_2 RIE plasma, as well as an $O_2 + SF_6$ RIE plasma, which is a much more aggressive etchant. The full results can be found in the appendix, but Figure 44 and Figure 46 summarize the results. Each Kapton sample was measured on a profilometer after the etch was completed. Note that for purposes of graphing data, each profilometer measurement taken was counted as a sample, rather than graphing a group of measurements taken on each Kapton sample.

This allowed a graph of thickness vs. time. If each Kapton sample were graphed

separately, the linearity of the etch could not be seen. However, each Kapton sample can

be clearly seen, since there are two 5-minute and three 10-minute samples taken for the

$O_2 + SF_6$ RIE plasma, and one of each of the remaining times. For more details, please

refer to the related data in the appendix.

For the $O_2 + SF_6$ RIE plasma, experiments were carried out in two separate

categories of experiments: etching on one side of the Kapton film, and etching on both

sides. For etching on boths sides, the time on each side was added up in order to graph

the results. The results showed that the amount of Kapton etched is roughly linear in

time. The RIE plasma is not entirely steady for the first couple of minutes, but steadies

afterward, and the results were seen to be fairly consistent.
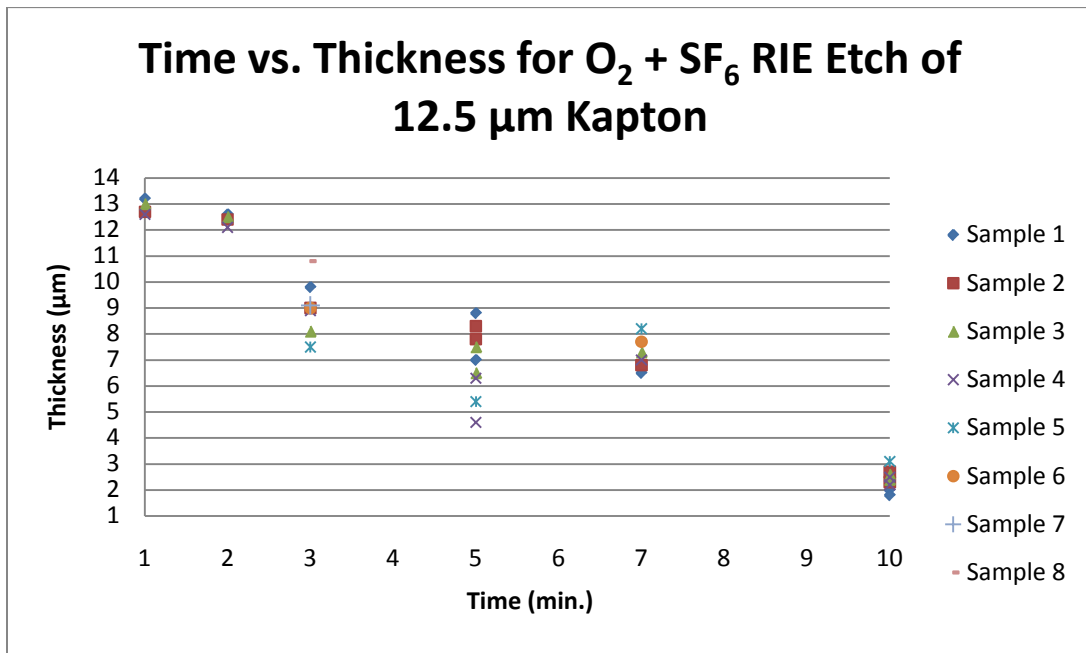
Figure 44: Results of etching Kapton with an $O_2 + SF_6$ plasma in an RIE over a

range of times

A second experiment was carried out to test the loading effect of the RIE. When

a significant portion of the area in the RIE is used, it etches more slowly than when there

is only a small sample to be etched. Samples of increasing size were etched for

increasing times, and each sample was measured to find how much of the Kapton was

etched. Figure 45 shows that a rough rate of etch was calculated from these numbers.

Based on these data, an additional etch was carried out for 31 minutes, and the resulting

Kapton sample was measured to be within predicted thickness parameters. For the

Jupiter March III in the AFIT cleanroom, these data can be used predictively.
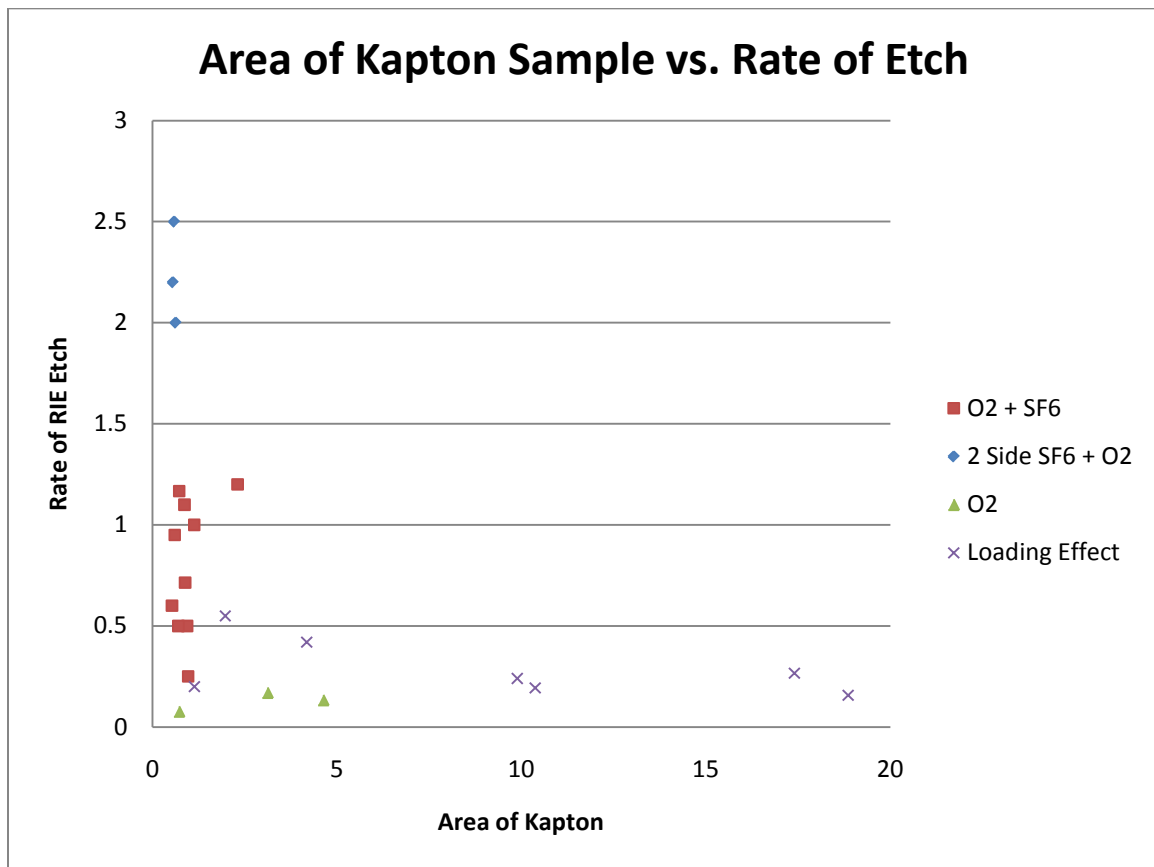
Figure 45: There is a loading effect for larger samples of Kapton, due to the reduced

effect of the plasma on a larger area

For O_2 RIE plasma, fewer experiments were carried out once it was discovered that the longer etch tended to be more uniform over the sample. There was still variation from sample to sample, as seen in Figure 46, but the profilometer showed less surface variation overall than did the O_2 + SF_6 RIE plasma. Note that, although the time for each etch was greater, the amount of Kapton etched away was much less. The O_2 plasma provides a far less aggressive etch than does the O_2 + SF_6 plasma.

Time vs. Thickness for O_2 RIE Etch of 12.5 μm Kapton
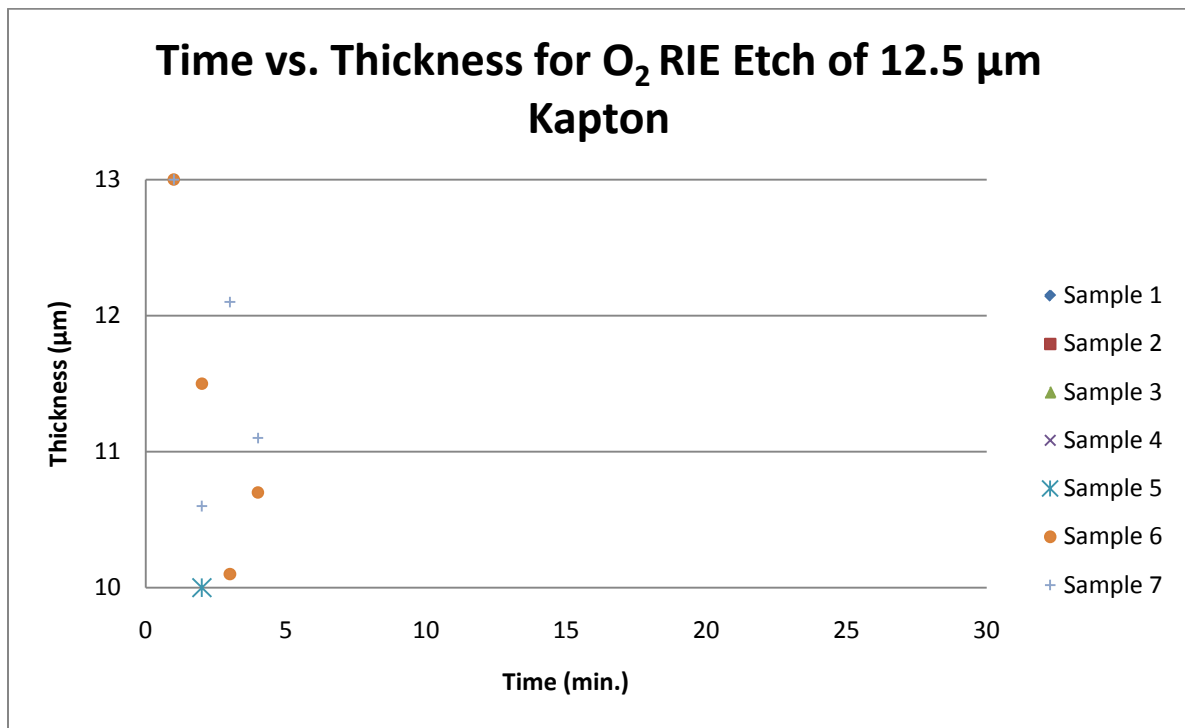
Figure 46: Thickness vs. time plot for Kapton etched with an O_2 plasma in an RIE

One additional experiment was carried out to test the feasibility of etching the Kapton after it was applied to the wing structure. A carbon fiber wing with a Kapton

membrane was etched in the $O_2 + SF_6$ plasma for 23 minutes, etching the Kapton to approximately two microns. Unfortunately, thermal effects of the RIE caused portions of the membrane to etch more rapidly, as seen in Figure 47. An RIE chamber is cooled through the chamber floor, but the membrane was insulated from much of that cooling effect by the carbon fiber structure, and part of the wing was etched away much more quickly than the rest. A shorter etch should be used to avoid this result. Though the Kapton member will be thicker and heavier, it will be intact. Another possibility may be two etches of shorter times, rotating the specimen between etches. If there are "hot spots" in the etching chamber, this solution will help to average the thermal effects across the Kapton membrane.
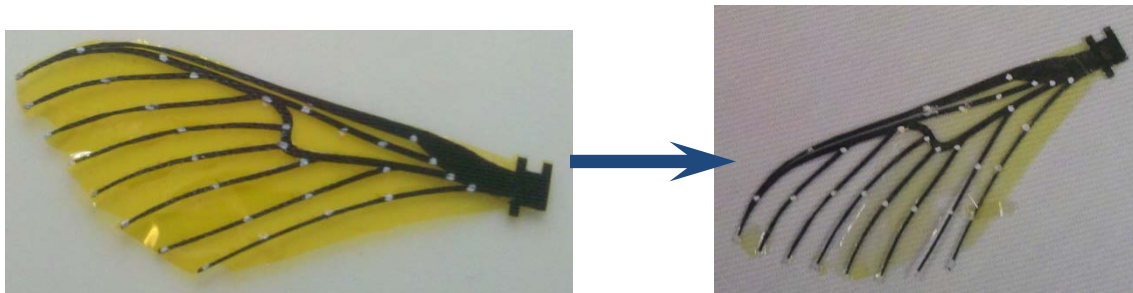
Figure 47: Kapton on Carbon fiber wing A) before RIE etch and B) after RIE etch; uneven etch was likely caused by thermal effects in the RIE chamber

4.2.7 Final Run

Once the process was set and the steps familiar, a final run was made to confirm the time needed to finish an entire wing. These wings were also characterized for repeatability and quality.

4.2.7.1 Time

Since the final run did not require a learning curve, the times were assumed to be representative of the process overall. Since the above wings were made using the pattern for a carbon fiber wing, which is much stiffer than titanium, it was decided to make wings with thicker, stiffer members. The members were given a roughly 10:1 ratio of thickness from base to tip of each member. This ratio was taken from the first wings designed by Maj. Ryan O'Hara for titanium wings. Then, because the former wing members were easily broken during processing, the new wing tips were thickened. The resulting wings can be seen in Figure 48. This process included opening the .dxf file in DraftSight to manipulate it, exporting it as a .bmp file, then opening the .bmp file in Microsoft Paint and making further manipulations. The entire process took an hour.
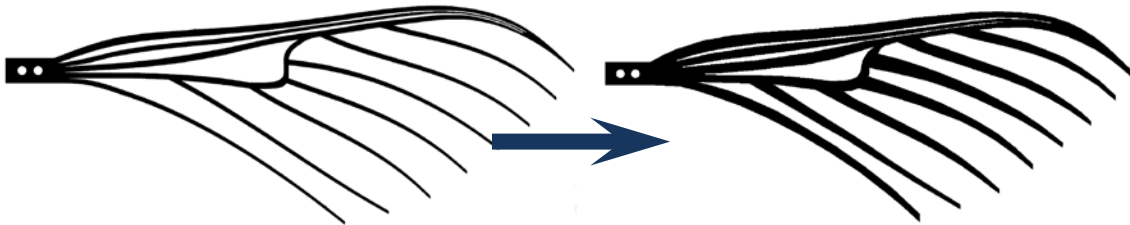
Figure 48: Wing members were thickened for greater stiffness in order to change the properties of the former wing, which was designed for carbon fiber fabrication, so the titanium will more closely resemble the hawk moth wing

Once the new file was saved in the proper format, it was loaded into the Heidelberg laser writer, and a mask was exposed. While the mask was being written, titanium samples were prepared with a positive photoresist. Once the mask was finished

and processed, the titanium samples were exposed and developed. This process took an hour and a half.

The masked titanium samples were then ready for etching. The etch itself took 26-29 minutes for the four wings. The variation was due to slightly different acid strengths when the 49% HF was mixed with HF in a 10:1 ratio using a beaker. The finished wings were soaked in water to neutralize the HF, cleaned with acetone, rinsed in water, and dried with N_2. Despite the new design, two members were destroyed during processing. One was due to a scratch in the photoresist that allowed the HF to cut the member in half. The other was caught on the still-masked titanium that was left after the etch and bent. The process of straightening overstressed the material and the member came off.   The entire etch process from setup to cleanup was 45 minutes. The resulting etch can be seen in Figure 49. Note that the first wings to come out of the etch, on the left of the figure, were left in the acid slightly longer, and demonstrate a better isotropic etch gradient.
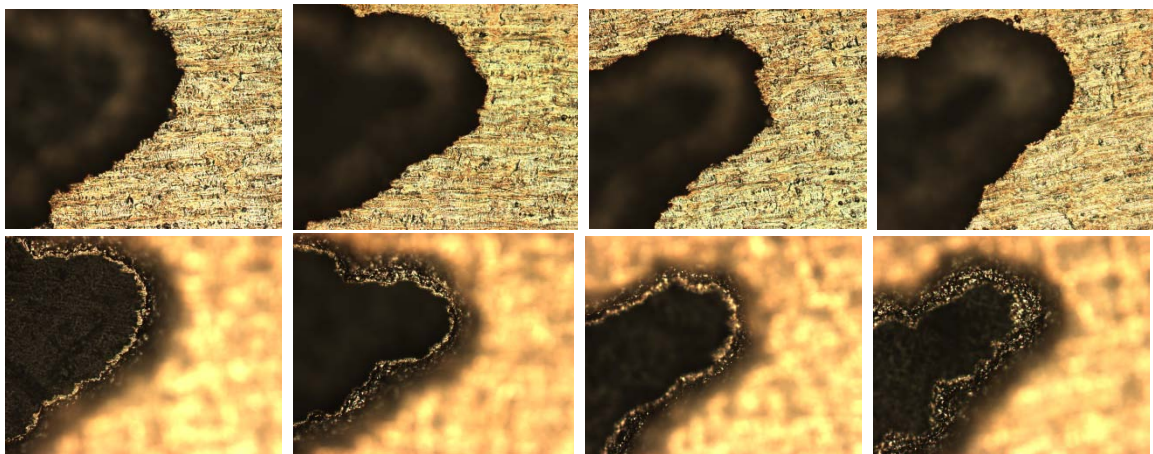
Figure 49: Top and bottom of the structure joining the spars; bottom shows anisoptopic HF gradient; pictures are ordered form 1 to 4 in order that etch was

finished, wing 1 being in a stronger acid; etch gradient is less pronounced in those samples that finished etching first, and were left in the acid slightly longer

The new wings were cambered, and Kapton membranes were etched to 5.5μm thickness using the RIE etch data presented above. The RIE etch took 31 minutes, and provided enough Kapton for all four membranes. The RIE Kapton etching process, however, could be performed during the mask writing or HF etching process. The process of imparting camber to the four wings, applying membranes, and removing the excess Kapton took 22 minutes. The membranes add 10 mg to the weight of the titanium wing structures.

The entire process took three and a half hours. Because this is a batch process, twice as many wings would take less than four hours to complete. The resulting wings can be seen in Figure 50. Notice that the right and left wings have been cambered appropriately: wings 2 and 4 could be used as a pair.
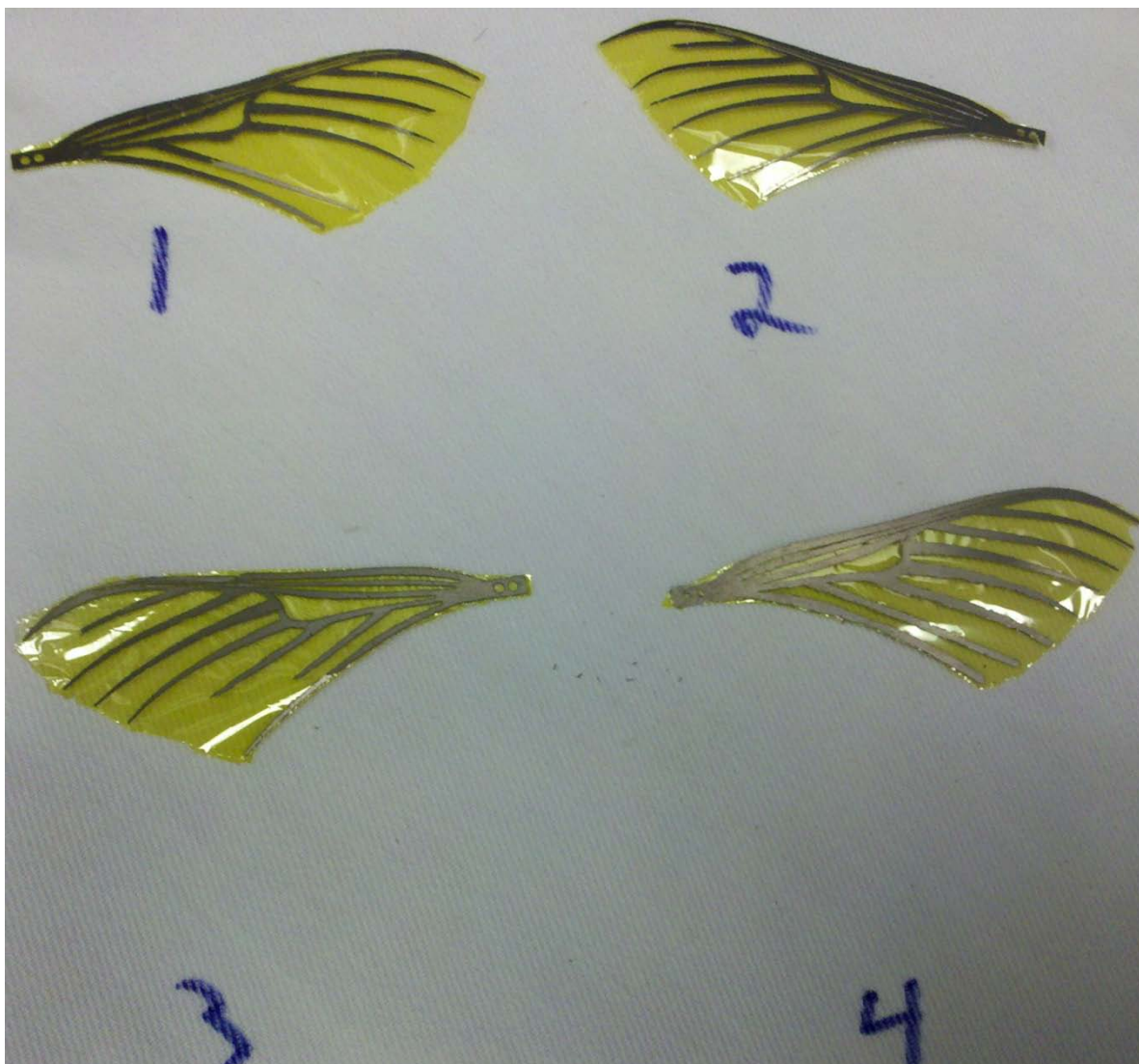
Figure 50: Final wings were made in four hours and forty minutes, from design change to final product 1) weighed 98.6 mg because of the broken wing structure, and weighted 108.3 mg with the membrane; 2) weighed 108.0 mg, and 118.1 mg with the membrane; 3) weighed 99.1 mg because of the three members that were cut off during the etching process, and 108.1 mg with the membrane; 4) weighed 118.4 mg, and 127.8 mg with the membrane

4.3 Investigative Questions Answered

4.3.1 Can MEMS Fabrication Techniques be Repeatedly Used to Manufacture Reliable MAV Wings?

The wings manufactured using the MEMS fabrication techniques described above are extremely consistent. The finish, shown at the base in Figure 51, is the same on each of them, preserved from the titanium foil by the photoresist.
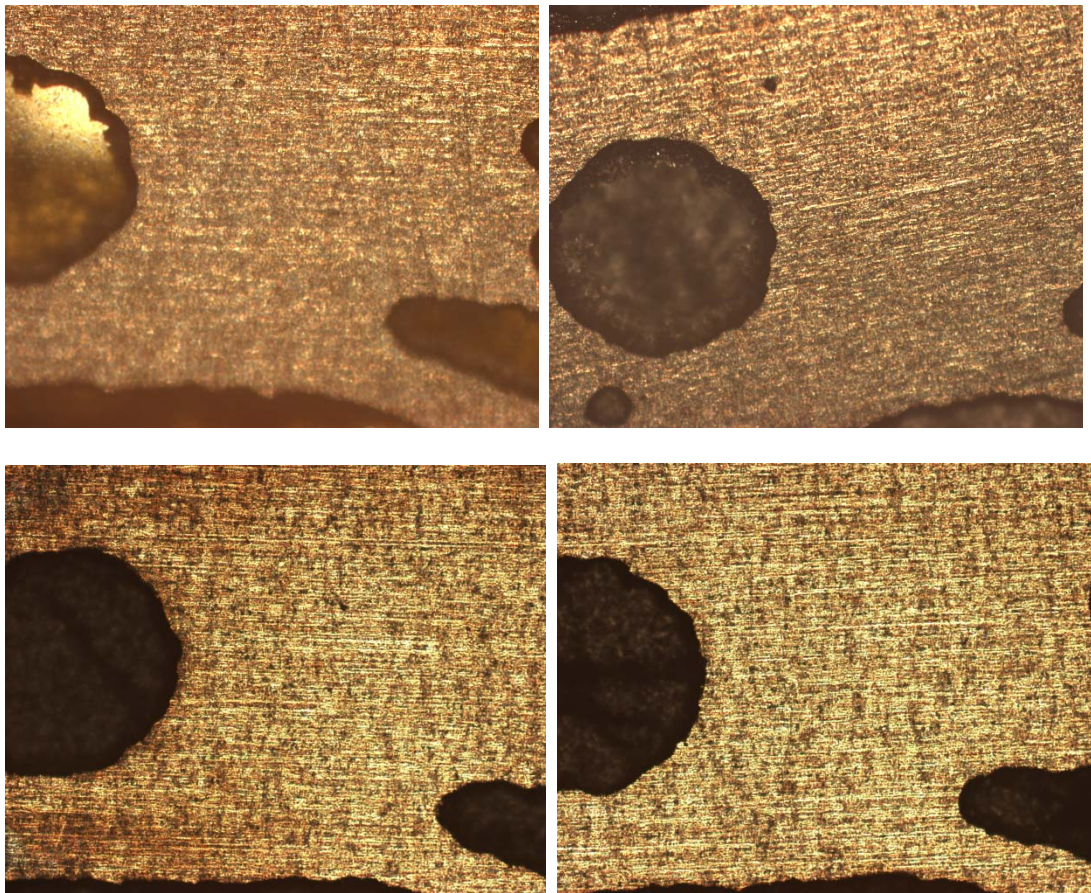
Figure 51: Surface finish of 4 titanium wings, made as a batch, shows the wing is consistently protected by the positive photoresist

Several features were also photographed with a microscope in order to demonstrate the consistency of the process. While there was some human error causing some features to break, the process itself was consistent. The pictures in Figure 52 show the wing base, wing tip, and the corner of the structural loop farthest from the wing base. Both the surface and the bottom of the structural loop corner were photographed in order to show that the gradient caused by the anisotropic etch gave a consistent slope to the sides of the wing features. These pictures show that, while there are variations from etch to etch, the structures, finish, and gradient of the etch are consistent for a given mask.
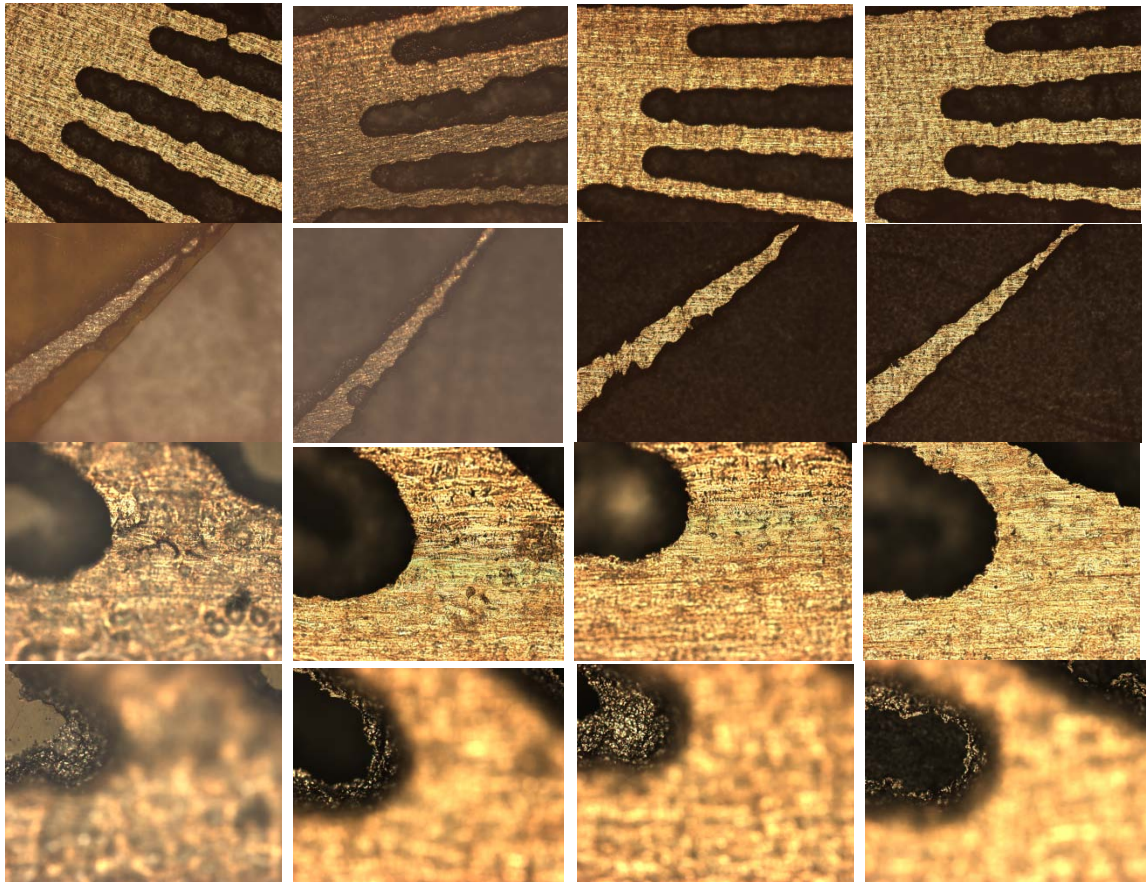
Figure 52: Features of four wings made as a batch; features were taken at 5x magnification: Row A) base of wing structure from which all structure branches

out; Row B) tip of wing where three structures join at top corner; Row C) corner of

structural loop furthest from wing base; Row D) microscope focused on bottom of

each loop pictures in Row C), showing the gradient of the slope caused by the

anisotropic acid etch

4.3.2 Can This Method of Manufacture be Used to Control Changes to Wings so

that these Changes can be Tested Against a Control to Yield Quantifiable,

Comparable Results?

Once the wing has been made into a .cif or .bmp file, it would be a simple matter to change it. For example, if it was required to remove a spar and write another mask in order to test whether that spar is structurally necessary, the entire process would take only a few hours from change to full-scale manufacturing. This is a short time for such a large scale change in a manufacturing process.

This manufacture process could easily be used for parametric studies of hawkmoth wings. One study that will need to be made is to remove one structural member at a time test structural stability vs. weight savings. Other studies may add a structural trailing edge and compare the aerodynamic changes vs. the weight penalty. These results will be directly comparable because the rest of the structure between the various wings will be exactly the same.

4.3.3 Are there any additional Manufacturing Methods Needed to Complete the Wing, such as Processes for Placing the Membrane or Imparting Wing Camber?

The answers to this question were explored in sections 4.2.5 and 4.2.6. In order for the manufactured wings to closely approximate the properties and motion of the *Manduca Sexta* wing, they were given similar properties, including comparable camber and light membranes.

4.3.4 Can these Methods be Used in Micro-MAV Mass Production?

This is one of the most important questions explored in this thesis. It was determined that once a mask is made, the titanium structure of the wing can easily be used for mass production. With the slot in the camber mold to accommodate the shoulder plate, the camber can also be used in mass production.

The two parts of the process that need improvement before they can be used in mass production are applying the membrane to the wing structure, and trimming the excess membrane from the finished wing. If a suitably thin membrane were to be cut into uniform strips, a weight could easily be applied to the edges to tension the membrane. The glue was easily applied, but the the process of trimming the excess membrane was not easily solved.

Figure 53: Manufactured wing side by side with a hawkmoth wing shows they are indeed similar in size and structure

4.4 Summary

Other ongoing AFIT research provided the background research and models needed to characterize the hawkmoth wing structure and movements ((50)**,** (51), (39) with drawings courtesy of Maj. Ryan O'Hara**)**. Their research directed the development of a file that could be used to write a mask using the Heidelberg μpg 101 mask writer. The mask was used to pattern a titanium foil sample with the wing structure, which was etched in a dilute HF solution. Camber was added to the wing structure by use of a cylinder and a fitting cylinder mold. A Kapton membrane was glued to the structure. This process is predicted to have properties similar to a *Manduca Sexta* wing. The manufacture process was successful in reliably making batches of structurally similar wings, with differences only due to human error in handling. Finally, the research questions posed at the beginning of the research were sequentially answered.

V. Conclusions and Recommendations

5.1 Chapter Overview

This chapter summarizes the conclusions and suggestions made in the previous chapter, and adds recommendations for further research.

5.2 Conclusions of Research

The process for making a Micro-MAV wing structure out of titanium, using MEMS fabrication techniques, is relatively simple. Once details such as acid strength needed for a reasonable etch rate, titanium spring-back and conversion to files that can be read by the mask writer were discovered experimentally, the process of making a batch of wings, from starting the mask to finishing the membranes, was less than four hours.

Camber and wing membrane application are important to constructing a working wing. These are innate to the passive structure and dynamics of the *Manduca Sexta* wing, and a comparable wing cannot be manufactured without at least approximating their properties.

5.3 Significance of Research

Two advantages can be found in this research. First, as Micro-MAV research is advanced, wings based on natural flyers will likely stand out as the best fit for research needs. Parametric studies will benefit from a repeatable process that can control variables exactly. Second, once research progresses beyond the laboratory, a repeatable process will make the transition from bench to mass production straightforward and relatively uncomplicated.

Wings found on unsteady-state flyers in nature have been optimized for the type of flight that is estimated to be best for Micro-MAVs. The challenge in manufacturing Micro-MAV wings is to take the design from nature and distill from it the important functions that can be manufactured with the current level of technology. The *Manduca Sexta* wing is light and strong, and titanium and Kapton are not a perfect match to the natural wing. Now that the thesis' reliably repeatable process can be used to manufacture the wings, small changes can be made to the design to discover which structural members are most important, and which can be removed to lighten the wing without impacting performance. These wings will be directly comparable to each other because changes can be controlled exactly in each mask that is made. An optimal wing can be found by comparing the performance of these wings.

As workable prototypes are made, functions for the Micro-MAV will create a demand for them. A process for mass producing and assembling them will be desirable. Most of the processes described in this thesis can easily be used in mass production. This research will allow a lower price and higher quality Micro-MAV to be used for essential functions such as intelligence gathering, search and rescue, hazardous environment exploration, and remote exploration, to possibly include other planets(52). These exciting options depend greatly the ability to mass produce commercial Micro-MAVs and on the quality of production.

5.4 Recommendations for Action

Since the research presented herein was instigated to facilitate the implementation of parametric studies, that is the one recommendation included here. Immediate parametric studies can be executed by using masks made in the processes described in

this thesis. These parametric studies can be used to iterate designs and make the best possible wing.

The processes described in this thesis were designed with the implementation of mass production as an end goal. Research is not yet at a stage where mass production is feasible, since research in this area is still very much in the laboratories. Mass production suggestions are not expected to be implementable in the near future.

5.5 Recommendations for Future Research

There are a number of questions left unanswered, or opened up, by the research presented in this paper. The answers to these questions have the potential to make wings that perform better than the ones presented herein. The pinnacle of success would be to create a wing that performs as well as the *Manduca Sexta* wing. The following topics are recommended for future research.

a. Find etchants for other materials that may be stronger and lighter than titanium. It has been suggested that stainless steel, though more dense than titanium, can be made to have the same properties in a much thinner foil. Other materials might similarly be used. Pure titanium was used for ease in this thesis, but many titanium alloys are known to have better properties and be much stiffer than pure titanium. Caltech/UCLA used the common Ti-6Al-4V alloy, which is an alloy of 88% titanium, 6% aluminum, 4% vanadium, and 2% other elements such as iron, carbon, hydrogen and oxygen(13). Nitinol was also considered for these wings, but the expense and lead time was too great. Aside from its shape retention properties, a suitable mold at the proper temperature may be used to

96

impart the exact camber of a natural hawkmoth wing. For any substrate, if a suitable etchant can be found, the process described in this thesis can be quickly applied to manufacture wings to be tested.

b. Membranes other than Kapton could be used. One area of reasearch that could facilitate the repeatable manufacture of wings would to find membranes that can be applied before camber is endowed, that will not affect the camber properties when the wing is pressed into a camber mold. Such a material could be cut exactly before application, so each membrane is exactly the same, cutting disharmonies between left and right wings during MAV wing flapping. Alternatively, finding lighter and stronger membrane material that can be applied after the camber has been imparted would be beneficial. Mylar, for instance, can be found in 2 μm sheets, which should be much lighter than Kapton. Focus of the research should be on a lighter, stronger membrane material, and should include testing and comparison of the material properties.

c. Mass production or automated methods of attaching membrane and removing excess should be studied. A razor can be used to remove excess in the method described in this paper, but mass production will require a more automated, easier process for removing excess membrane material. It is far too easy to introduce abberations between left and right hand wings through uneven membranes. This, in turn, could cause differential forces in flapping, making the MAV more difficult to control. Unless this aspect is made moot by the application process described in bullet (b), excess membrane removal will be an important step in the mass production process. One possibility may be to stamp

the membrane out after being glued onto the cambered wing superstructure. If this step is taken, the wing will have to be held in the exact same position each time, perhaps in a manner such as that used to hold the superstructure in place for imparting camber in 4.2.5. Another possibility may be to pre-cut the membranes, leaving two to three long "stringers" attached, to which the weights may be applied in order to keep tension. These "stringers" may be cut off exactly, without producing uneven membranes.

d. Production of wings with more elaborate features that may help the Micro-MAV fly better should be explored. Examples might be different structural member cross-sections (if possible), microsensors, etc. The wings may also be made to receive signals, as antenna, in order to better control movement.

e. Test the effect of wing structural member cross section caused by the anisotropic etch. It was hypothesized that the wing cross section caused by the anisotropic etch of the HF may add to the stiffness, and perhaps other properties of the wing. When the process of transferring the drawing to the mask is better controlled, a mask can be made to make wings of exact size to compare the wing to those wings manufactured by other techniques. This will be another measure of the quality of MEMS etching compared to other wing manufacturing techniques.

5.6 Summary

The manufacturing process described in this thesis will work well to perform parametric studies, and many parts will be easily applicable to mass production. There are still steps in the process that will be benefitted by additional research. These include

wing structural material, membrane material, and membrane attachment method improvements. This manufacturing process will facilitate parametric studies as the Air Force researches optimal Micro-MAV wings. Then, once feasible Micro-MAVs are fabricated, the wings can be mass-produced with this manufacturing technique.

Appendices

A1.1 Butterfly

Butterflies are unsteady-state flyers with an impressive variety of wing structure and form, as seen in figure 1-1. While the some butterfly wing structures are similar to the hawk moth wing, their flying style is completely different. The flying style, is not precisely controlled, and could not be used for the precise and controlled flying needed for Micro-MAVs.

Figure1- 1: Example butterfly wings, some of which are similar to hawkmoth wings; A) *Rhetus dysonii***, family** *Nemeobiidae***; B)** *Trogonoptera brookiana***, family** *Papilionidae;* **C)** *Chaetocneme denitza***; D)** *Hesperilla idothea* **has wings that look similar to hawk moth wing in structure, but do not fly in fashion needed for Micro-MAVs (thanks to http://www.chebucto.ns.ca/Environment/NHR/lep_images.html**

A1.2 Beetle

Beetles are also unsteady-state flyers, and are much more controlled than the butterfly. An example beetle wing, shown in Figure 1-2, shows structure that could be manufactured. While their flight is straighter than the butterfly, it is still not sufficiently controlled to be used for Micro-MAV flight.

Figure1- 2: The Goliath beetle, Eupatorius gracilicornis pictured here, flies in a more controlled fashion than the butterfly, but is not sufficiently so for a Micro-MAV (courtesy of http://www.science-store.com/life/specimens/la460.htm, [Accessed April 2010])

A1.3 Housefly

Early in the research for wing structure, the housefly was shown to be a precise flyer. The housefly is a highly controlled flyer in the unsteady state regime. There has been much work in the past couple of years done, as presented by Dr. Sanjay Sane in a lecture at Wright State University. The following information is from that lecture, while

information from his research presented in the body of the paper cites his research articles. This research has helped to understand the mechanisms behind its flight mechanisms, in which inertial stresses act at the wingbeat frequency. The coriolis strain information is communicated at a rate much too fast for the eye to respond to, and it was postulated that direct communication between the organs stabilized the flight. The haltere, which looks like a stub of a wing, and is small enough that it cannot be discerned in the wing detail in Figure 1-3, is in direct antiphase to the wing. The haltere was found to be directly coupled through the exoskeleton rather than through the nervous system. When the exoskeleton was cut, the housefly could no longer fly.

While the use of the haltere was one factor that discouraged use of this research in wing design for the Micro-MAVs, the research was found to be relative to hawkmoth flight. This information may be helpful in finding a method of transmission to control Micro-MAV flight without the technology to mimic, or even approximate, the function of internal muscles used by natural flyers. These fine muscles may not be needed to control the wings precisely.
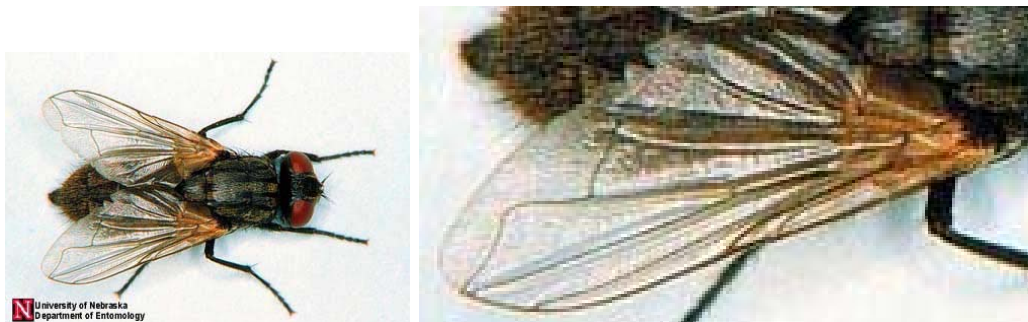
Figure1- 3: Musca domestica Linnaeus, the housefly, is a controlled and agile flyer in the unsteady state regime, but is much smaller than the Micro-MAV. The housefly flight mechanism may be too complex for the Micro-MAV, but could help

in understanding how to control and coordinate flight without internal muscles

(courtesy of http://entomology.ifas.ufl.edu/creatures/urban/flies/house_fly06.htm

[accessed April 2010])

A1.4 Bat

The bat is an outstanding flyer, as highlighted during a scholarly presentation to the Air Force Institute of Technology by Prof. Kenny Breuer. As before, his research cited in the body of this paper is established through published research articles, but this is a summary of his presentation, as relevant to Micro-MAV flight. Bats are very nimble in the air and able to make hairpin turns. They come in a variety of sizes, and can hover and even land upside down. Their flight mechanism, however, is highly complex, and would be very difficult to reproduce mechanically. The bat wing has a highly compliant membrane of variable stiffness in spanwise and chordwise directions, deforming bones, numerous articulated joints, and hair "flight sensors" on their wings. Like the hummingbird and the hawk moth, the tip vortex that helps to sustain unsteady-state flight is strong, then is dissipates at the upstroke to avoid drag by retracting the wings. This seems to be a purely passive motion. The complexity of the bat wing can be seen in Figure 1-4.
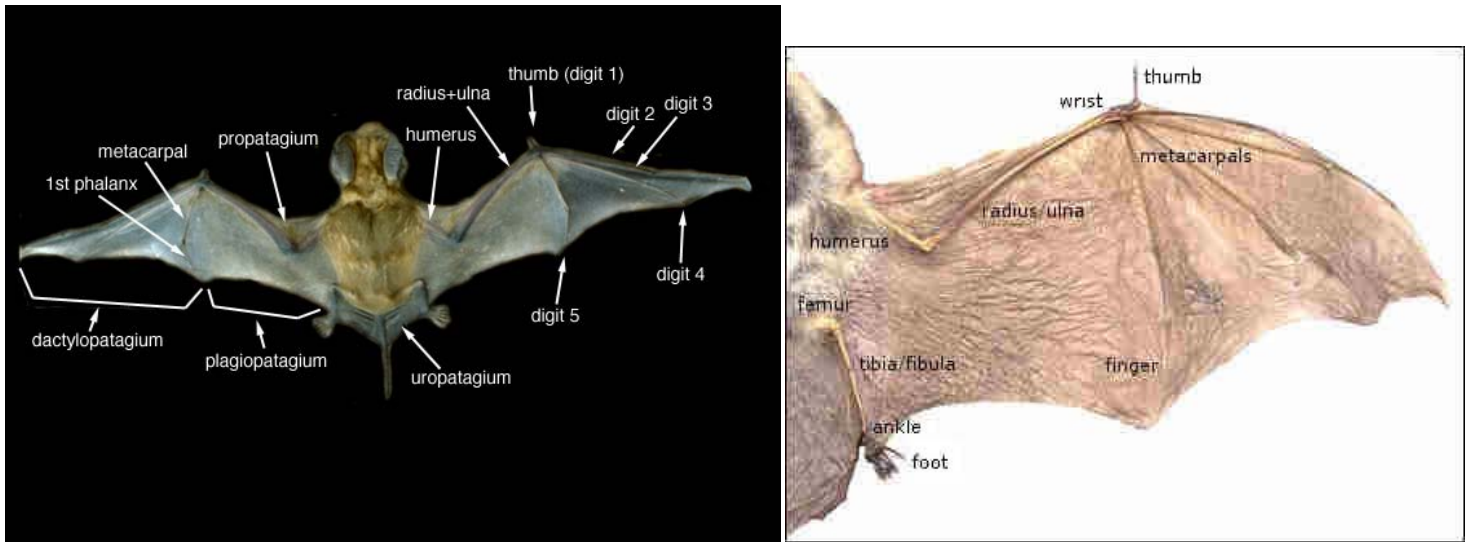
Figure1- 4: The bat wing is highly complex and would be very difficult to accurately reproduce through manufacturing (pictures courtesy of http://animaldiversity.ummz.umich.edu/site/resources/anatomical_images/bat_wings.jpg?XTHEME=POPUP and http://museum2.utep.edu/mammalogy/taxa/chiroptera1.htm [accessed Feb. 2011])

The wing membrane is stiffer in the spanwise than the chordwise direction, as seen in Figure 1-4. It expands up to 100% during the downstoke in the spanwise direction. The bat wing membrane is highly compliant, and has variable stiffness in spanwise and chordwise directions, being stiffer in the spanwise than the chordwise direction, as seen in Figure 1-5. The wing membrane It expands up to 100% during the downstoke in the spanwise direction. Additionally, the wing flight mechanisms include deforming bones, numerous articulated joints, and hair "flight sensors" on their wings. The sensor hairs are different from other hairs, and are sensitive to flow, possibly acting

as flow separation sensors to detect attached flow. The bat flies very clumsily without them. The possibility of recreating sensors of that caliber mechanically is zero.
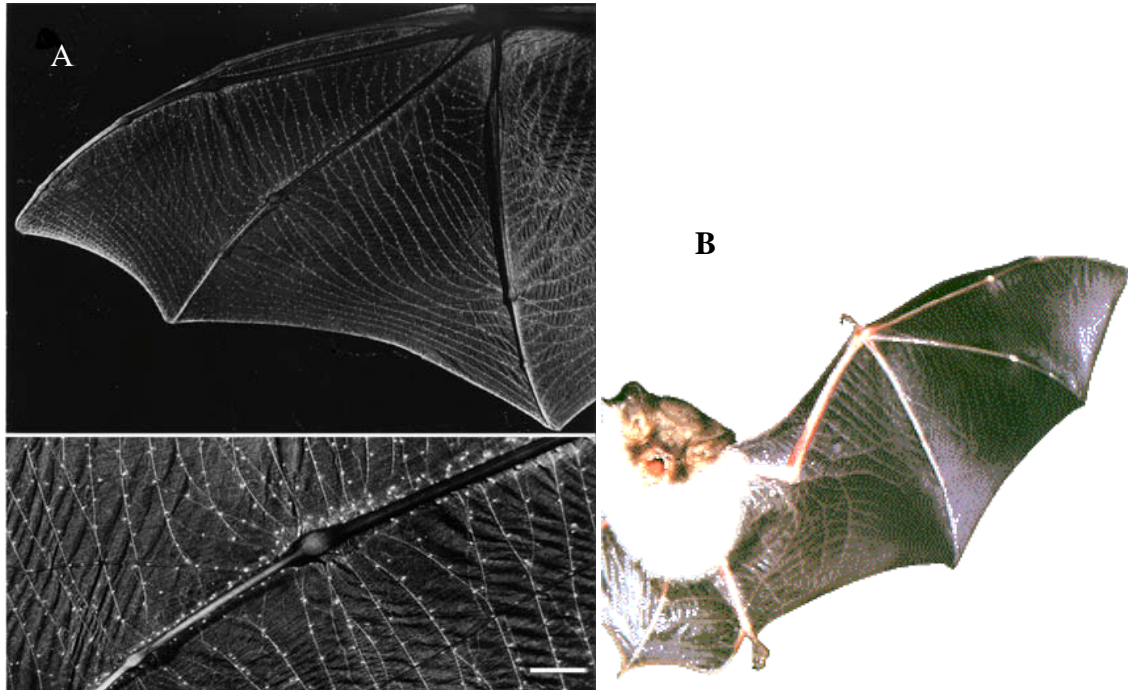
Figure1- 5: Highly anisotropic bat wing; A) Bat wings are compliant and highly anisotropic spanwise, but chordwise are essentially fixed length due to muscles embedded in wing arm B) bat wing during downstroke, expanded in spanwise direction (courtesy of http://i.livescience.com/images/051216_bat_wing_02.jpg for A and http://www.transitionrig.com/bat.htm for B, [accessed February 2011])

A1.5 Dragonfly

The dragonfly has all the characteristics a Micro-MAV needs in order to carry out the missions assigned to it. The size is just right, also. However, like the bat, the dragonfly flying mechanisms would be difficult to reproduce, as would the wing. The wing is

corrugated and has a structure that would be very heavy if reproduced mechanically. The interaction between the wings would be very difficult to accurately reproduce mechanically, and even more difficult to control for hovering and other aspects of flight.

Figure1- 6: The dragonfly wing can be reproduced in a laboratory, but would be heavy, structurally (pictures courtesy of http://www.ask.com/wiki/Dragonfly for A and B, and http://www.treknature.com/gallery/Asia/photo68607.htm for C [accessed April 2010])

A1.6 Hummingbird

Hummingbirds are celebrated agile flyers. They hover, fly complex patterns, but can also fly forward at high speeds, as seen in Figure 1-7. Not only do hummingbirds fly with the precision necessary for Micro_MAV design, but their flight control mechanisms are more easily reproduced mechanically. Dr. Bret Tobalske spoke at Wright State University on the flight process for a hummingbird. Once again, all research done by him that is cited in the body of this paper is from research papers, but his lecture is summarized in this appendix.
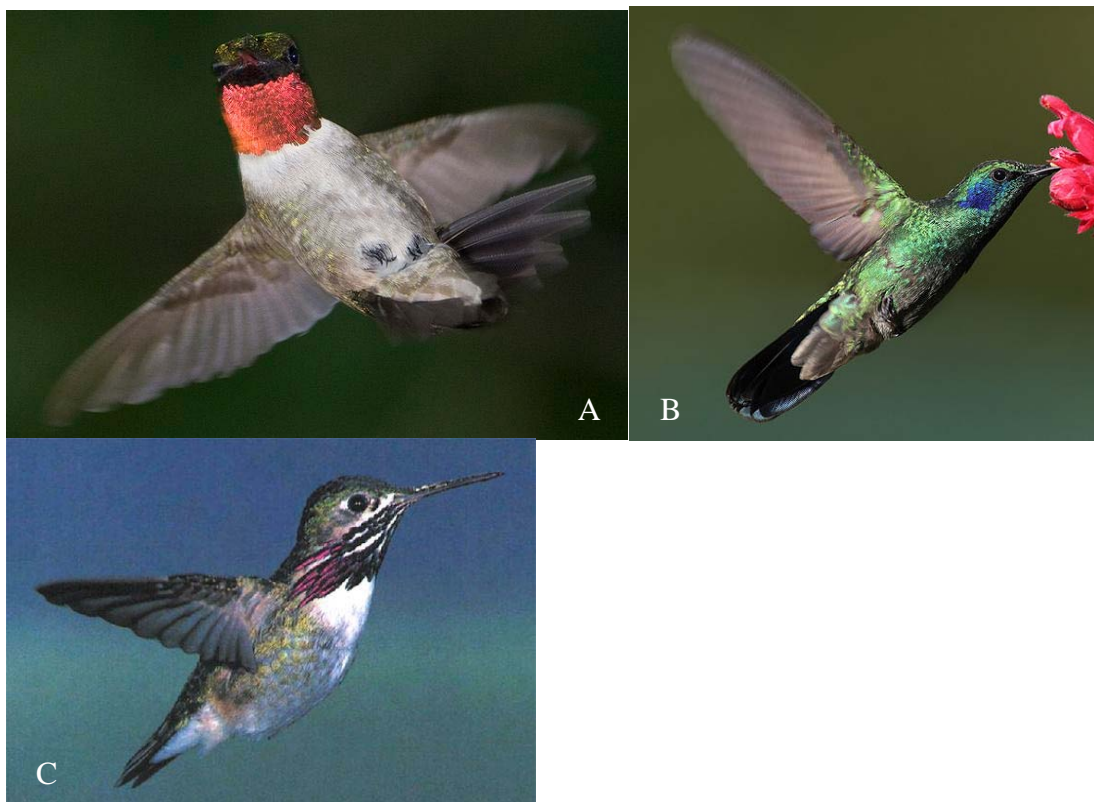
Figure1- 7: Hummingbirds very agile, with the ability to A) fly backward; B) hover; and C) fly forward at high speeds with great facility (pictures courtesy of

The cycle of supination during upstroke, followed by pronation during downstroke, seen in Figure 1-8, helps to shed tip vortices before changing stroke direction, decreasing drag and increasing lift. This motion may be passive, due to channel locking between the ulna and the radius, as a 4-bar linkage with joints that allow for twisting between them ("open articular surfaces"). This is similar to the hawk moth flying, and may be reproducible through controlling only two degrees of freedom, as discussed in the body of the paper.
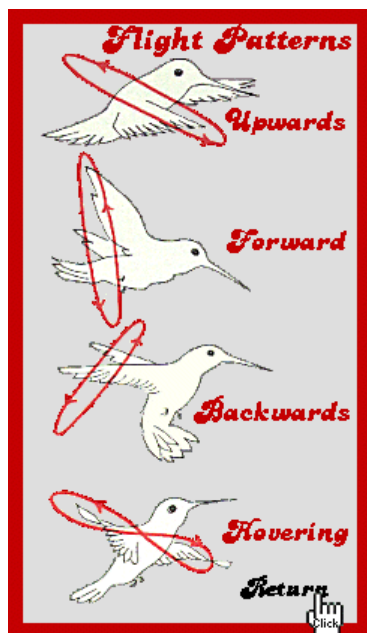
Figure1- 8: Hummingbird wing strokes during hovering and forward flight (graphic

courtesy of http://www.mschloe.com/hummer/huminfo.htm [accessed April 2010])

However, the structure of the wing would be difficult to reproduce. The tiny humerous and long hand wing, even compared to the hand wing of other birds, only extend along ~20% of the wing. The rest of the length of the wing is made up of feathers, as can be seen in Figure 1-9. The feathers bend ~35%, and are very important to flight. These characteristics would be very difficult to reproduce mechanically.
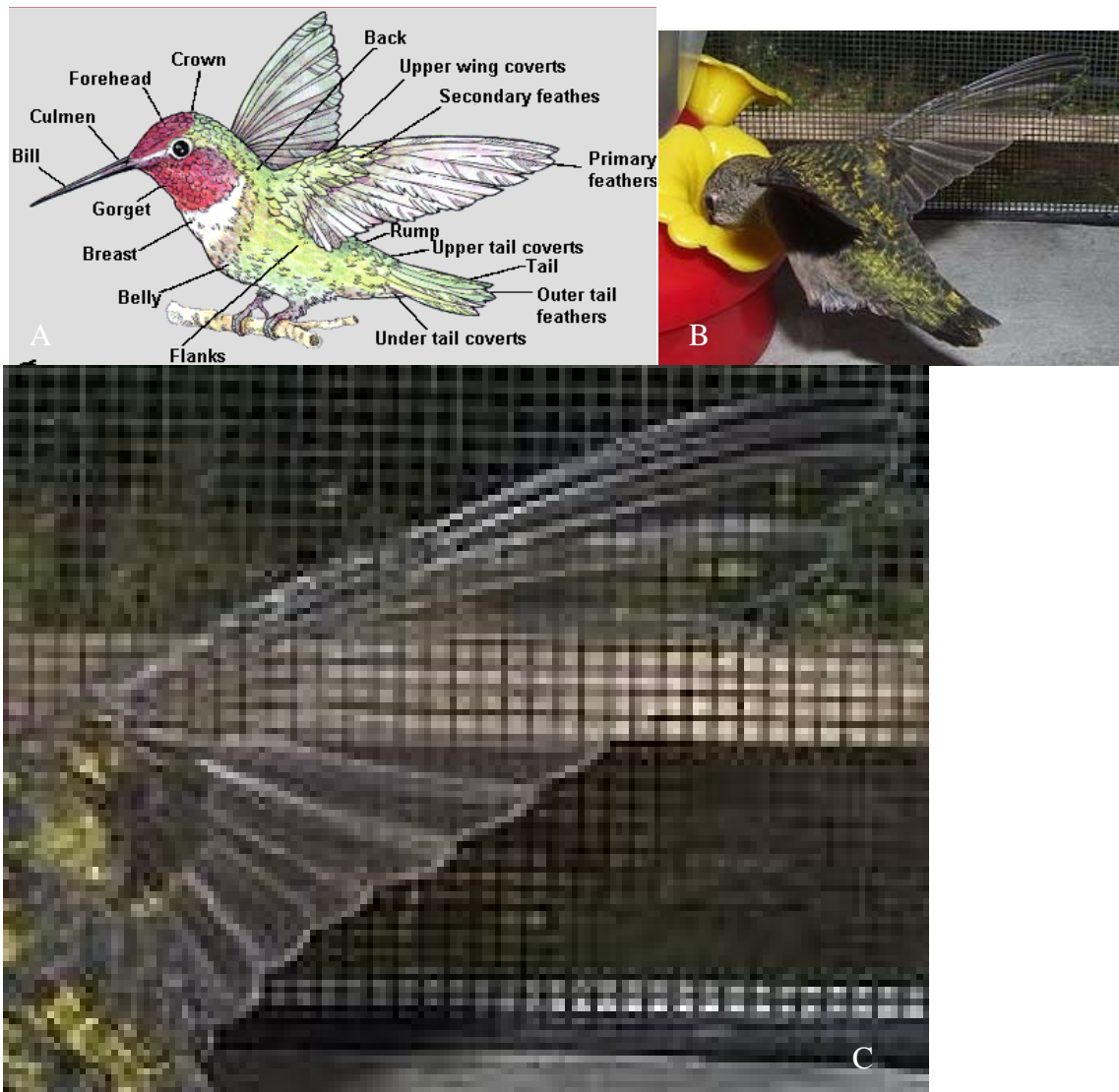
Figure1- 9: Hummingbird wings have a small portion of the superstructure made of bones, but are mainly feathers, making them very difficult to produce mechanically

A1.7 Hawkmoth

Hawkmoths (order lepidoptera, family sphingidae) are a large subset of all moths. They are generally large moths, with streamlined bodies, long narrow fore wings, and smaller hind wings, as seen in Figure 1-10. They are able to hover, and to fly at extremely high speeds (one of the fastest insects in the world - they have been clocked at 53 km/h) . They are also sometimes called Sphinx Moths or Hummingbird Moths because of the distinctive hum that can be heard while flying.

Figure1- 10: Members of the hawkmoth familyA) & B) show rich detail in the wings of *Macroglossum stellatarum*; C) shows the *Hemaris Thysbe* or hummingbird clearwing hawkmoth, and D) is a detail of C to show wing structure (courtesy of http://www.ask.com/wiki/Macroglossum_stellatarum for A and B and http://www.howardfamilyhomepage.net/page5b.html, for C and D [accessed April 2010])

the manner of flight and flight mechanisms of the hawk moth are very similar to the hummingbird. The pictures in Figure 1-11, covering the next two pages, show various hawk moths, along with details of their wings, enlarged to show wing structure.

112
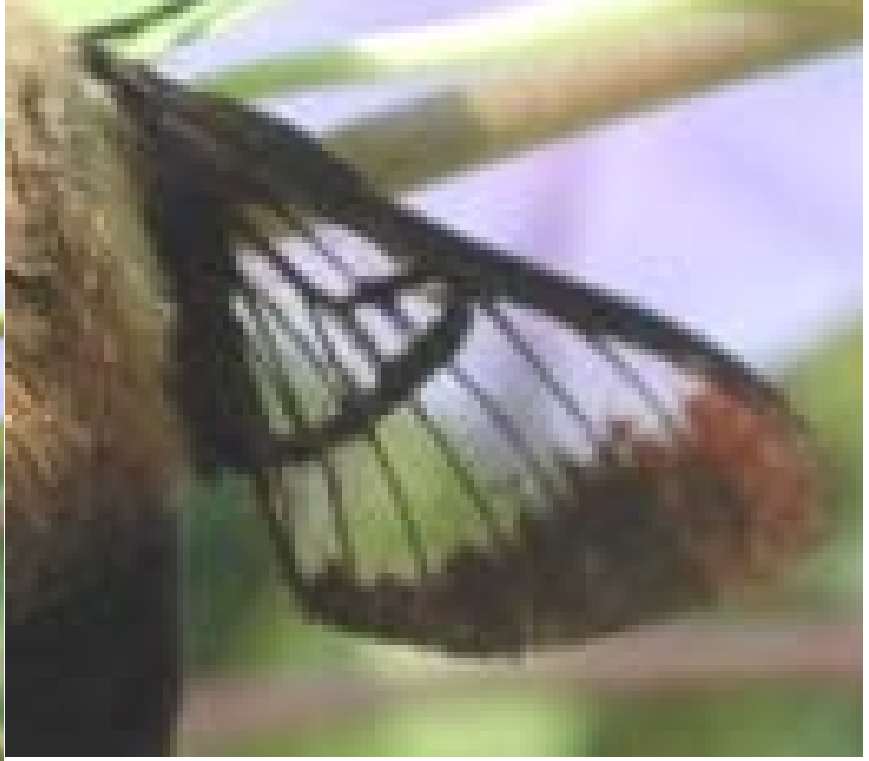
Figure1- 11: Various hawkmoths with details of their respective wings, showing wing structure; A) *Daphnis nerii* **(Oleander Hawkmoth); B)** *Cephonodes kingii* **(Bee**

Hawkmoth); C) *Hemaris diffinis* (Snowberry Clearwing Moth); and *D) Manduca Sexta* (courtesy of www.ask.com/wiki/Sphingidae for A, B, and C, and http://waynesword.palomar.edu/manduca2.htm for D [accessed April 2010])

In order to find an etch rate that was sufficiently fast for a manufacture process, but would not undercut the photoresist mask too much, or cause an overly uneven finish, tests were performed on small titanium squares, approximately 1cm x 1cm. Table 2-1 includes the raw data from those tests. The tests were performed with increasingly dilute HF and timed to the entire dissolution of the sample. The resulting times were converted into rates, assuming the sample is 125 µm thick, which should be a uniform thickness for the titanium foil.

Table 2- 1: Raw data from dissolution tests on titanium samples for various dilutions of HF

sample	thickness (µm)	HF dilution	time to hole (min.)	time to dissolve	1-side time	rate
1	125	0.01		2	4	31.25
2	125	3	5.25	6.25	12.5	10
3	125	5	9	10	20	6.25
4	125	8	12.92	13.75	27.5	4.545455
5	125	10	26		31	4.032258
*note: times for samples 1-4 are for two sides, but sample five was etched on only one side.						
	rate calculation is adjusted to account for this measurement					

The graphic in Figure 2-1 compares the rates of dissolution with the dilution of the HF. The green line is a logarithmic rate for comparison. The samples seem to approach a time between 3 and 4 minutes as dilution increases. The dilution chosen for the manufacturing process seems to approach that etch rate, indicating that the aggressive

etch has settled to a more even etch rate, and the dilution chosen is optimum for

minimizing surface finish and mask undercutting.
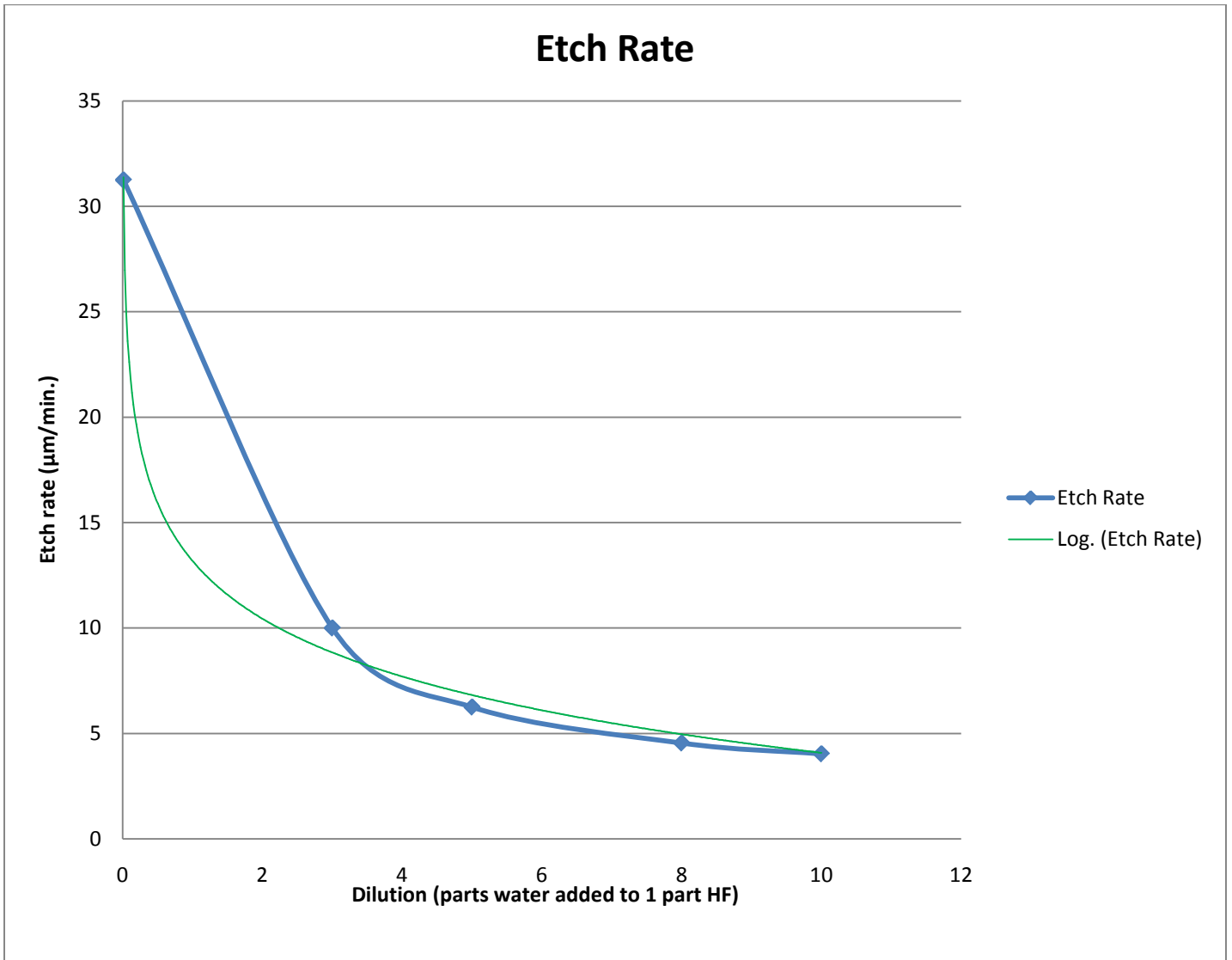
Figure 2- 1: Rate of dissolution decreases dramatically with increasing HF dilution;

shown with logarithmic decrease line for comparison

Appendix 3: Wing Camber Study Data

Many samples of titanium were pressed into different "camber molds" to measure their springback. Each camber mold consists of a cylinder of a given diameter and a tight fitting mold. The titanium sample is pressed into the tight fitting mold by the cylinder. The camber is then measured and recorded. The titanium sample is then pressed into the camber mold two more times to measure change in camber due to repeated bending.

The initial camber molds were made of pine and manufactured with drill bits and hole saws, and finished with sandpaper. The last two camber molds were printed on a rapid prototype. Table 3-1 shows the raw data from each of those experiments, and some notes from anomalous readings or anomalous test conditions.

Table 3- 1: Raw data from titanium springback testing of 1 cm and 2 cm long samples, pressed into cylinrical molds of varying diameters in order to estimate camber created

arc (cm)	5% camber	7% camber	10% camber		Design camber: 4x actual camber for springback			
1	0.05	0.07	0.1		Design	5%	7%	10%
1.5	0.075	0.105	0.15		radius (cm)	4.9832	3.54785	2.46592
2	**0.1**	**0.14**	**0.2**		dia. (cm)	9.9665	7.0957	4.93184
					radius(in)	1.9619	1.396791	0.970834646
					dia. (in)	3.9238	2.793583	1.941669291
Results for 0.775" diameter cylinder			Slightly smaller than what I calculated for 10% camber fixture					
width	length	1st press (in)	camber	3 presses (in)	camber			
0.026	0.87	0.048	5.5%	0.065	7.5%			
0.05	0.807			0.047	5.8%			
0.125	0.83			0.05	6.0%			
0.126	0.816			0.043	5.3%			

width	length	1st press (in)	camber	3 presses (in)	camber			
0.133	0.892	0.045	5.0%	0.051	5.7%			
0.212	0.892			0.036	4.0%			
0.255	0.87	0.032	3.7%	0.043	4.9%			
0.405	0.803			0.035	4.4%			
0.408	0.691			0.03	4.3%			
0.07	0.503	0.03	6.0%	0.03	6.0%			
0.096	0.408	0.021	5.1%	0.025	6.1%			
0.112	0.344	0.009	2.6%	0.016	4.7%			
0.125	0.421	0.014	3.3%	0.017	4.0%			
0.132	0.404	0.014	3.5%	0.017	4.2%			
0.322	0.457	0.012	2.6%	0.015	3.3%			

Actual yield: 5% camber

Hypothesis: springback is about 8x the bend of the diameter I put in the cylinder

Results for 0.51" diameter cylinder

width	length	1st press (in)	camber	3 presses (in)	camber			
0.018	0.438	0.038	8.7%	0.048	11.0%	stuck in mold*		
0.095	0.479	0.039	8.1%	0.045	9.4%			
0.463	0.51	0.04	7.8%	0.053	10.4%			
0.02	0.845	0.117	13.8%	0.149	17.6%	stuck in mold*		
0.104	0.839	0.103	12.3%	0.121	14.4%			
0.457	0.811	0.07	8.6%	0.1	12.3%			

Results for 0.625" diameter cylinder

width	length	1st press (in)	camber	3 presses (in)	camber			
0.139	0.787	0.05	6.4%	0.061	7.8%			
0.172	0.817	0.063	7.7%	0.071	8.7%	weakened by HF?		
0.405	0.823	0.038	4.6%	0.059	7.2%			
0.025	0.494	0.026	5.3%	0.028	5.7%	stuck in mold*		
0.159	0.473	0.019	4.0%	0.025	5.3%			
0.403	0.396	0.013	3.3%	0.016	4.0%			

*Those pieces stuck in the mold were weakened by extraction process and imparted greater camber than normal

Results for 0.756" diameter cylinder

width	length	1st press (in)	camber	3 presses (in)	camber			
0.333	0.721	0.015	2.08%	0.022	3.05%			
0.088	0.808	0.024	2.97%	0.034	4.21%			
0.08	0.466	0.015	3.22%	0.016	3.43%			

0.137	0.311	0.011	3.54%	0.013	4.18%			
Any cylinder has a camber of 1/π. That is one unit of height over π units of arc, or about 31.83% camber.								
In order to get 5% camber, the arc needs to have a (31.83/5)*2*π circumference, so r=6.36 cm; d=5.01 in.								
	Actual moth wing							
length	width	h	camber					
2.25	0.991	0.09	9.08%					
2.021	0.771	0.097	12.58%					

Figure 3-1 plots the raw data from the 2 cm long samples of titanium, plotted against the sample widths. The camber measurements are grouped by diameter of the camber mold into which it was pressed and the number of times it was pressed into the cylinder. A correlation between the width of the titanium sample and the amount of springback can be observed.

Each group of sample widths is also loosely represented by a line. This line is solely present to give a visual representation of what the average springback is, for a quick comparison. The lines should not be interpreted to be the slope of a curve for titanium springback.

Figure 3- 1: Measured camber vs. width of titanium sample pressed into camber mold for all samples of 2 cm length; measurements grouped by diameter of camber mold and number of times pressed into camber mold

Figure 3-2 plots the raw data from the 1 cm long samples of titanium, noting their

widths. Once again, there is a correlation between the width of the titanium sample and

the amount of springback. It is also to be noted that there is more springback for the

shorter samples than the longer samples mesured in Figure 3-1, so the camber is less

pronounced.   Since these samples are closer in length to the main structural cross

member of the designed wings, this data was given more weight when deciding the final

diameter of the camber cylinder to be used for pressing the manufactured wings.

Once again, each group of sample widths is also loosely represented by a line.

This line is solely present to give a visual representation of what the average springback

is, for a quick comparison. The lines should not be interpreted to be the slope of a curve
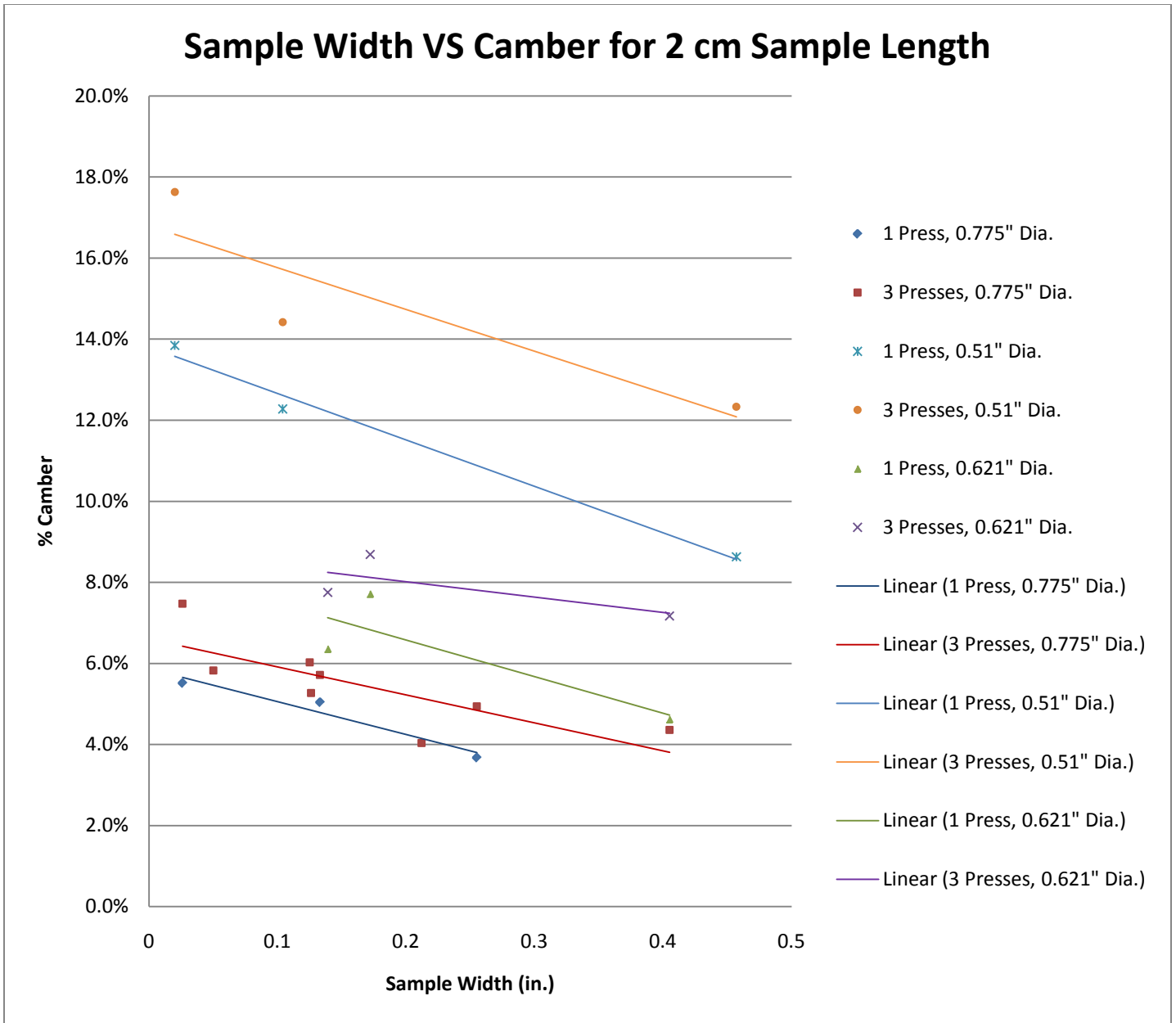
for titanium springback.
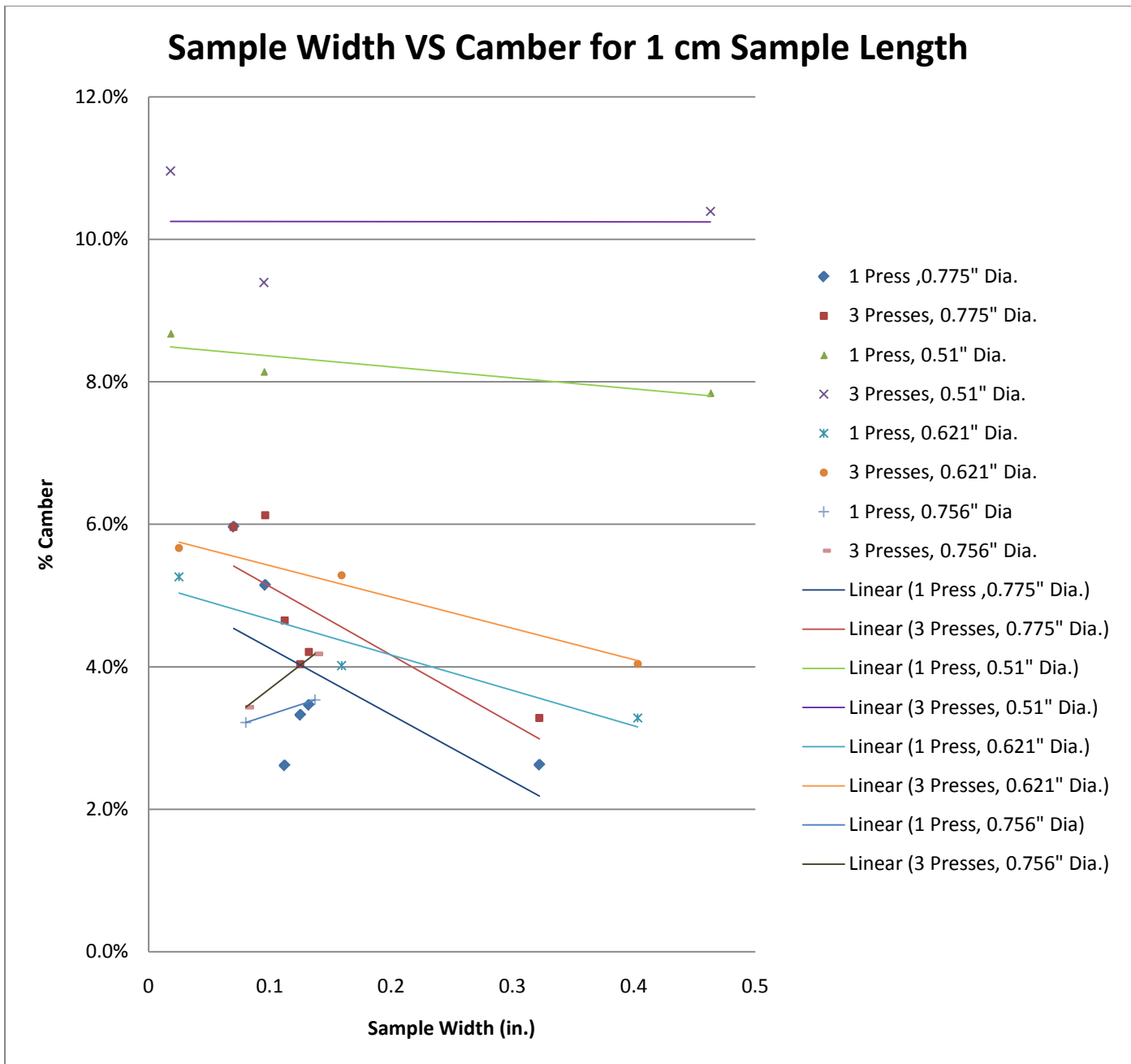
Figure 3- 2: Measured camber vs. width of titanium sample pressed into camber mold for all samples of 1 cm length; measurements grouped by diameter of camber mold and number of times pressed into camber mold

Appendix 4: Kapton Study Data

One of the great weight penalties for the manufactured wings was found to be the membrane. In order to save weight, the Kapton can be etched in an RIE. In order to measure the rate at which samples are etched, various samples of approximately 1 cm x 2 cm were etched, as well as larger samples. Table 4-1 shows the raw data from those etches. Across the top is the time in minutes the sample was etched. Down the left side is the number of sample measurements taken by a profilometer. The measurement of the sample is recorded next to the sample number. The measurements vary along the edge of the sample, so a semi-accurate picture of how much Kapton was etched by the RIE etcher in the stated period of time by observing all of the samples. An average etch rate is estimated based on this observation. Note that there are two types of RIE etch performed. The first is with a plasma composed of O_2 and SF_6, which provides an aggressive etch. The second is with a plasma composed of O_2 only. It is a less aggressive etch, and appears to be etch more evenly. Anomolies from the etch and measurements are noted at the end of the table.

Table 4- 1: Measurements taken along the edge of Kapton samples etched in an RIE

with plasma made of O_2 and SF_6, as well as a plasma made of O_2 only

O_2+SF_6 etch

TWO SIDE (min/side)

time (min)	0	1	2	3	5	5	7	10	10	10	10	3	4	5
sample 1	13.9	13.2	12.6	9.8	7	8.8	6.5	2	1.8	8.8	7.5	7.7	2.8	1
sample 2	13.7	12.7	12.4	9	8.3	7.8	6.8	2.3	2.7	8.9	5.9	5.5	1.9	2.1
sample 3	13.9	13	12.5	8.1	6.5	7.5	7.3	2.6	2.4	7.4	5	6.5	2.7	2.8
sample 4	13.6	12.6	12.1	8.9	4.6	6.3	7	2.5	2.2	6.5	3.2	5	5	0.9
sample 5				7.5		5.4	8.2		3.1	6	3.6	4.2	1.5	2
sample 6				9			7.7			8.2	5.2	6.9	2.1	1.9
sample 7				9.1							9	4.4	2.3	1.3
sample 8				10.8								3.4		1.1
Estimated etch	N/A	0.5	0.5	3.5	6	5.5	5	10	9.5	5	6	6	10	11
Width	N/A	0.81	0.71	0.64	1.97	0.67	0.73	0.96	0.63	0.58	0.55	0.54	0.5	0.45
Height	N/A	1.16	1.36	1.13	1.17	1.29	1.21	1.18	0.95	1.21	0.96	1.16	1.17	1.22
area	N/A	0.94	0.966	0.723	2.305	0.864	0.883	1.133	0.599	0.702	0.528	0.63	0.59	0.549
rate		0.5	0.25	1.167	1.2	1.1	0.714	1	0.95	0.5	0.6	2	2.5	2.2

O_2 etch only

time (min)	0	10	15	30
sample 1	13	11.5	10.1	10.7
sample 2	13	10.6	12.1	11.1
sample 3		12.7	11	10.7
sample 4			11.4	10.7
sample 5			11	
sample 6			11	
sample 7			11	
Estimated etch	N/A	1.7	2	2.3
Width	N/A	1.53	2.27	0.6
Height	N/A	2.04	2.04	1.21
area	N/A	3.121	4.631	0.726
rate		0.17	0.133	0.077

Loading Effects, SF_6+O_2

time (min)	10	20	25	25	30	35		
sample 1	11	1	0.7	7.8	2.2	5.1		
sample 2	12.1	3	2.4	6.3	2.5	9.2		
sample 3	12	2.3	3.3	10.1	2	6		
sample 4	11.1	0.7	1.4	10.3	1.2	8.6		
sample 5	11.3	1	1	5.3	5.6	9.3		
sample 6	9.9	2.6	1.3	5.7	6.6	0.9		
sample 7	12.1	1.2	1.4	4.9	4.1	1.8		
sample 8	12	0.7	2	5.7		0.9		
sample 9	11.7	1.1	1.6					
sample 10	12	1.9	2.6					
Estimated etch	2	11	10.5	6	8	5.5		
Width	1.07	0.94	1.99	2.9	4			
Height	1.06	2.1	2.1	3.41	4.35			
area	1.134	1.974	4.179	9.889	17.4	18.86		
rate	0.2	0.55	0.42	0.24	0.267	0.157		

First "no etching" measurement, using inaccurate "leveling" was 10µm, so it was not included
Several measurements of 10 & 15 min. O2 came out 17-29 µm.   Could be due to the other end of the sample hanging off the silicon wafer, which was used for smoothness and to keep the sample level. I have not included measurements over the original sample height.
The last listed 10 min. O2 + SF6 etch is anomolous. I have no idea why, nor does the technician who operated the RIE.   Due to this uncertainty, I did not include them with the graphed data.
The last two loading effect samples were ragged around the edges, so I cut a piece off the corner, and measured the inside of the cut, which gave me a more accurate measure of the etch the very small measurements on these samples were taken at the edge
The loading area of the RIE is a 5" dia. circle, so the area of the 35 min etch was $(4.9/2)^2*\pi$

Figure 4-1 compares the sample thickness after the etch for each sample etched by

the plasma consisting of O_2 and SF_6. A representative line, drawn only to visualize the

average amount of Kapton etched during the given time period, appears with each

sample. No rate information is meant to be conferred by use of these lines.
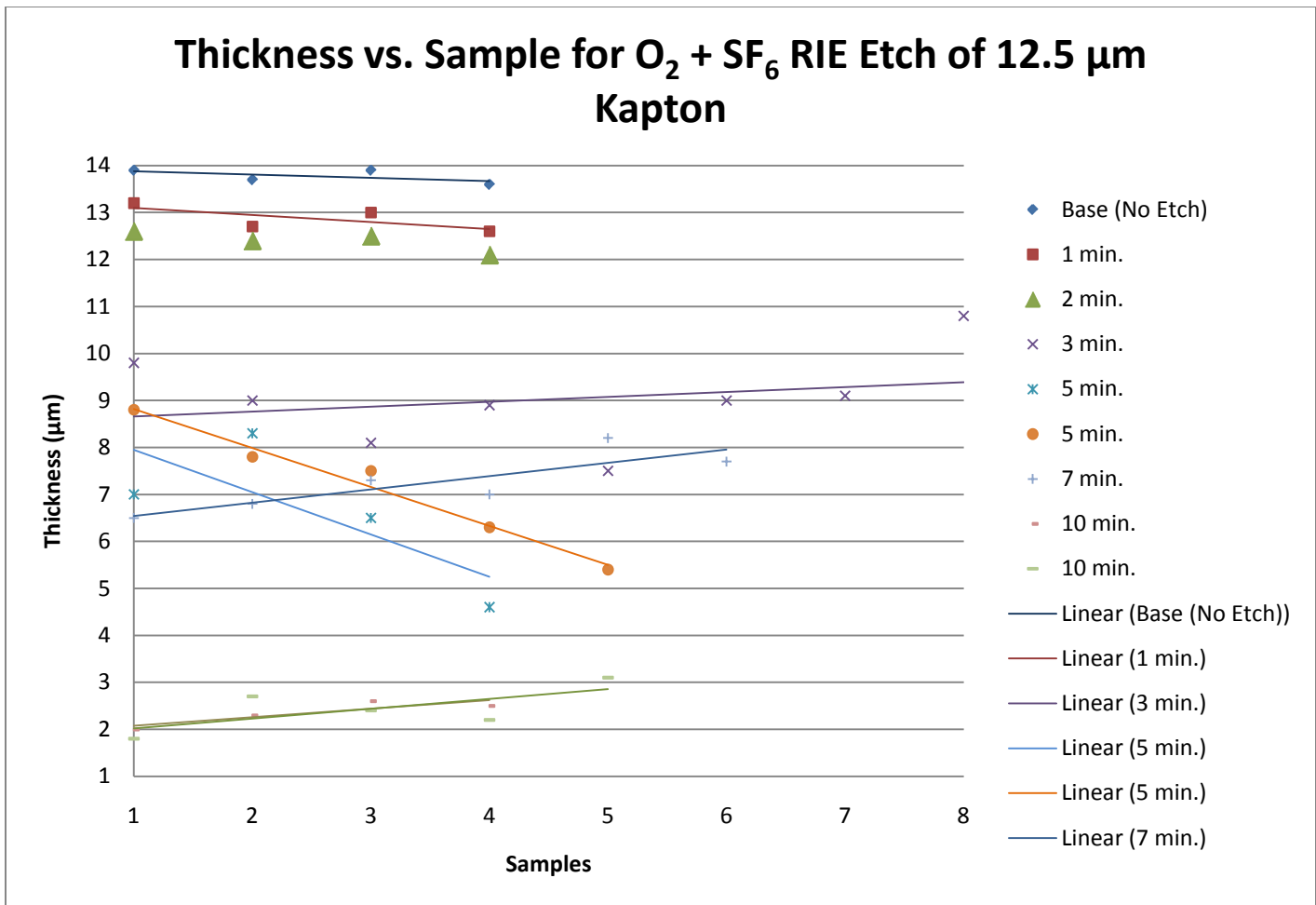
Figure 4- 1: Thickness measurements of Kapton samples after etch by plasma

consisting of O2 and SF6

Figure 4-2 compares the sample thickness vs. time etched by the plasma consisting of O_2 and SF_6. The samples show that the etching process is not entirely linear, but linear enough that a prediction of how much will be etched can be made.
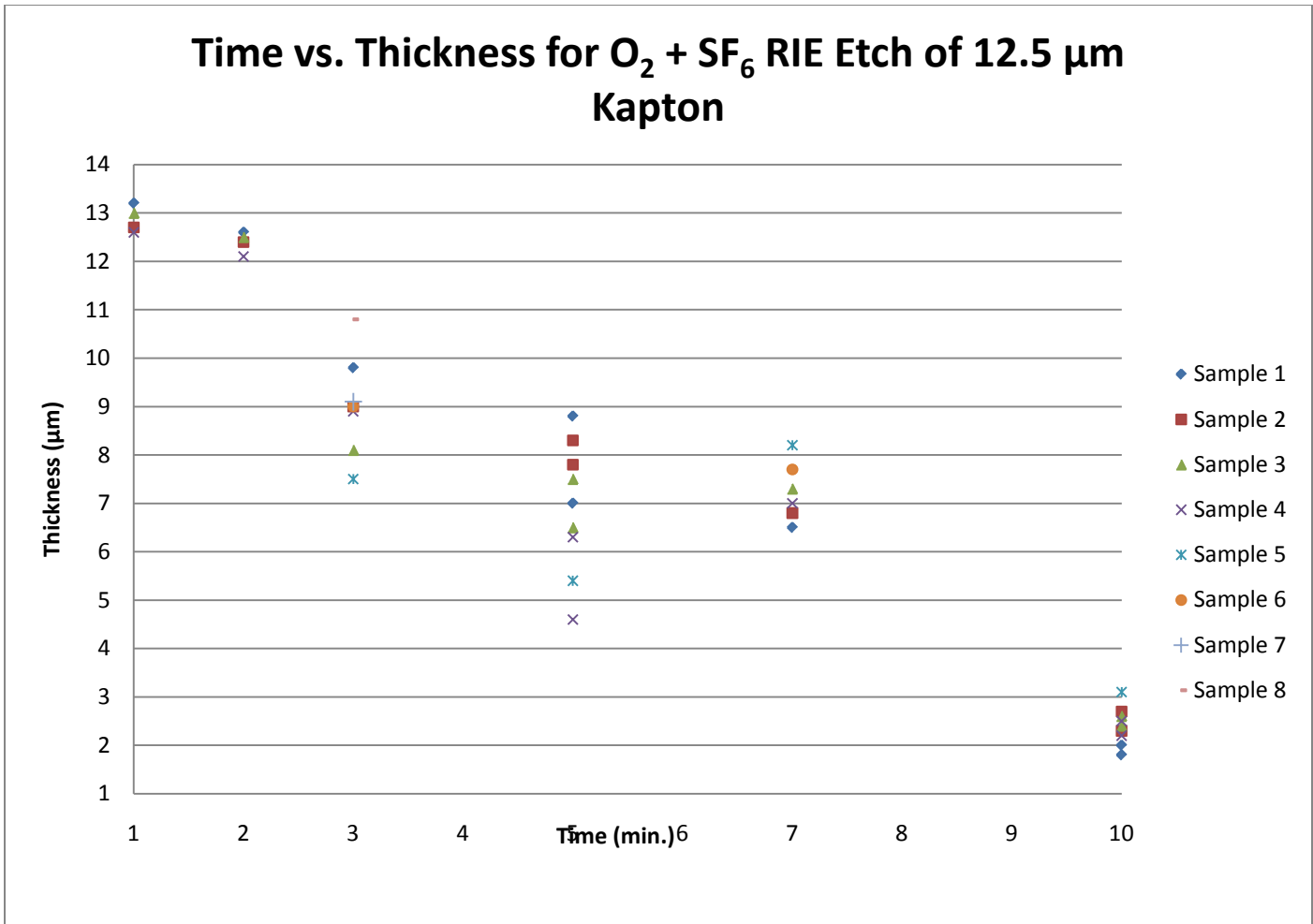
Figure 4- 2: Thickness of Kapton samples vs. time etched in a plasma consisting of O2 and SF6 shows the roughly linear nature of the etching process

Figure 4-3 compares the sample thickness after the etch for each sample etched by the plasma consisting only of O_2. Once again, representative line appears with each sample, drawn only to visualize the average amount of Kapton etched during the given time period. No rate information is meant to be conferred by use of these lines.
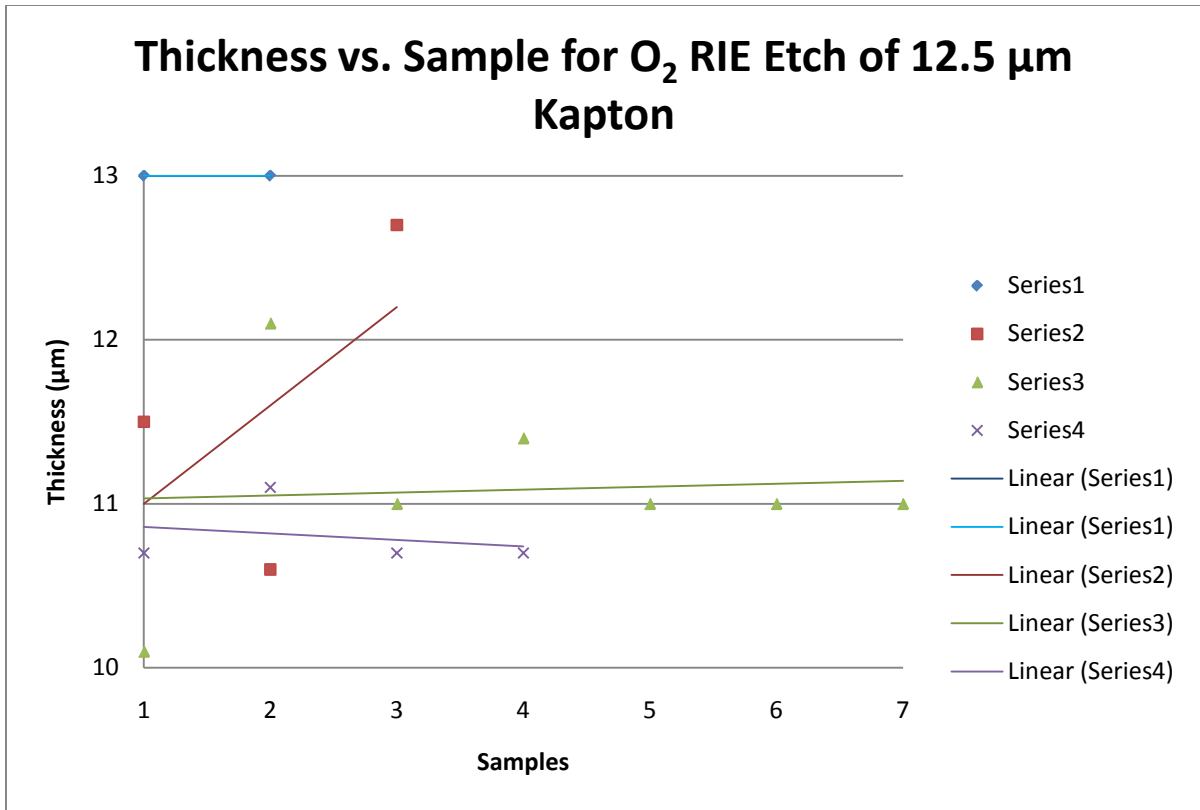
Figure 4- 3: Thickness of Kapton samples measured after etch in an O$_2$ plasma

Figure 4-4 compares the sample thickness vs. time etched by the plasma consisting of only of O$_2$. Once again, the samples show that the etching process is not entirely linear, but is smoother than the more aggressive SF$_6$ + O$_2$ etch.
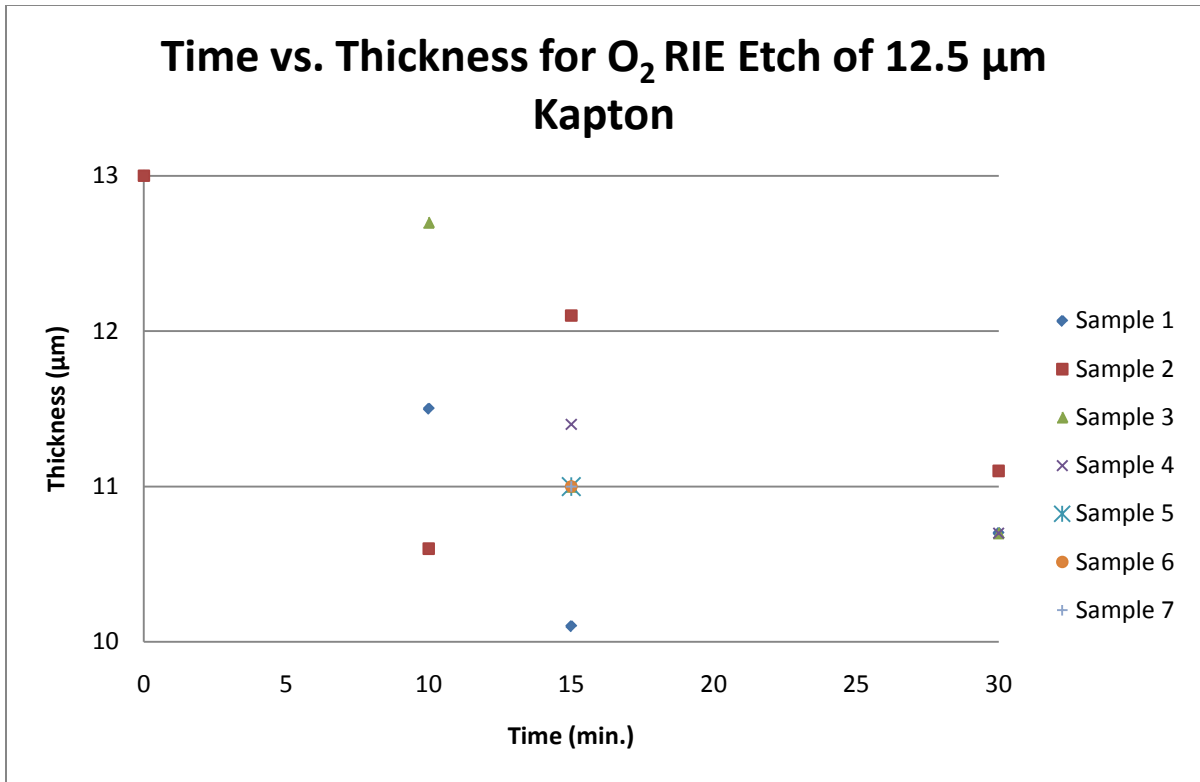
Figure 4- 4: Time vs. thickness for Kapton samples etched in RIE plasma consisting

of O_2 molecules
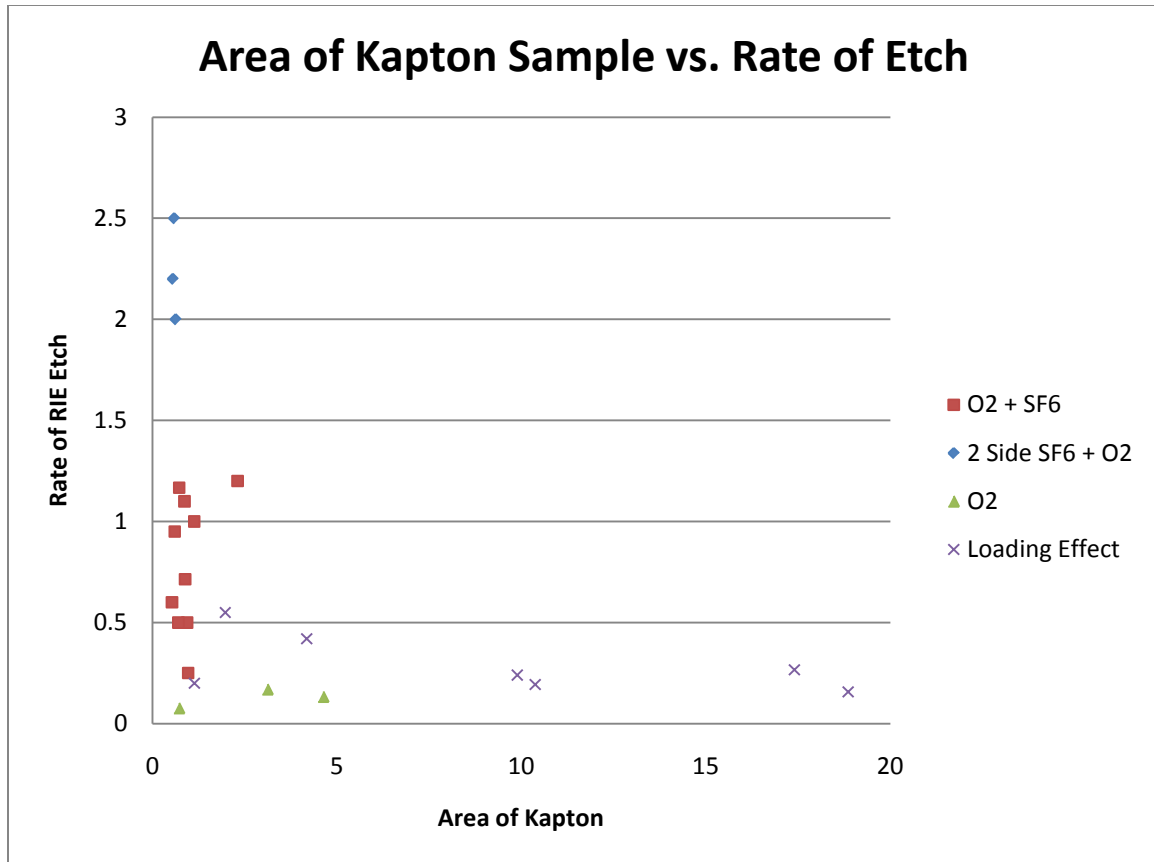
Figure 4- 5: Etch rate of various size samples of Kapton show the loading effect on RIE plasma in the chamber; the rate is much higher for smaller samples, but stabilizes near 0.25 μm/min. for samples with larger total areas

In order to fully characterize the etch rates, the loading effect of the RIE chamber must be taken into effect. When a larger sample is placed in the chamber, the plasma is spread across the area, decreasing the effect somewhat. Figure 4- 5 shows that the effect seems to stabilize around 0.25 μm/min. Once that rate was known, it was shown that the thickness of the Kapton after the etch could be predicted based on these data.

Bibliography

1. **Anderson, John D.** *Fundamentals of Aerodynamics.* New York, NY : McGraw-Hill, 2007.

2. **Chabak, Kelson D.** *Conceptual Study of Rotary-wing Microrobots.* Wright-Patterson Air Force Base : AFIT Thesis, 2008.

3. **Madou, Marc J.** *Fundamentals of Microfabrication: The Science of Miniaturization.* s.l. : CRC Press, 1997.

4. **Gardner, Julian W., Varadan, Vijay K. and Awadelkarim, Osama O.** *Microsensors, MEMS and Smart Devices.* s.l. : Wiley, 2001.

5. **Wood, Robert J.** *The First Takeoff of a Biologically Inspired At-Scale Robotic Insect.* s.l. : IEEE Transactions on Robots, April 2008.

6. **Wood, R. J., et al.** *Microrobotics Using Composite Materials: The Micromechanical Flying Insect Thorax.* Berkeley, CA : UCLA.

7. **Wood, R. J., et al.** *Microrobot Design Using Fiber Reinforced Composites.* Berkeley : Journal of Mechanical Design, 2008.

8. **Avandhanula, S., et al.** *Lift Force Improvements for the Micromechanical Flying Insect.* Berkeley : s.n.

9. **Pornsin-sirirak, T. Nick, et al.** *MEMS WING TECHNOLOGY FOR A BATTERY-POWERED ORNITHOPTER.* Miyazaki, Japan : 13th IEEE Annual International Conference on MEMS, 2000. pp. 709-804.

10. **Pornsin-Sirirak, Nick, Liger, Matthieu and Tai, Yu-Chong.** *Flexible Parylene-valved Skin for Adaptive Flow Control.* UCLA, Los Angeles : s.n.

11. **Fearing, R. S., et al.** *Wing Transmission for a Micromechanical Flying Insect.* Berkeley : IEEE International Conference on Robotics and Automation.

12. **Frye, Mark A.** *Multisensory Systems Integration for High-performance Motor Control in Flies.* Los Angeles, CA : Current Opinion in Neurobiology, 2010.

13. **Pornsin-Sirirak, T. Nick, et al.** *Ti-Alloy MEMS Wing Technology for a Micromechanical Flying Insect.* Caltech : s.n.

14. **Wood, R. J.** *Design, fabrication, and analysis of a 3DOF, 3cm flapping-wing MAV.* San Diego, CA : Proceedings of the 2007 IEEE/RSJ International Conference on Intellingent Robots and Systems, 2007.

15. **Dickinson, Michael H., Lehmann, Fritz-Olaf and Sane, Sanjay P.** Wing Rotation and the Aerodynamic Basis of Insect Flight. *Science Magazine Research Articles.* 2007.

16. **Sane, Sanjay P.** *The Aerodynamics of Insect Flight.* Seattle, WA : The Journal of Experimental Biology, 2003.

17. **Zhao, Liang, et al.** *Aerodynamic Effects of Flexibility in Flapping Wings.* s.l. : Interface, Journal of the Royal Society, 2009.

18. **Hubel, Tatjana Y., et al.** *Time-resolved Wake Structure and Kinematics of Bat Flight.* s.l. : Experimental Fluids, 2009.

19. **Warrick, Douglas R., Tobalske, Bret W. and Powers, Donald R.** *Aerodynamics of the Hovering Hummingbird.* s.l. : Nature Publishing Group, 2005.

20. **Van Den Berg, Coen and Ellington, Charles P.** *The Vortex Wake of a 'Hovering' Model Hawkmoth.* s.l. : The Royal Society, 1997.

21. **Anderson, Michael.** *Design and Control of Flapping Wing Micro Air Vehicles Dissertation Prospectus.* 2010.

22. **Wang, Z. Jane.** *Dragonfly Flight.* s.l. : American Institute of Physics, Oct 2008.

23. **Montealegre, Fernando, Jonsson, Thorin Thorin and Robert, Daniel.** *Understanding Wing Mechanics in Actively Stridulating Ensiferan (Orthoptera: Ensifera) Using Laser Vibrometry and Neuro-active Substances.* Prague : Society for Experimental Biology, 2010.

24. **Riskin, Daniel K., et al.** Quantifying the Complexity of Bat Wing Kinematics. *Journal of Theoretical Biology.* 2008.

25. **Margerie, D de, et al.** *Artificial Evolution of the Morphology and Kinematics in a Flapping-Wing Mini-UAV.* s.l. : IOP Publishing, Bioinspirationand Biomimetics, 2007.

26. **Tobalske, Bret W.** *Biomechanics of Bird Flight.* Portland : The Journal of Experimental Biology, 2007.

27. **Tobalske, Bret W., et al.** *Three-dimensional kinematics of hummingbird flight.* Portland, OR : The Journal of Experimental Biology, 2007.

28. **Hubel, Tatjana Y., et al.** Wake Structure and Wing Kinematics: The Flight of the Lesser Dog-faced Fruit Bat, Cynopterus Brachyotis. *The Journal of Experimental Biology.* 2010.

29. **Tian, Xiaodong, et al.** Direct Measurement of teh Kinematics and Dynamics of Bat Flight. *Institute of Physics Publishing, Bioinspiration and Biomimetics.* 2006.

30. **Usherwood, James R. and Ellington, Charles P.** *The Aerodynamics of Revolving Wings, Model hawkmoth wings.* Cambridge : The Journal of Experimental Biology, 2002.

31. **Lua, K. B., et al.** *On the Aerodynamic Characteristics of Hovering Rigid and Flexible Hawkmoth-like Wings.* s.l. : Experimental Fluids, 2010.

32. **Wu, Guanhao and Zeng, Lijiang.** *Measuring the Kinematics of a Free-flying Hawk-moth (Macroglossum Stellatarum) by a Comb-fringe Projection Method.* s.l. : Chinese Society of Theroetical and Applied Mechanics and Springer-Berlag BmbH, 2009.

33. **Willmott, Alexander P. and Ellington, Charles P.** *Measuring the Angle of Attack of Beating Insect Wings: Robust Three-Dimensional Reconstruction from Two-Dimensional Images.* Cambridge : The Journal of Experimental Biology, 1997.

34. **Wu, Pin and Ifju, Peter.** *Experimental Method for FW Structure Optimization for MAVs.* FL : 51st AIAA/ASME/ASCE/AHS/ASC Structures, Structureal Dynamics, and Materials Conference, 2010.

35. **Wood, R. J. and Fearing, R. S.** *Flight Force Measurement for a Micromechanical Flying Insect.* CA : Berkeley.

36. **Xie, Lunxu, Wu, Pin and Ifju, Peter.** *Advanced Flapping Wing Structure Fabrication for Biologically-Inspired Hovering Flight.* Orlando, FL : 51st AIAA/ASME/AHS/ASC Structures, Structural Synamics, and Materials Conference, 2010.

37. **Daniel, Thomas L. and Combes, Stacey A.** *Flexible Wings and Fins: Bending by Inertial of Fluid-Dynamic Forces.* University of Washington : Integr. Comp. Biology, 2002.

38. **Usherwood, James Richard.** Aerodynamics and Energetics of Animal Flight Based on Propeller Models. *A dissertation for the degree of Doctor of Philosophy in the University of Cambridge.* Cambridge, England : s.n., 2001.

39. **Deleon, Nathan.** Manufacturing and Evaluation of a Biologically Inspired Engineered MAV Wing Compared to the Manduca Sexta Wing Under Simulate Flapping Conditions. *2011.* 2011.

40. **Technology, Georgia Institute of.** Artificial Butterfly: Wing Scaled Provide Template for Complex Photonic Structures. *Science Daily.* 2006.

41. **Society, American Chemical.** Natural Solar Collectors on Butterfly Wings Inspire more Powerful Solar Cells. *Lepidopterology.* 2009.

42. **Davidson, Michael W.** Butterfly Wing Scales. *Molecular Expressions.* [Online] 1998-2010. [Cited: February 11, 2011.] http://micro.magnet.fsu.edu/primer/techniques/phasegallery/butterflywing.html.

43. **Cox, Adam, et al.** *The Development of Elastodynamic Components for Piezoelectrically Actuated Flapping Micro-Air Vehicles.* s.l. : Journal of Intelligent Material Systems and Structures, 2002.

44. **Materials, Rohm and Haas Electronic.** Microposit S1800 G2 Series Photoresists. 2006.

45. **Chem, Micro.** SU8 2-25. *Process Guidelines.* 2002.

46. **May, Gary S. and Sze, Simon M.** *Fundamentals of Semiconductor Fabrication.* Hoboken, NJ : John Wiley & Sons, 2004.

47. Selective Chemical Etchants.

48. **Williams, Kirt R., Gupta, Kishan and Wasilik, Matthew.** *Etch Rates for Micromachining Processing.* s.l. : IEEE, 2003.

49. **1728 Software Systems.** Circle Sector, Segment, Chord and Arc Calculator. *Geometry Calculators.* [Online] January 27, 2011. [Cited: January 27, 2011.] http://www.1728.com/circpart.htm.

50. **Michelson, Robert C. and Naqvi, Messam A.** *Extraterrestrial Flight.* s.l. : RTO-AVT von Karman Institute for Fluid Dynamics Lecture Series, 2003.

51. **Yan, Joseph and Fearing, Ronald S.** *Wing Force Map Characterization and Simulation for the Micromechanical Flying Insect.* Berkeley : s.n.

52. **Coutu, Ron.** EENG636, MEMS lecture slides. 2009.

53. SU8 2-25. *Process Guidelines.*

54. **Dickson, W. B. and Dickinson, M. H.** *The Effect of Advance Ratio on the Aerodynamics of Revolving Wings.* Pasadena, CA : Journal of Experimental Biology, 2004.

55. **Stanford, Bret, et al.** *Shape Structure and Kinematically Optimized Hovering Wing.* s.l. : 51st Annual AIAA/ASME/ASCE/AHS/ASC Structures, Structural dynamics, and Materials Conference, 2010.

56. **Wang, Ji Kang and Sun, Mao.** *A Computational Study of the Aerodynamics and forwing-hindwing Interaction of a Model Dragonfly in Forward Flight.* Beijing : The Journal of Experimental Biology, 2005.

Vita

Bob Dawson was born in Provo, Utah. He graduated from Brigham Young University with a degree in Mechanical Engineering and was comissioned into the Air Force that same month. After two assignments he was accepted to the Air Force Institute of Technology to earn a Masters of Science in Aeronautical Engineering, Control Systems Design. In both degrees his secondary emphasis was MEMS.

1. REPORT DATE *(DD-MM-YYYY)* 24-03-2011	2. REPORT TYPE Master's Thesis	3. DATES COVERED *(From – To)* June 2009 – March 2011

TITLE AND SUBTITLE Repeatable Manufacture of Wings for Flapping Wing Micro Air Vehicles Using Microelectromechanical System (MEMS) Fabrication Techniques	5a. CONTRACT NUMBER
	5b. GRANT NUMBER
	5c. PROGRAM ELEMENT NUMBER
6. AUTHOR(S) Dawson, David "Bob", Captain, USAF	5d. PROJECT NUMBER ENR # 10-152
	5e. TASK NUMBER
	5f. WORK UNIT NUMBER

7. PERFORMING ORGANIZATION NAMES(S) AND ADDRESS(S) Air Force Institute of Technology Graduate School of Engineering and Management (AFIT/ENY) 2950 Hobson Way, Building 640 WPAFB OH 45433-8865	8. PERFORMING ORGANIZATION REPORT NUMBER AFIT/GAE/ENY/11-M06
9. SPONSORING/MONITORING AGENCY NAME(S) AND ADDRESS(ES) Air Force Research Laboratory, Air Vehicles Directorate Attn: Dr. Greg Parker gregory.parker@wpafb.af.mil 2130 8th St, bldg 45 Wright Patterson AFB 45433 (937) 255-7750 (DSN: 785-7750)	10. SPONSOR/MONITOR'S ACRONYM(S) AFRL/RBAA
	11. SPONSOR/MONITOR'S REPORT NUMBER(S)

12. DISTRIBUTION/AVAILABILITY STATEMENT
    Approved for public release, distribution unlimited

13. SUPPLEMENTARY NOTES
This material is declared a work of the U.S. Government and is not subject to copyright protection in the United States

14. ABSTRACT
While there have been great advances in the area of Flapping Wing Micro Air Vehicles (FWMAV), prototype parts have been constructed with the objective of scientific discovery and basic research. There has been little effort to make parts that could be consistently and repeatedly manufactured. Until recently, there has been little, if any, focus on methods that could be used and verified by subsequent researchers. It is herein proposed that Microelectromechanical System fabrication methods will provide a fast, cheap, and highly repeatable manufacturing method for the FWMAV wings. The wings manufactured to demonstrate this process, bio-inspired by the *Manduca Sexta*, were patterned and manufactured from titanium. The process took a relatively short amount of time: three and a half hours from start to finish. Multiple wings were fabricated as a batch during this time. A repeatable method for producing camber in the wing and mounting a membrane on the titanium structure is also presented. These processes will allow parametric testing of FWMAV wings. These wings will be exactly the same, except for specific changes made by the designer, so wing iterations can be compared and studied precisely. The best possible FWMAV wing can be discovered and exactly recreated in this manner. This process may also be easily adapted to mass manufacture of FWMAV wings in industry.

15. SUBJECT TERMS
        Flapping Wing Micro Air Vehicles (FWMAVs), Microelectromechanical Systems (MEMS), wing fabrication, repeatable

16. SECURITY CLASSIFICATION OF:			17. LIMITATION OF ABSTRACT	18. NUMBER OF PAGES	19a. NAME OF RESPONSIBLE PERSON Richard G. Cobb, Asst. Prof., USAF
a. REPORT U	b. ABSTRACT U	c. THIS PAGE U	UU	157	19b. TELEPHONE NUMBER *(Include area code)* (937) 255-3636, x4559 Richard.Cobb@afit.edu

Standard Form 298 (Rev. 8-98)
Prescribed by ANSI Std. Z39-18